FZK 353
15 March 1968

APOLLO RADIATION SURVEY METER AND PERSONAL RADIATION DOSIMETER

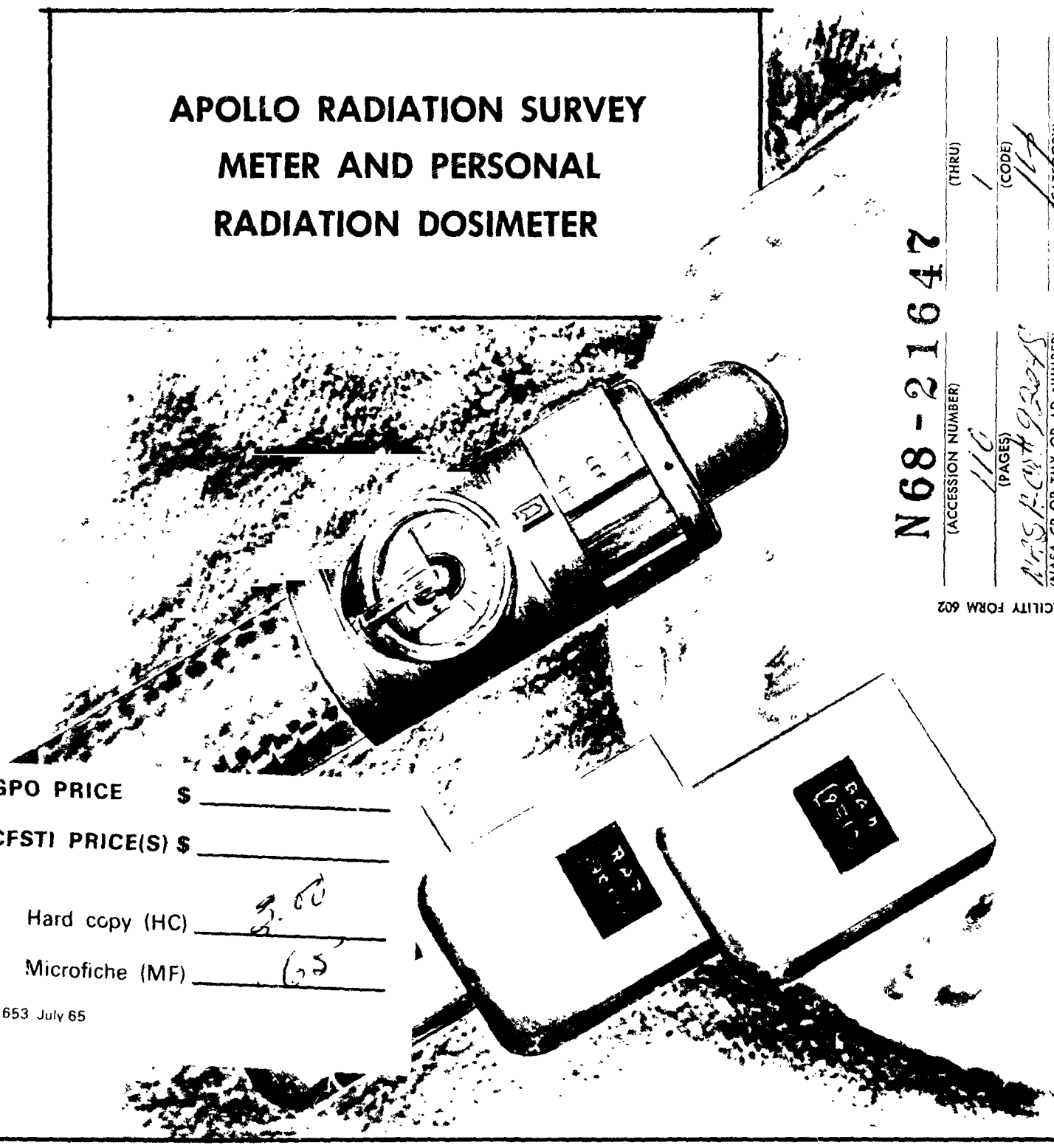

N68-21647
(ACCESSION NUMBER) (THRU) 1
(PAGES) (CODE)
(NASA CR OR TMX OR AD NUMBER) (CATEGORY)
FACILITY FORM 602

GPO PRICE $ _____
CFSTI PRICE(S) $ _____
Hard copy (HC) 3.00
Microfiche (MF) .65
ff 653 July 65

NUCLEAR AEROSPACE RESEARCH FACILITY

operated by

GENERAL DYNAMICS | *Fort Worth Division*

APR 1968

FZK 353
15 March 1968

NUCLEAR AEROSRACE RESEARCH FACILITY

APOLLO RADIATION SURVEY METER AND PERSONAL RADIATION DOSIMETER

Prepared For
MANNED SPACECRAFT CENTER
NATIONAL AERONAUTICS AND SPACE ADMINISTRATION
HOUSTON, TEXAS

Contract No. NAS9-6287

GENERAL DYNAMICS
Fort Worth Division

TABLE OF CONTENTS

TABLE OF CONTENTS (Cont'd)

LIST OF FIGURES

LIST OF FIGURES (Cont'd)

LIST OF FIGURES (Cont'd)

PRECED[illegible] FILMED.

LIST OF TABLES

I. INTRODUCTION

Two types of Apollo radiation instruments have been successfully fabricated to meet all the Apollo environmental and reliability requirements. One type, the Personal Radiation Dosimeter, integrates incident radiation and displays the total dose on a five-digit register. The other type, the Radiation Survey Meter, measures radiation rate on a linear meter readout. Three dosimeters and one survey meter are shown in Figure 1-1, along with a bracket for holding the meter and a black plastic case designed for the safe transport of the instruments. The interior of the case is fitted with cloth-covered foam rubber with cutouts shaped for the individual instruments, as shown in Figure 1-2. Both latches on the case can be locked.

Early prototype modes of these radiation measuring systems were developed by the NASA Manned Spacecraft Center, the Fort Worth Division of General Dynamics, and several other companies. Most of the final circuit designs and basic physical configurations were developed by the Manned Spacecraft Center. During this contract work General Dynamics performed the detail design, fabrication, qualification, and delivery of the flight hardware. In addition to the flight hardware, training units were furnished for use by the astronauts.

The structural and operational designs of the Personal Radiation Dosimeter and the Radiation Survey Meter are described in Sections II and III, respectively. The various calibration and linearity tests to which the instruments were subjected are described in Section IV, results of these tests are also presented. Recommendations are given in Section V.

NASA quality assurance and reliability procedures were used to manage and control the program, and documentation commensurate to these procedures was prepared and submitted to MSC. Other aspects of the program that have been documented are discussed in Appendix A

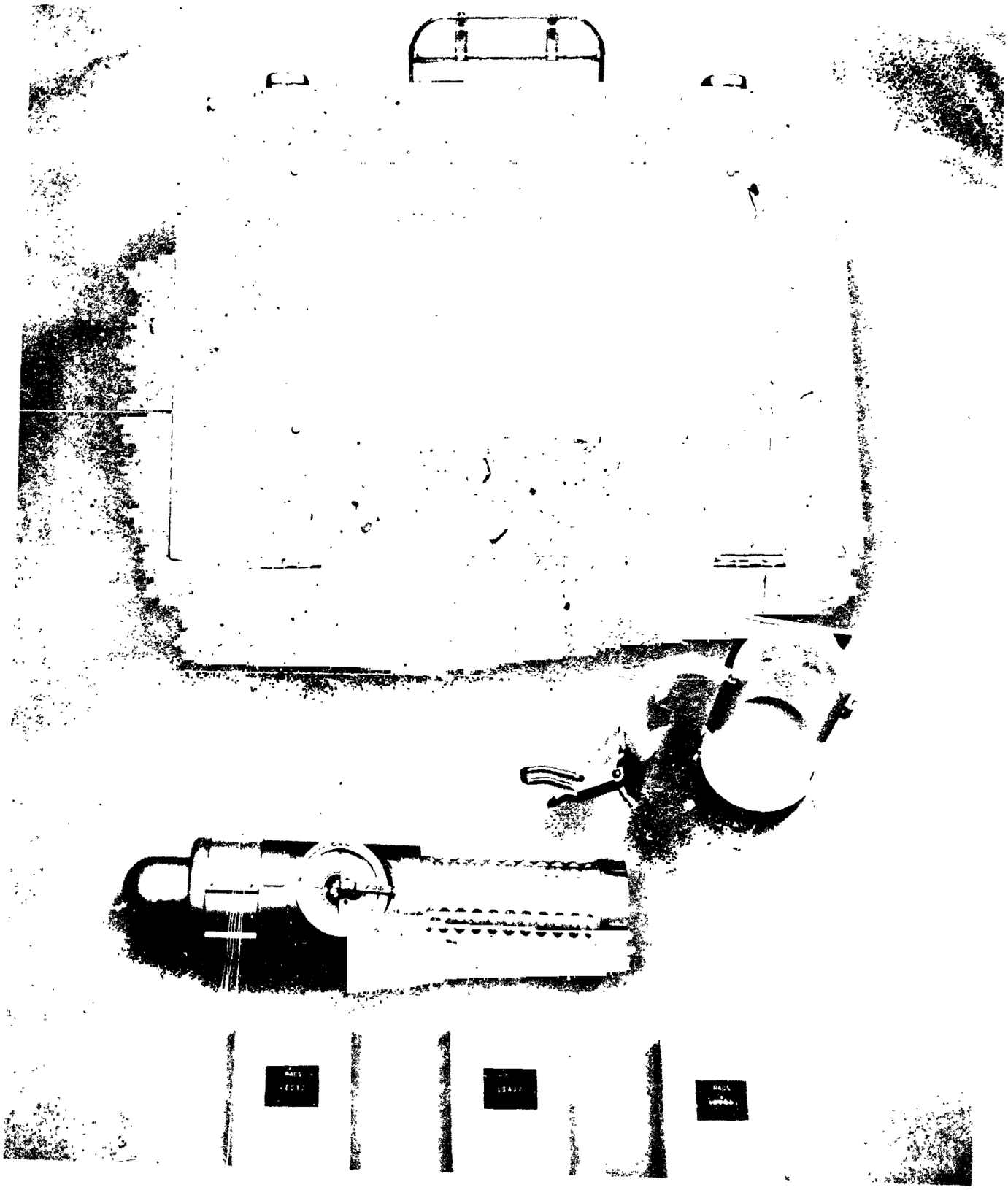

Figure 1-1 Apollo Carrying Case, Radiation Survey Meter and Bracket, and Three Personal Radiation Dosimeters

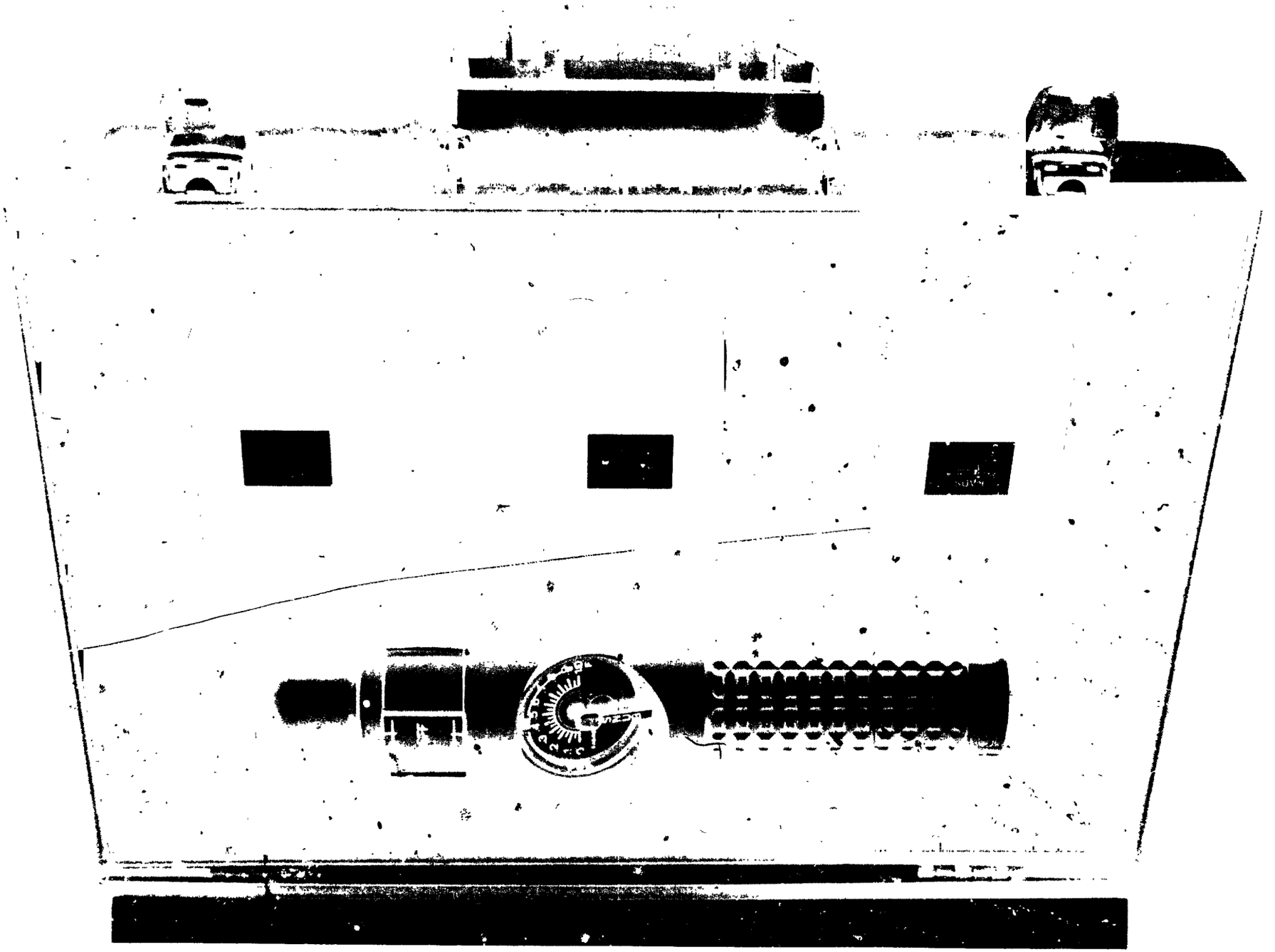

Figure 1-2 Interior of Apollo Carrying Case

II. PERSONAL RADIATION DOSIMETER

The Personal Radiation Dosimeter (PRD), shown in Figure 2-1, was designed to monitor the radiation dose resulting from exposure to solar flares and the Van Allen radiation belt. The PRD has a 0- to 1000-rad range in 0.01-rad increments and will measure cobalt-60 gamma fields of less than 60 rad/h to within $\pm$ 10% and fields greater than 60 rad/h to within 20% with a reproducibility of $\pm$ 3%. The batteries are capable of supplying power continuously in excess of 250 hours, or for a total integrated count of 99,999 (1000 rad). The complete unit occupies a volume of 5.46 $in.^3$ and weighs 0.38 lb.

2.1 Structural Design

The PRD is packaged in a rectangular aluminum shell finished with a flat white pain (3M400 series) manufactured by the Minnesota Mining and Manufacturing Company. The various components that make up the dosimeter are shown in Figure 2-2. These components are (1) an ionization chamber, (2) a high-impedance module, (3) an electronic (low-impedance) module and a readout register, and (4) a battery container. This modular design permits the replacement of any component or electronic module without adversely affecting the operation of the whole system. Also, any component from one dosimeter may be used to replace a like component in another dosimeter.

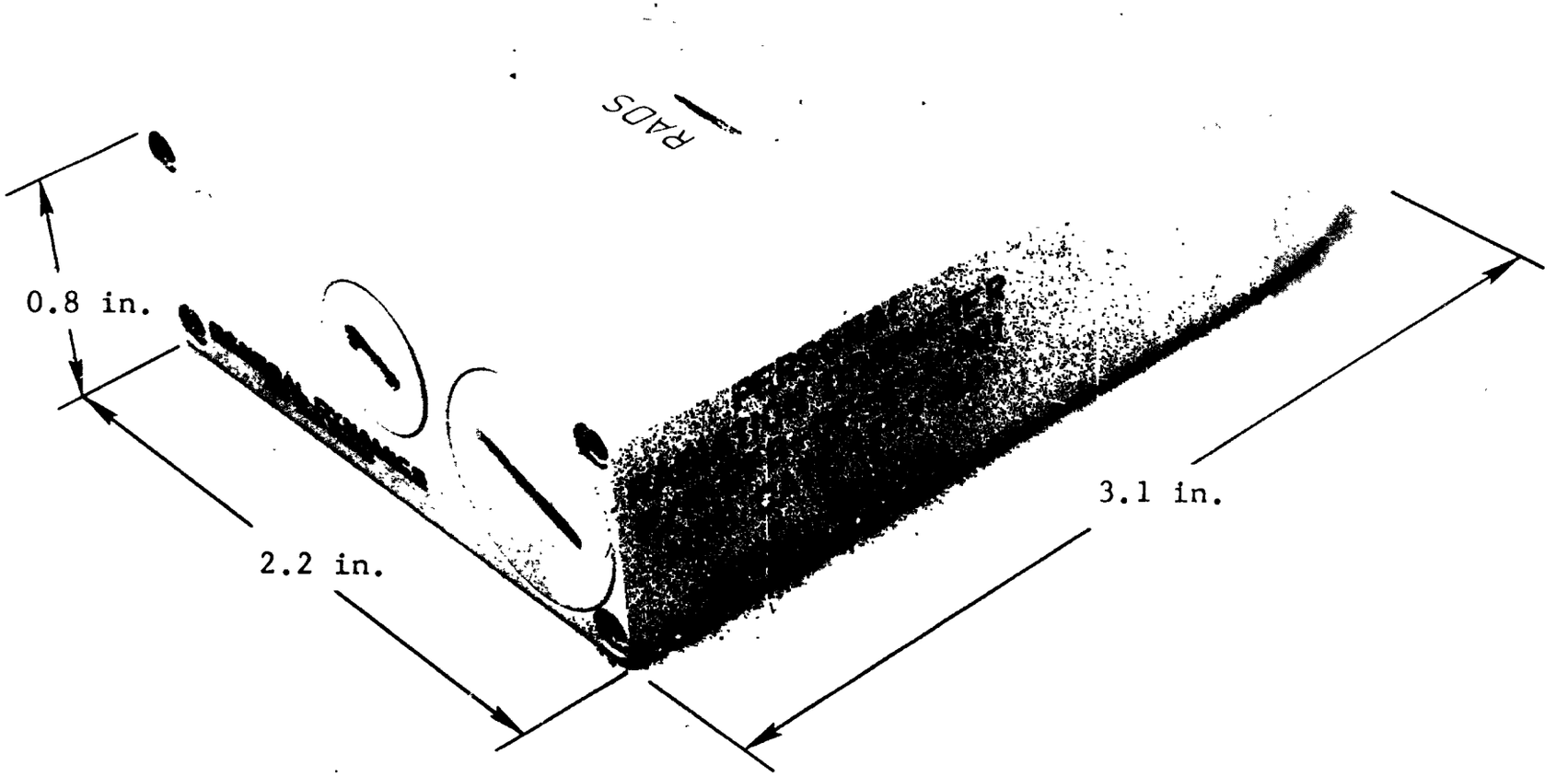

Figure 2-1 Apollo Personal Radiation Dosimeter

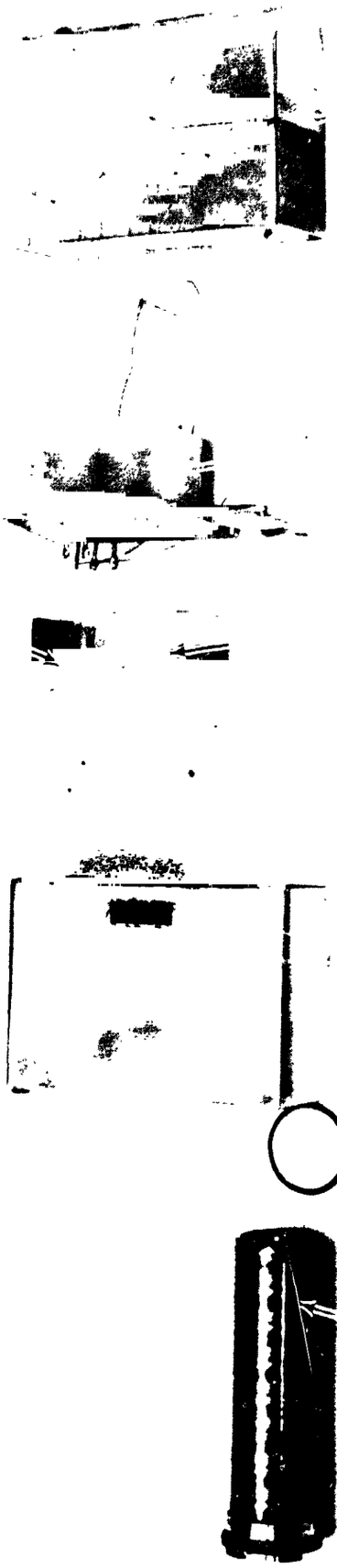

Figure 2-2 Disassembled Personal Radiation Dosimeter

Access to the batteries and electronic circuitry test points is provided by the two hermetically sealed caps visible in Figure 2-1. The larger cap provides access to the battery container, the smaller to four test points used to check out the electronics. Indium and silicon rubber gaskets are used to hermetically seal the unit

2.1.1 Ionization Chamber

A cross-sectional drawing of the ionization chamber is shown in Figure 2-3. As indicated in the figure, the electrodes are made of high-density polyethylene, partially aluminized for electrical conductivity. The chamber is housed in a thin aluminum shell 0.015 in. thick; the total thickness into the active volume is 0.219 g/cm^2.

A more detailed presentation appears in General Dynamics Drawings NLM 224-B and 250-B. The assembly procedure is described in NIP-2.

2.1.2 Electronic Modules

The high-impedance electronic piece parts are resistance-welded and mounted in a block of high-density polyethylene to provide maximum insulation resistance along with a rigidly constructed module (see NLM 228-B). The low-impedance electronic piece parts are in a welded, cordwood-type module potted with

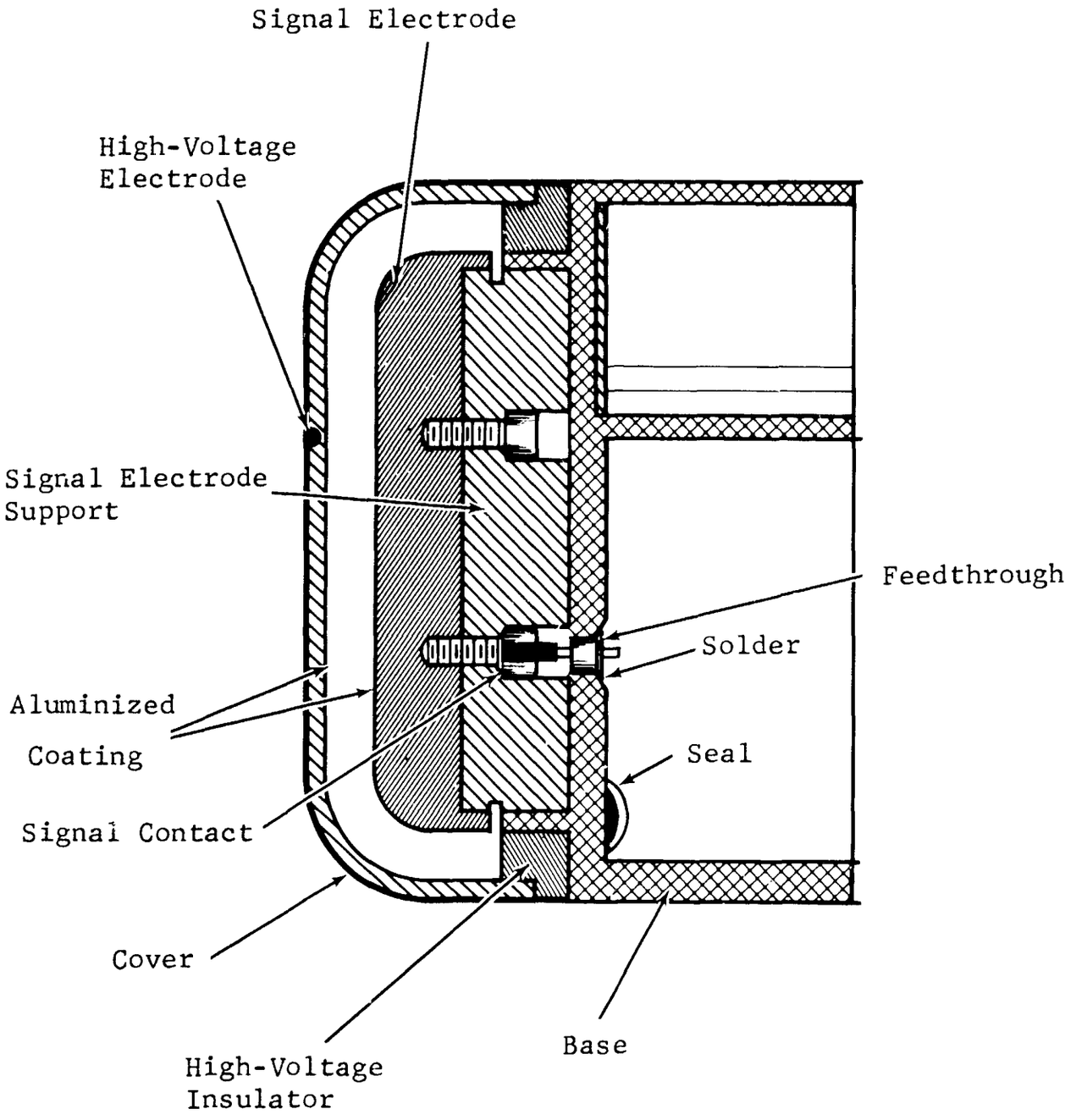

Figure 2-3 Cross-Sectional View of PRD Ionization Chamber

Emerson and Cuming Stycast 1090 SI (see NLM 252-B). Detailed fabrication and assembly procedures for each module are given in NIP-3 and NIP-4.

2.1.3 Readout Register

A drawing of the readout register is presented in Figure 2-4. This device is enclosed in a hermetically sealed housing; the electrical connections are made through two glass-sealed terminals. The five-digit readout has white letters on a black background and is read through a magnifying window (Fig. 2-4). This window is made of polished polystyrene rod and has a magnification of approximately two. It is made by General Dynamics and installed by the A. W. Haydon Company.

2.2 Operational Design

A simplified circuit schematic of the Personal Radiation Dosimeter is shown in Figure 2-5. Radiation-produced ionization pairs in the ion chamber cause current in the external circuit to charge a capacitor, C_1, positive according to the expression $V = Q/C_1$, where V is the voltage across C_1 and Q is the electronic charge, which is proportional to the radiation dose. The input resistance R_x is greater than 10^{15} ohms and is the parallel equivalent of the leakage resistance of capacitor C_1, relay K_1, the amplifier input, and the ionization chamber.

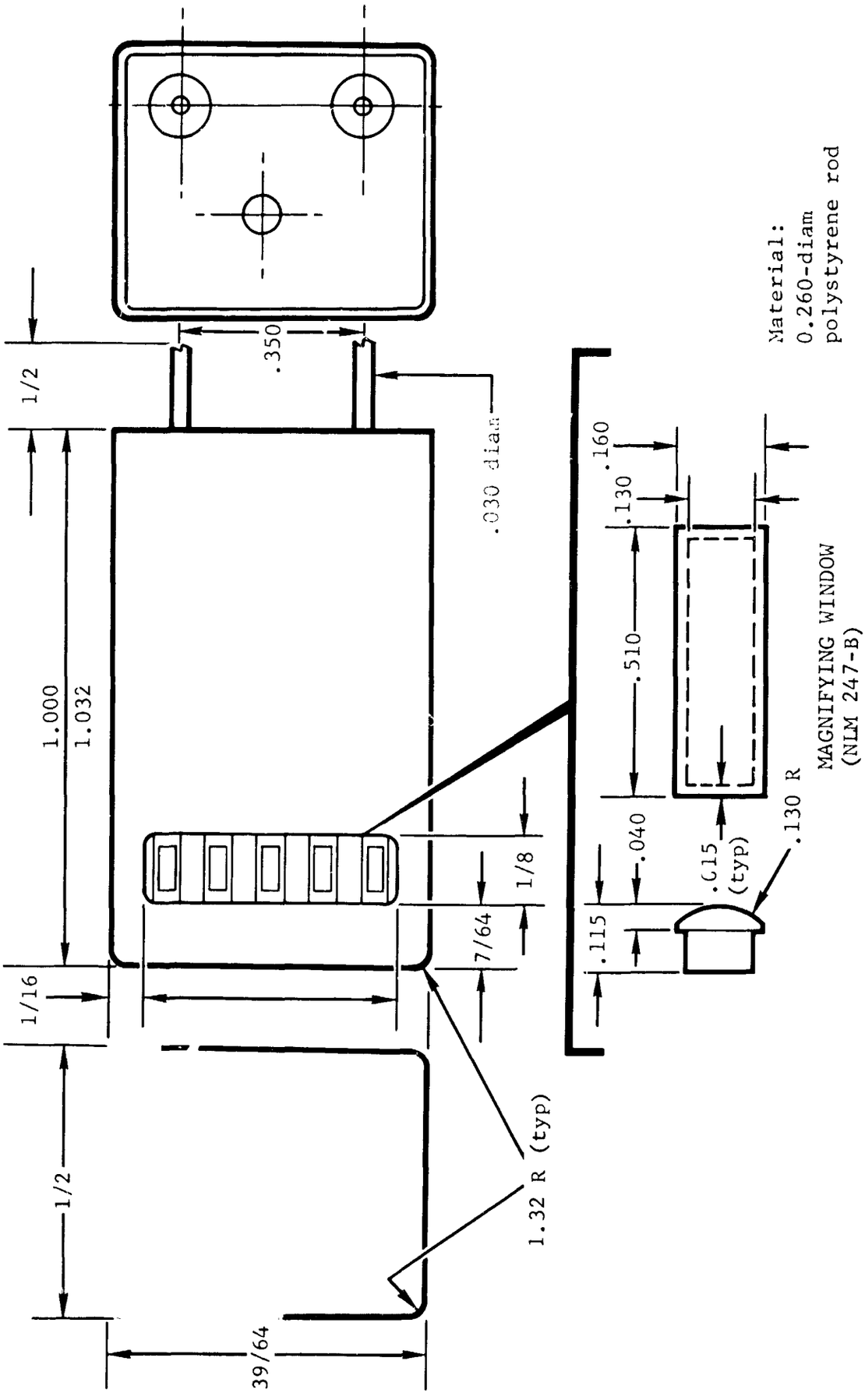

Figure 2-4 Five-Digit Readout Register for Dosimeter

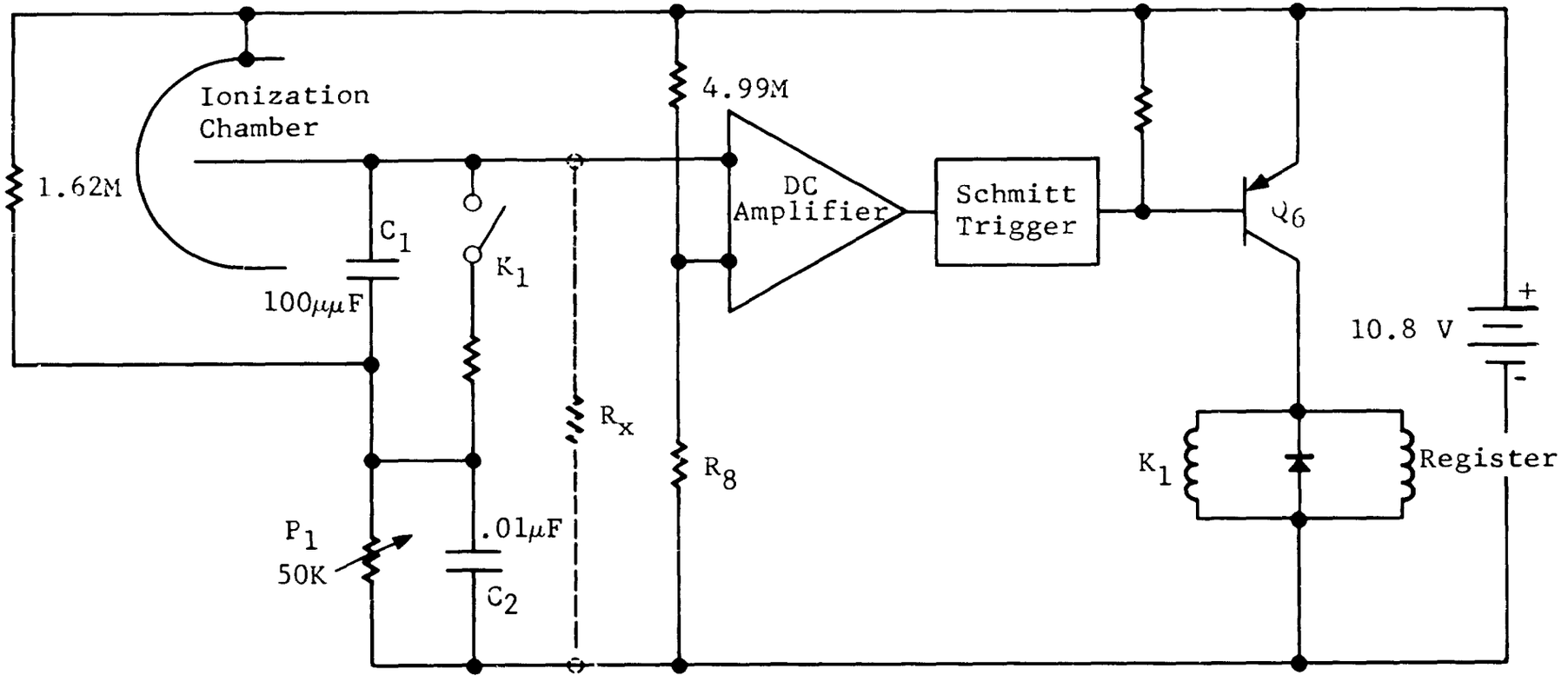

Figure 2-5 Simplified Circuit Schematic of the Personal Radiation Dosimeter

When C_1 charges to a preset voltage level V, the Schmitt trigger will trip, C_1 will be discharged by K_1, and the register will add one count to its total. Each count on the register represents 10 mrad.

2.2.1 Ionization Chamber

The PRD ionization chamber (Fig. 2-3) has an active volume of 6.5 cm^3 with a gamma sensitivity of 10^{-12} A/rad/h. The chambers are filled with ethylene gas to 1050 mm-Hg at 86°F and, at a dose rate of 90 rad/h, are 95% saturated at 6.0 V (Fig. 2-6).

2.2.2 High-Impedance Module

A schematic of the high-impedance circuit is shown in Figure 2-7. This high-impedance input circuit includes a dc differential amplifier using 2N3631 MOS Field Effect Transistors (Q_1 and Q_2). These units are matched for equal gate voltage ($\pm$ 0.010 V) at a drain current of 40 μA. The values of R_6 and R_8 set the input voltage and are selected for a minimum voltage shift over a temperature range of from 0° to 175°F. The input voltage is set at 0.5 $\pm$ 0.050 V and the maximum voltage shift over the temperature range is $\pm$ 0.015 V.

Included in the high-impedance module with the dc differential amplifier are relay K_1 and charging capacitor C_1. Made by Central Lab, C_1 is a 100-pF polystyrene capacitor, Type CPR-100J,

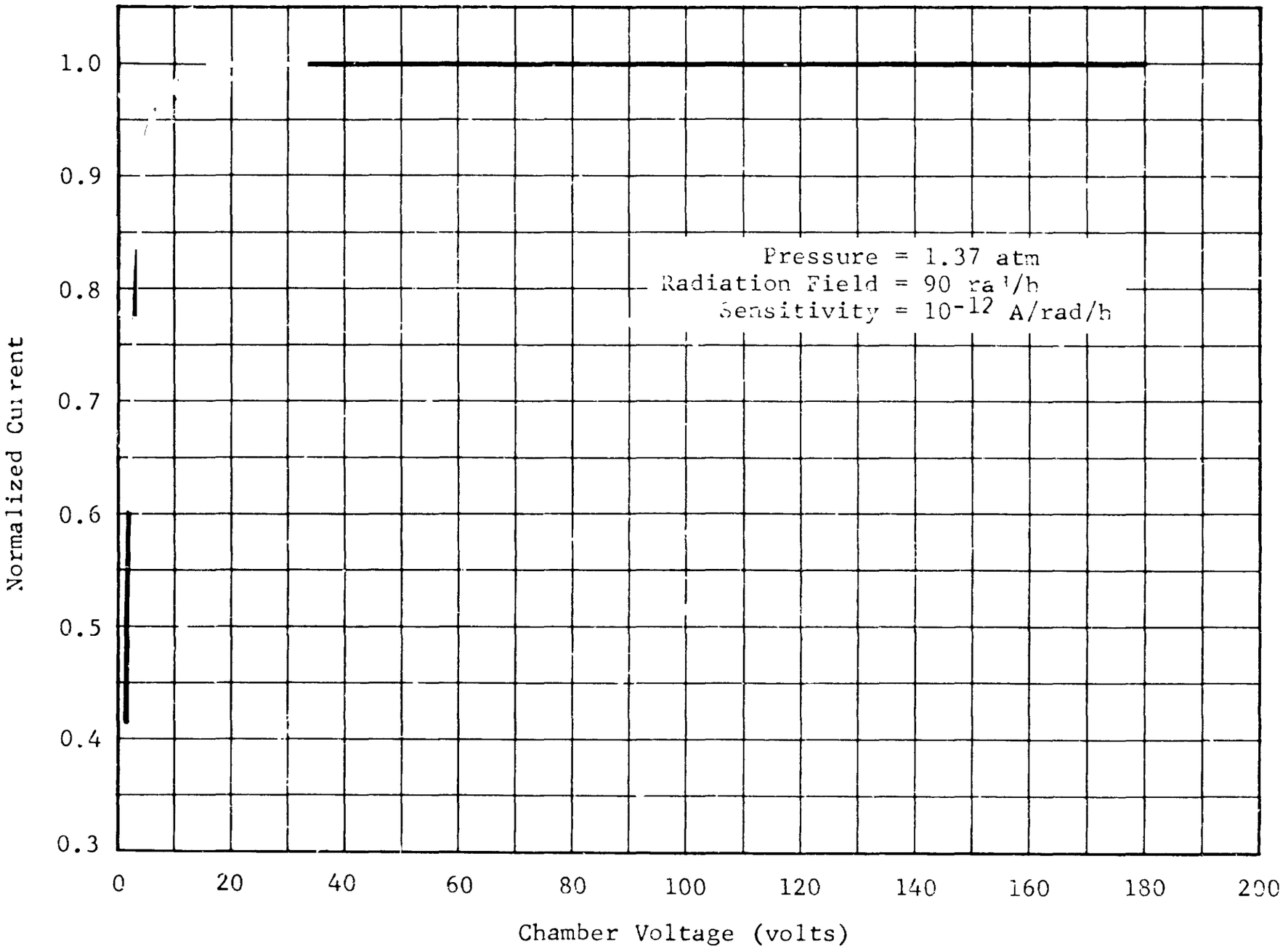

Figure 2-6 PRD Saturation Curve

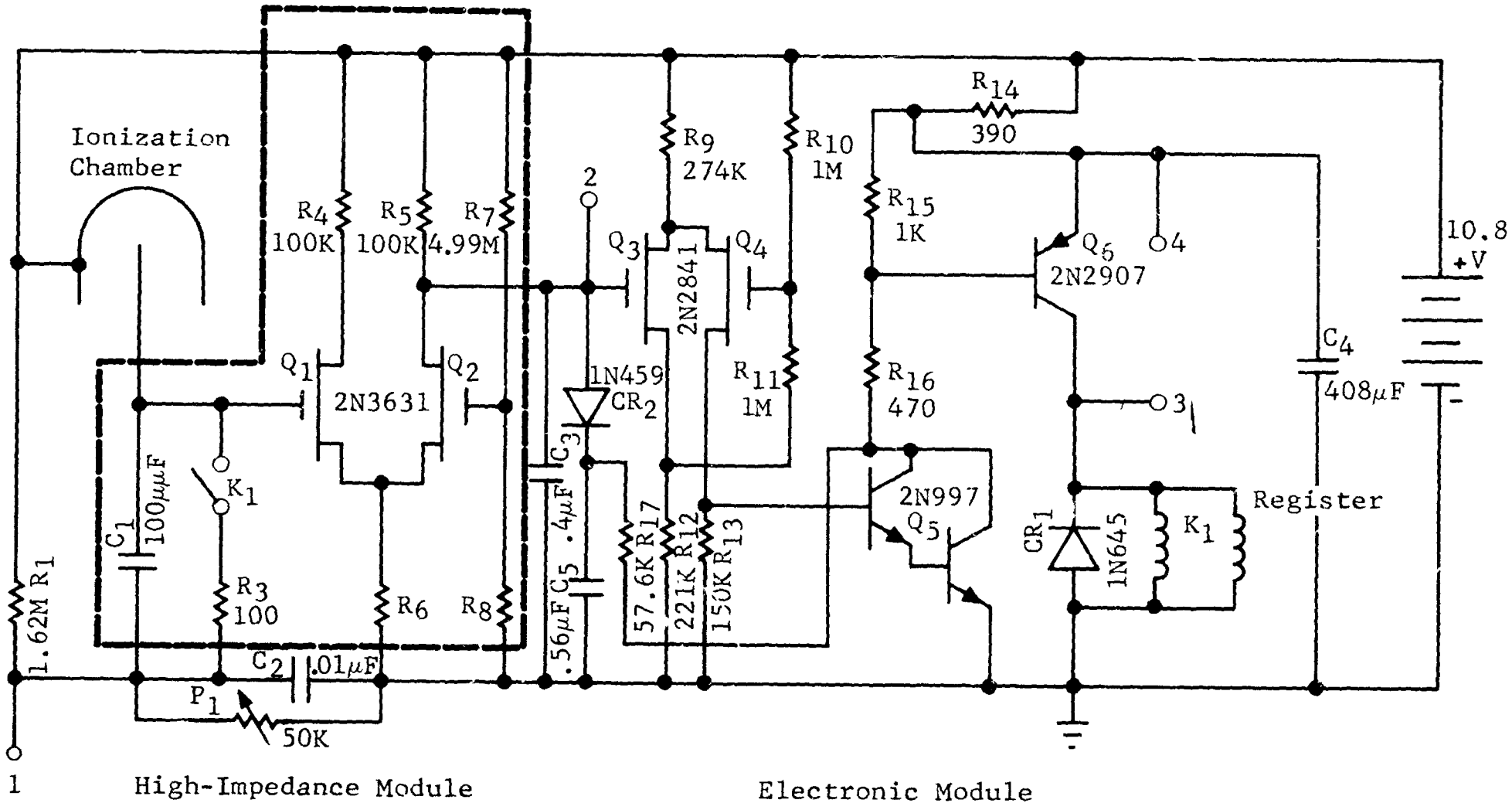

Figure 2-7 Electronic Schematic of Personal Radiation Dosimeter

with an insulation resistance of 10^{18} ohm. Relay K_1 is Type 410-9, made by Teledyne. The unit is in a TO-5 package and has a minimum insulation resistance of 10^{15} ohms.

2.2.3 Electronic Module

The schematic of the electronic module is shown in Figure 2-7. The output signal from the high-impedance module is fed to the Schmitt trigger circuit, consisting of Q_3 and Q_4. The 2N2841 Field Effect Transistors are used for low power consumption. These units are matched for equal gate voltage ($\pm$ 0.010 V) at a drain current of 20 μA. The pulse from the Schmitt trigger is amplified by Q_5 (2N997) and then fed to Q_6 (2N2907), which drives the relay K_1 and the register. The output pulse width is 25 msec; this is set by the value of C_5.

Calibration of individual units is made by adjusting potentiometer P_1. This sets the voltage at which C_1 discharges when relay K_1 is energized.

C_4 consists of six 68-μF capacitors in parallel for a total of 408 μF. This capacitance is charged to the battery voltage through R_{14} (390 ohms). When the circuit fires, the charge across C_4 causes the relay and register to energize. This capacitance will extend the battery life and ensure register operation at lower temperatures.

2.2.4 Readout Register

The readout register (C19525), built by the A. W. Haydon Company, has a five-digit counter that is actuated electromagnetically. The unit is designed to operate (1) with a coil voltage of from 7 to 11 Vdc, (2) at a maximum power input of 3.0 W at 77°F and 50% duty cycle, (3) at a maximum counting rate of 10 counts/sec, and (4) at a minimum impulse duration of 0.020 sec.

Each register was checked at General Dynamics for maximum count rate and minimum operating pulse width at 10.8 V and for the minimum operating dc voltage. The units were checked at ambient temperature using the test circuit shown in Figure 2-8. The maximum count rate at 10.8 V, using a 10-msec pulse width, was found to be 15 pulses/sec. The minimum pulse width at 10.8 V was found to be 4 msec, and the minimum dc operating voltage was found to be 4 V.

One of the registers and the test circuit of Figure 2-8 were placed in a temperature chamber and operated from -45° to +175°F. At ambient temperature all five digits stepped with a 10-msec pulse width, and the battery voltage remained at 10.8 V during the pulse. At +175°F all five digits stepped with a 5-msec pulse, and the battery voltage remained at 10.8 V during

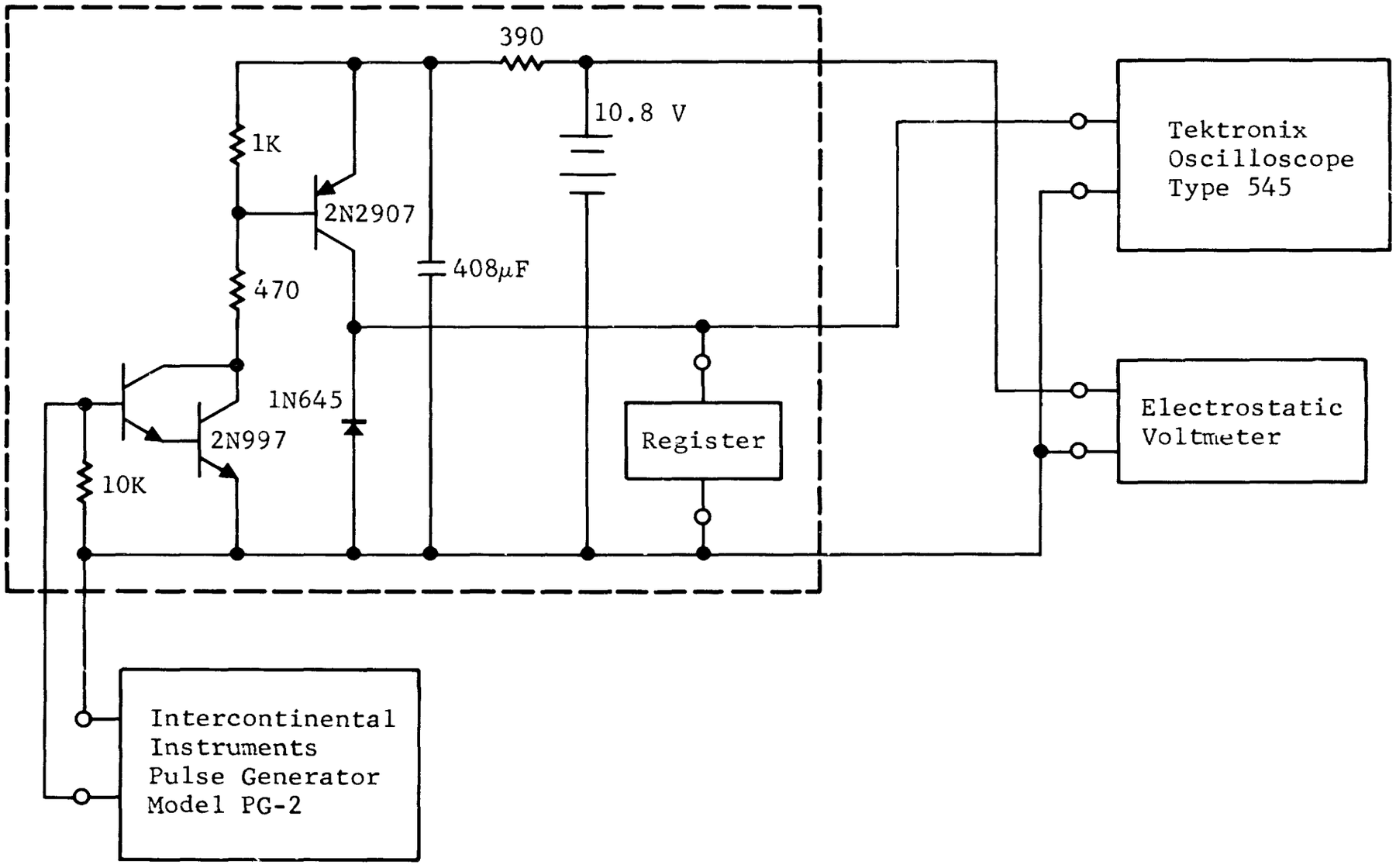

Figure 2-8 Checkout Circuit for Readout Register

the pulse. At -45°F all five digits stepped with a minimum pulse width of 10 msec. The battery voltage dropped to 8.0 V with no load and to 6.5 V during the pulse.

2.2.5 Power Supply

The dosimeter battery package is designed to contain eight mercury cells (Mallory Type RM625R), each with a capacity of 250 mA-h. These batteries are removable from the rear of the package.

The steady-state current drain of the dosimeter, excluding the register and relay, is approximately 120 μA. The register and FET gate discharge relay will operate one time for each 10 mrad of exposure. Each pulse is approximately 25 msec in width and the total register and relay resistance is approximately 45 ohms. With an operating voltage of 10.8 V, the current drain per pulse will be

$$\frac{10.8\ \text{V}}{45\ \text{ohm}} \times \frac{2.5 \times 10^{-2}\ \text{sec}}{3.6 \times 10^{3}\ \text{sec}} = 1.67 \times 10^{-3}\ \text{mA-h/pulse}$$

With a steady-state current of 120 μA, the total current drain for 10^5 pulses and a 250-h operation will be

$$(1.67 \times 10^{-3})\ (10^5) + (0.12)\ (250) = 197\ \text{mA-h}$$

2.3 Temperature and Stability Data

Leakage currents due to low insulation resistance could cause a charge to build up on C_1 (Fig. 2-7) great enough to

cause the dosimeter to count without a signal. Three dosimeters were monitored for a period of four days to check the static count rate. The results are shown below.

Table 2-1

LEAKAGE CURRENT PULSES ON DOSIMETERS OVER FOUR-DAY PERIOD
(rad)

S/N	3/22/67	3/23/67	3/24/67	3/25/67	2/26/67
003	000.00	000.01	000.02	000.02	000.04
007	000.00	000.00	000.00	000.00	000.00
008	000.00	000.00	000.00	000.00	000.00

Dosimeter 003 indicated 1 count/day; dosimeters 007 and 008 indicated zero counts. The maximum error in 003 would be 10 mrad per day, a small amount for any appreciable radiation field.

Dosimeter 003 was exposed to a low radiation field and operated over a temperature range of from -40° to $+140^{\circ}$F. The results, tabulated below, are shown graphically in Figure 2-9. The battery voltage, Schmitt trigger firing potential, and counts per minute were monitored at 18°F intervals. The data

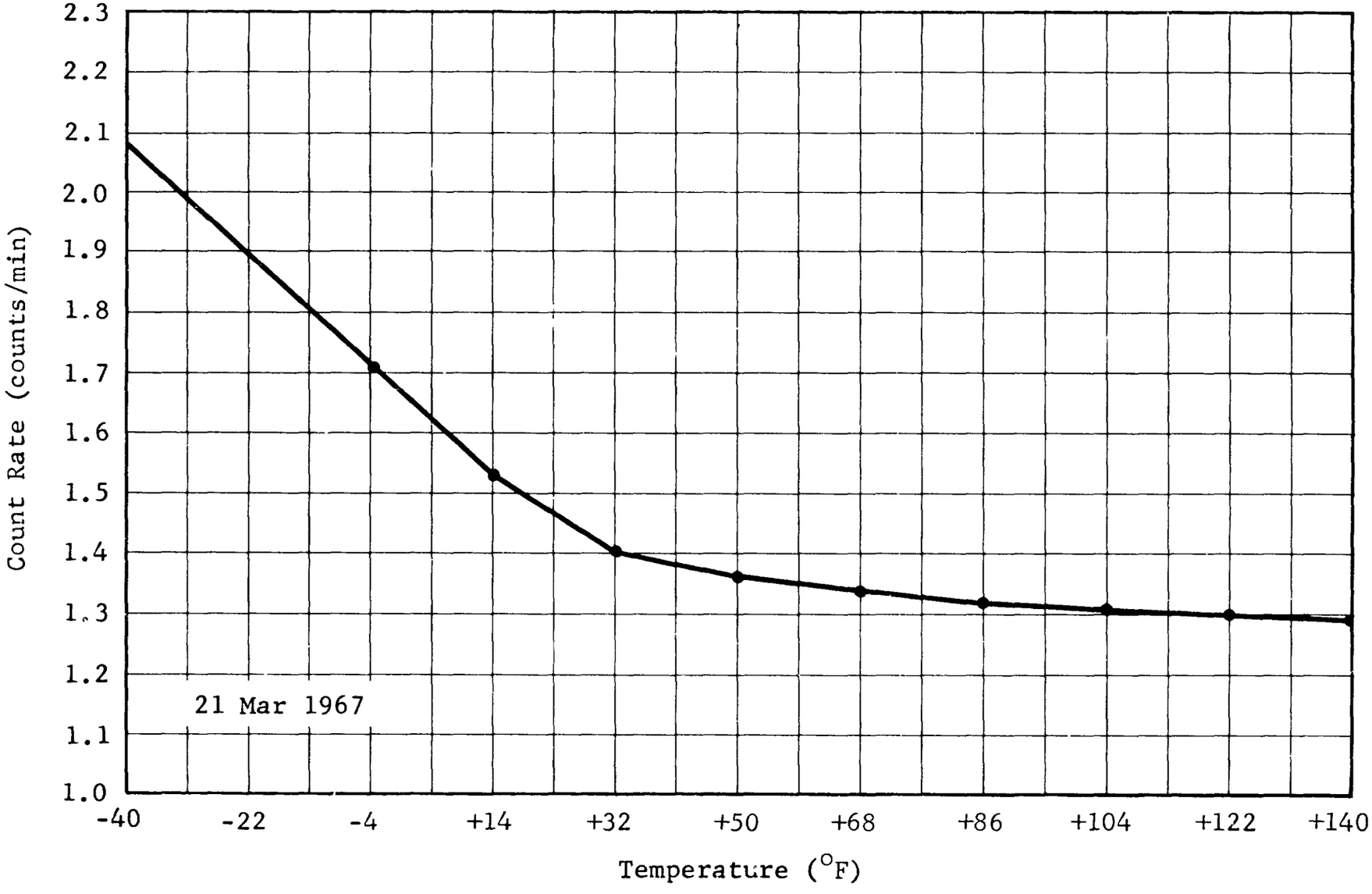

Figure 2-9 Count Rate vs Temperature for Apollo Personal Radiation Dosimeter No. 003

Count Rate vs Temperature for Apollo Personal Radiation Dosimeter No. 003

Temperature (°F)	Cts/Min	Schmitt Trigger Pt.	Battery Voltage
+140	1.29	7.07	10.7
+122	1.30	7.06	10.7
+104	1.31	7.06	10.7
+ 86	1.32	7.05	10.7
+ 68	1.34	7.05	10.7
+ 50	1.37	7.05	10.7
+ 32	1.40	7.05	10.7
+ 14	1.53	7.05	10.7
- 4	1.70	7.04	10.6
- 22	1.88	6.75	10.0
- 40	2.08	6.45	9.7

show that in a constant radiation field, the PRD temperature response is essentially flat from 32° to 140°F and below 32°F the output changes drastically because of the lower battery potential and the monotonically decreasing Schmitt trigger point.

During the environmental tests, two dosimeters were operated in a hard vacuum (10^{-6} torr) at an elevated temperature of 200°F. The units were suspended in the center of a cylindrical environmental chamber, the chamber pressure was then reduced to 10^{-6} torr, and the wall temperature was elevated to 200°F. The units were held in this environment for 6 hours. A radiation source was used to cause the units to operate at a low count rate. The

count rate and temperature over the 6-h period are shown in Figure 2-10. The data indicate two significant points: the PRDs reach equilibrium with the chamber walls in 4 hours (and at a much higher temperature than anticipated), and the count rate increases with temperature. (In the figure, the minutes/count decreases.) PRD 007 increased by 15% over the whole cycle and PRD 008 increased by 26%.

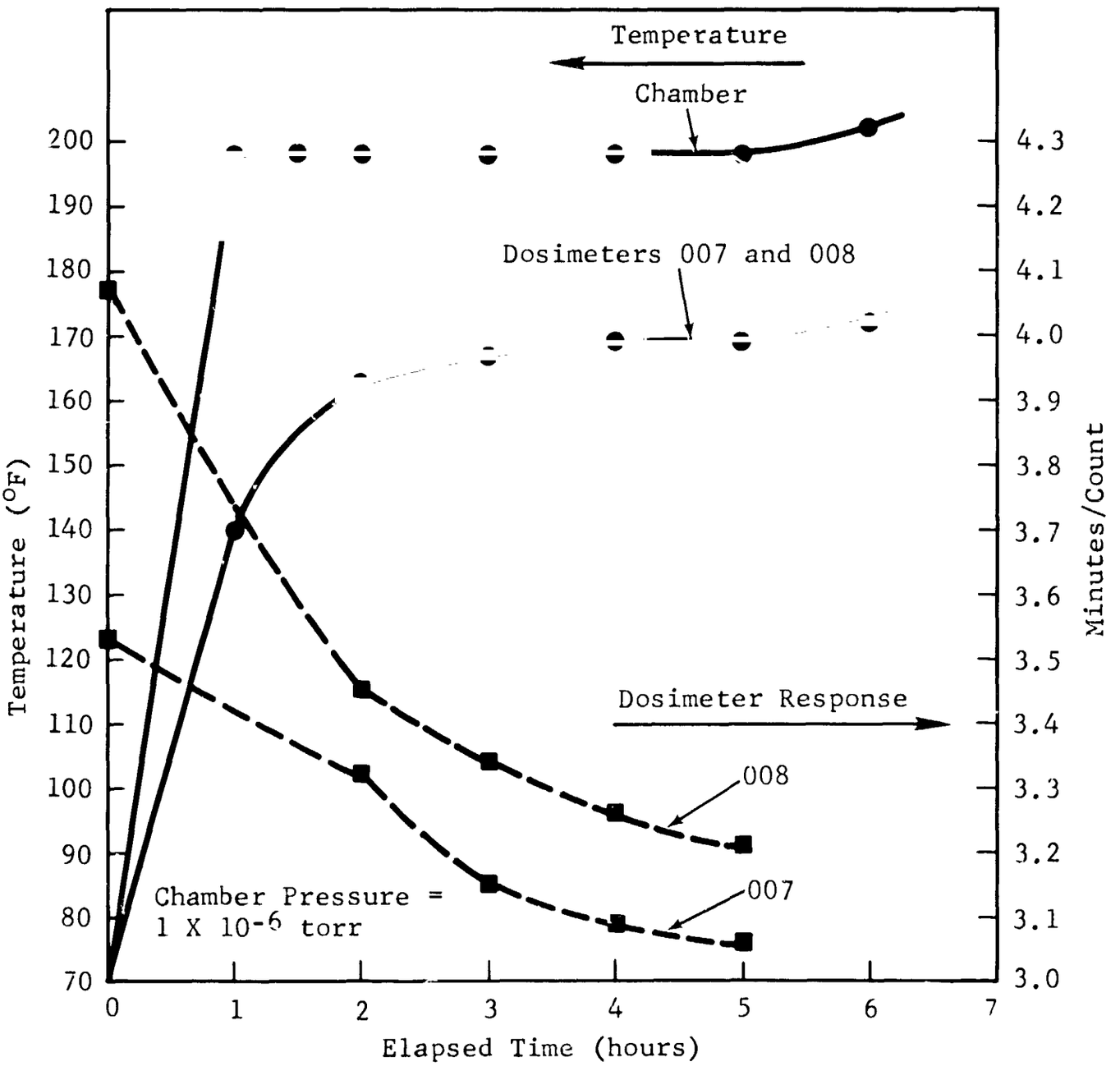

Figure 2-10 Dosimeter Response to a Hard Vacuum and Elevated Temperature

III. RADIATION SURVEY METER AND METER BRACKET

The Radiation Survey Meter (RSM) was designed to monitor the dose rates occurring as a result of exposure to solar flares and the Van Allen radiation belt. The RSM has four selectable ranges: 0-100 mrad/h, 0-1 rad/h, 0-10 rad/h, and 0-100 rad/h. The survey meter will measure cobalt-60 gamma dose rates to within ± 10% of full scale for each range with ± 3% reproducibility. The batteries have a liftime in excess of 1000 hours of continuous operation. The RSM weighs 1.58 lb and has an overall length of 9.560 in. and a maximum diameter of 2.324 in.

The RSM and the bracket designed to hold it are shown in Figures 3-1 and 3-2. The purpose of the bracket is to hold the survey meter in a firm, fixed position in the spacecraft and to protect it from shock and vibration during launch and reentry. The bracket weighs 0.625 lb and has a maximum height of 4.313 in. and a maximum diameter of 2.563 in.

3.1 Structural Design

The RSM is packaged in an anodized housing having a size and shape similar to that of a large flashlight. The various components that make up the RSM are shown in Figure 3-3. These are (1) an ionization chamber, (2) a high-impedance module,

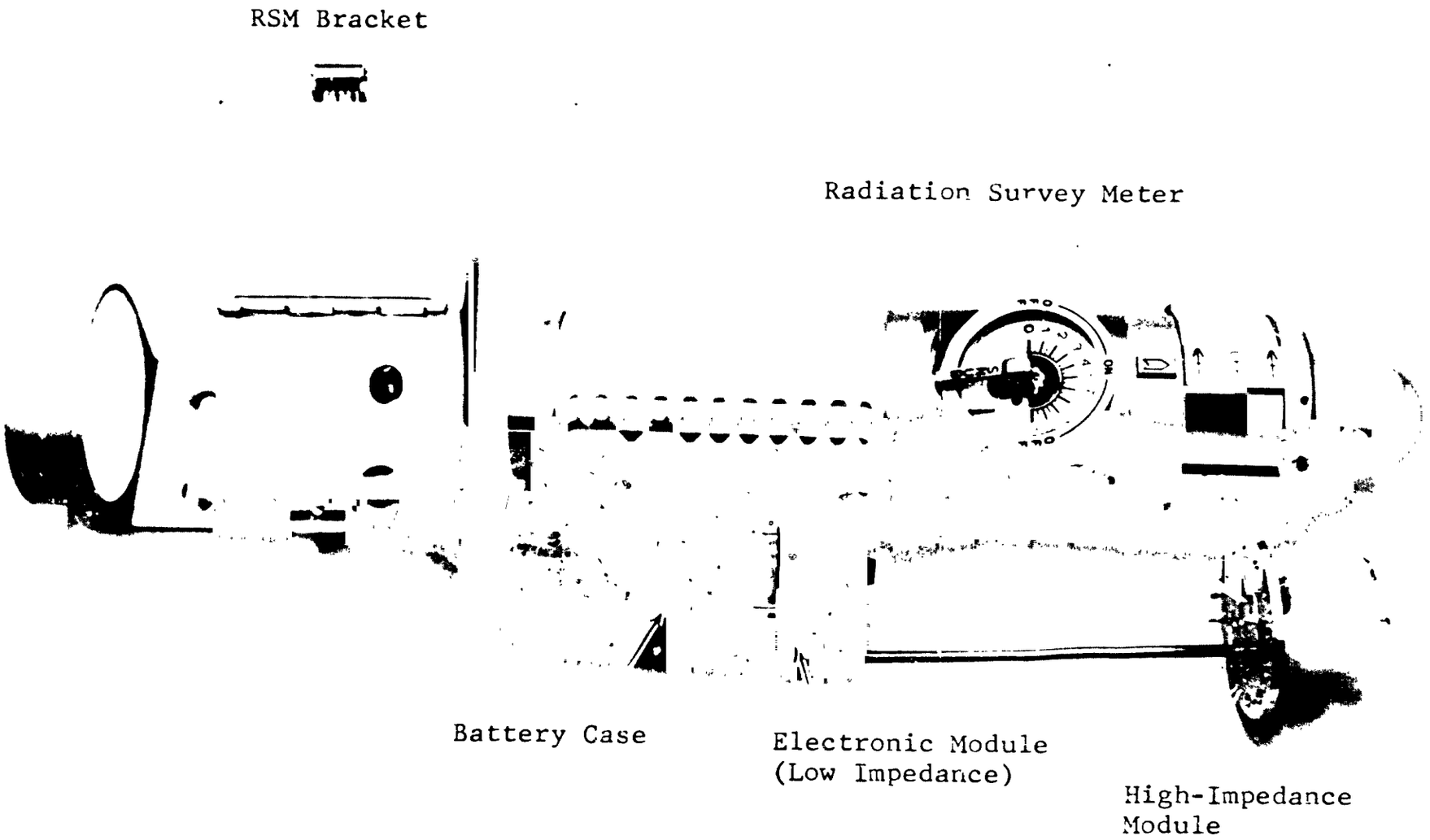

Figure 3-1 Radiation Survey Meter, Bracket, High-Impedance Module, Electronics Module, and Battery Pack

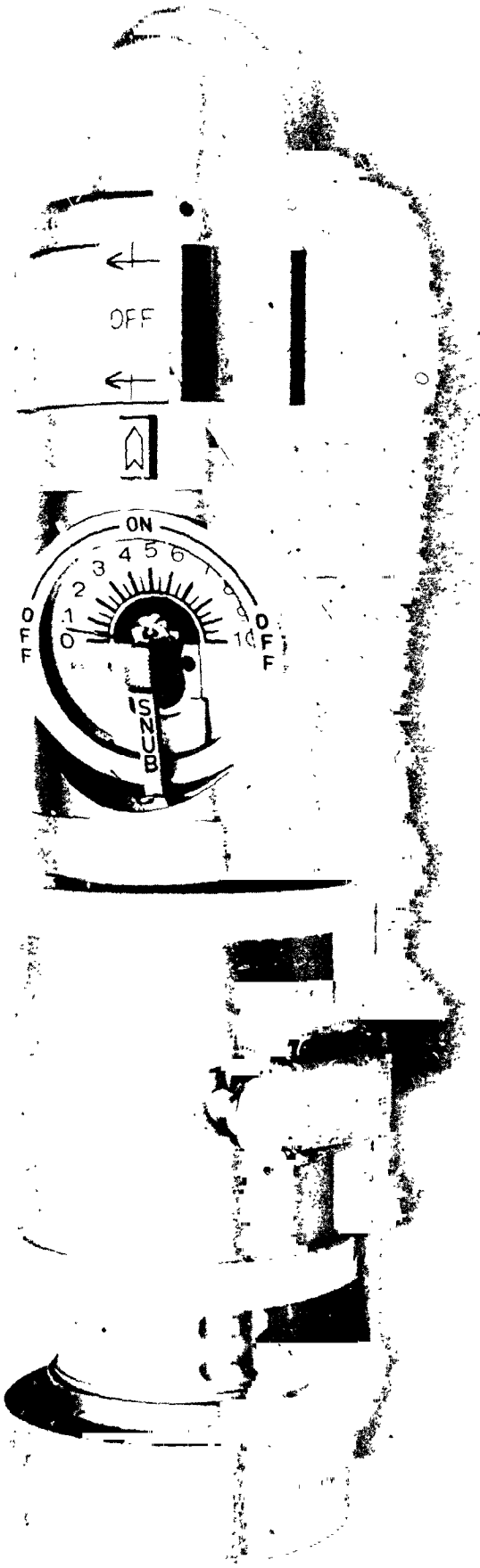

Figure 3-2 Radiation Survey Meter Secured in Bracket

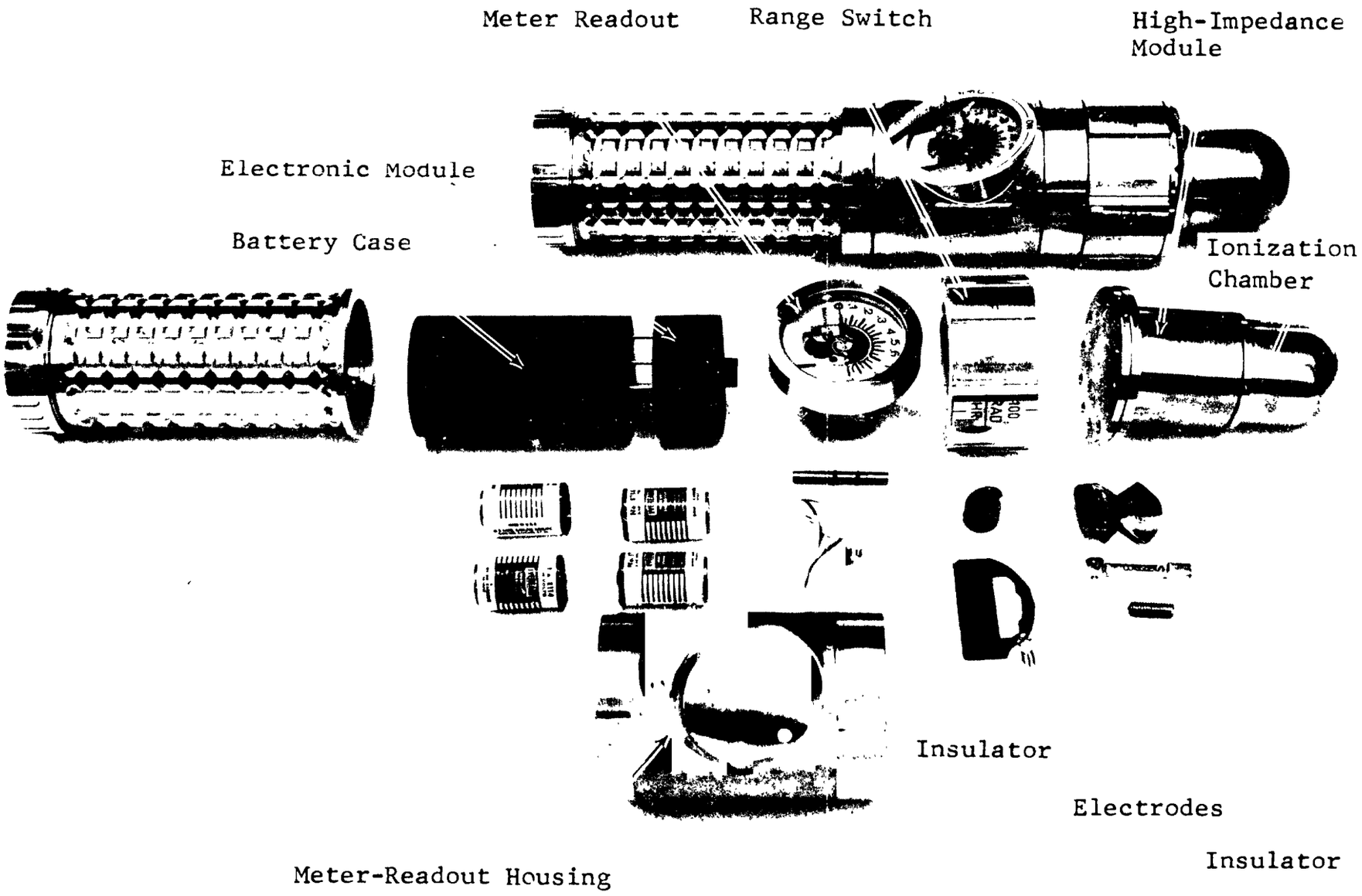

Figure 3-3 Disassembled Radiation Survey Meter and Its Major Subassemblies

(3) a range switch, (4) a meter readout and housing, (5) an electronic (low-impedance) module, and (6) a battery module. This modular design permits the replacement of any component or electronic module without adversely affecting the operation of the entire system. Also, any component from one RSM may be used to replace a like component in another RSM.

Four test points are provided for measuring the voltage across the meter readout and the battery potential without having to disassemble the unit. Access to these four test points is obtained by removing the end cap from the instrument.

3.1.1 Ionization Chamber

A cross-sectional drawing of the ionization chamber is shown in Figure 3-4. The electrodes are made of high-density polyethylene, partially aluminized for electrical conductivity. The thickness of the lower, cylindrical portion of the high-voltage electrode was reduced from 0.05 in. to 0.035 in. in order to preclude contact between the aluminum dome and the electrode. (Contact caused the meter needle to move up scale.) The flexibility of the dome made such contact possible whenever the meter was inadvertently squeezed during handling.

The mechanical drawing numbers are NLM 223-B and NLM 253-B. The assembly procedure is described in NIP-10.

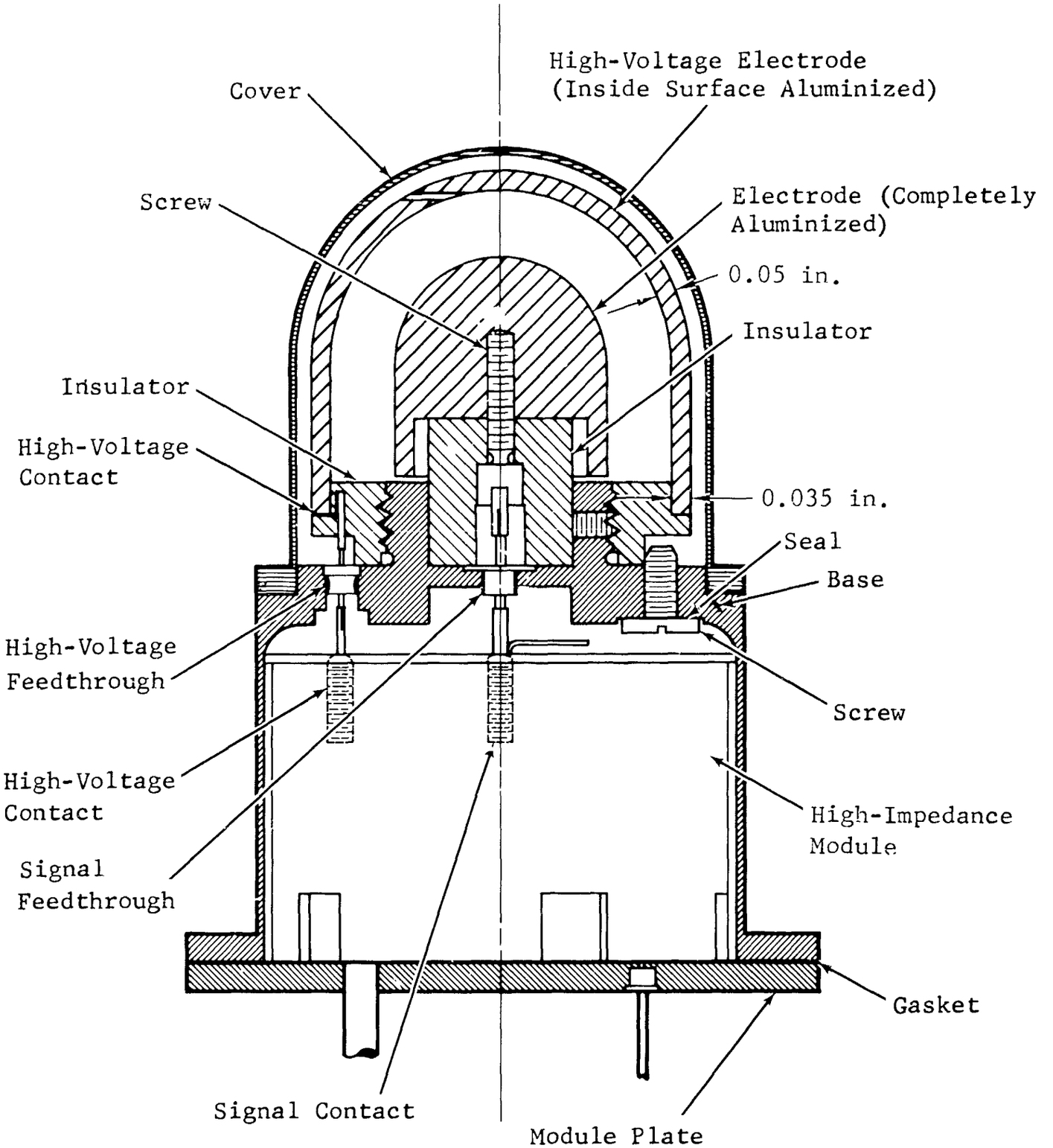

Figure 3-4 Cross-Sectional View of RSM Ionization

3.1.2 High-Impedance Module

The high-impedance module contains the range switches, power switches, and the input transistor and components for the amplifier. This module is directly connected to the output signal electrode of the ionization chamber and must be maintained at a high insulation resistance, approximately 10^{15} ohms. To achieve this high resistance the piece parts are placed in a precision machined cylinder of high-density polyethylene and the electronic connections made by resistance welding. Next, an aluminum feedthrough header plate is welded and soldered to the high-impedance module. After this completed unit is electronically checked, it is installed in the cavity behind the ionization chamber. This module is then hermetically sealed and evacuated, so that the ionization chamber and high-impedance module become one assembly.

The detailed mechanical drawing is NLM 231-B. The assembly procedure is described in NIP-12.

3.1.3 Electronics Module

The electronics module contains the low-impedance portion of the amplifier and the transistor that drives the current meter. Two externally adjustable potentiometers are located in this module and are used for meter zero and full-scale adjustment.

The parts are potted in Emerson Cuming 1090 SI epoxy. The mechanical drawing of the module mold is NLM 240-B and the electronics parts layout is NLE 301-B.

The electronic module is 1.560 in. in diameter by 0.800 in. in length and is inserted in the handle from the meter end of the handle. The module rests firmly against a silicon O-ring and is held firmly in the handle by a threaded insert. This threaded insert locking ring is called out as a -23 lock ring on NLM 234-B. The electronics module details can be readily seen in NLM 254-B.

3.1.4 Meter Assembly and Snub Mechanism

The meter assembly and snub mechanism can be seen in Figure 3-3. The basic meter movement - a Weston 100-μA, 180-deg taut-band unit - was removed from its commercial case and placed in a round, stainless-steel, hermetically sealed case. The meter face plate is calibrated in rad/h and is easily read at arm's length from the operator. The snubbing device was installed to dampen the meter pointer and movement during shock and vibration. A cutaway view of the meter and snubbing device is shown in NLM 254-B. The mechanical drawing of the meter case and face plate is given in NLM 229-B. The assembly procedure is described in NIP-15.

The snub mechanism consists of a lever-actuated piano wire that places tension on the meter needle when it is in the ON position. The snub lever has a positive detent for the ON and OFF positions. This is accomplished by means of a ball plunger with 5 lb of pressure applied to it; the plunger drops into a groove for a positive latch-up for the ON and OFF positions. Silicon O-rings are used to make a waterproof seal where the snub switch mechanism enters the housing. The snub device is shown in NLM 235-B and NLM 246-B. The procedure for assembling is given in NIP-17.

3.1.5 Range Switch

The range switch is used to externally change ranges and apply power to the unit (see Fig. 3-3). The switch turns on a smooth surface provided by two Teflon sleeves; the Teflon also serves as a dust seal. Three spring ball plungers used in the switch detent into a stainless steel lock ring at each range position. This gives a smooth positive action to the switch. The range switch can be easily operated by an astronaut wearing gloves and a pressurized suit.

The drawing and assembly procedure are given in NLM 230-B and NIP-16, respectively.

3.1 6 Battery Module

The battery module is cast from Emerson Cuming 1909 SI and is 1 560 in in diameter by 2.625 in. in length. It contains four E-114 Eveready mercury cells of 5.40 V each to provide the positive and negative 10.8 V needed for operation of the survey meter. The battery module is shown in Figure 3-3; the module mold drawing is NLM 232-B, Sheets 1, 2, and 3.

Test points are available on the rear end of the battery module for voltage and signal checks. The batteries are inserted into the module and held firmly in place by copper spring clips The handle cap can be removed and the batteries changed and/or signals tested without disturbing the hermetic seal in the other parts of the survey meter. The battery module plugs into the electronics module after the latter has been installed. Firm pressure is held on the battery module by a silicon rubber insert, or pad, between the module and the end cap of the handle The assembly procedure on this module is explained in NIP-13.

3.2 Operational Design

A simplified circuit schematic of the RSM is shown in Figure 3-5. The radiation dose rate is measured in terms of current produced by the ionization chamber. Ion pairs produced

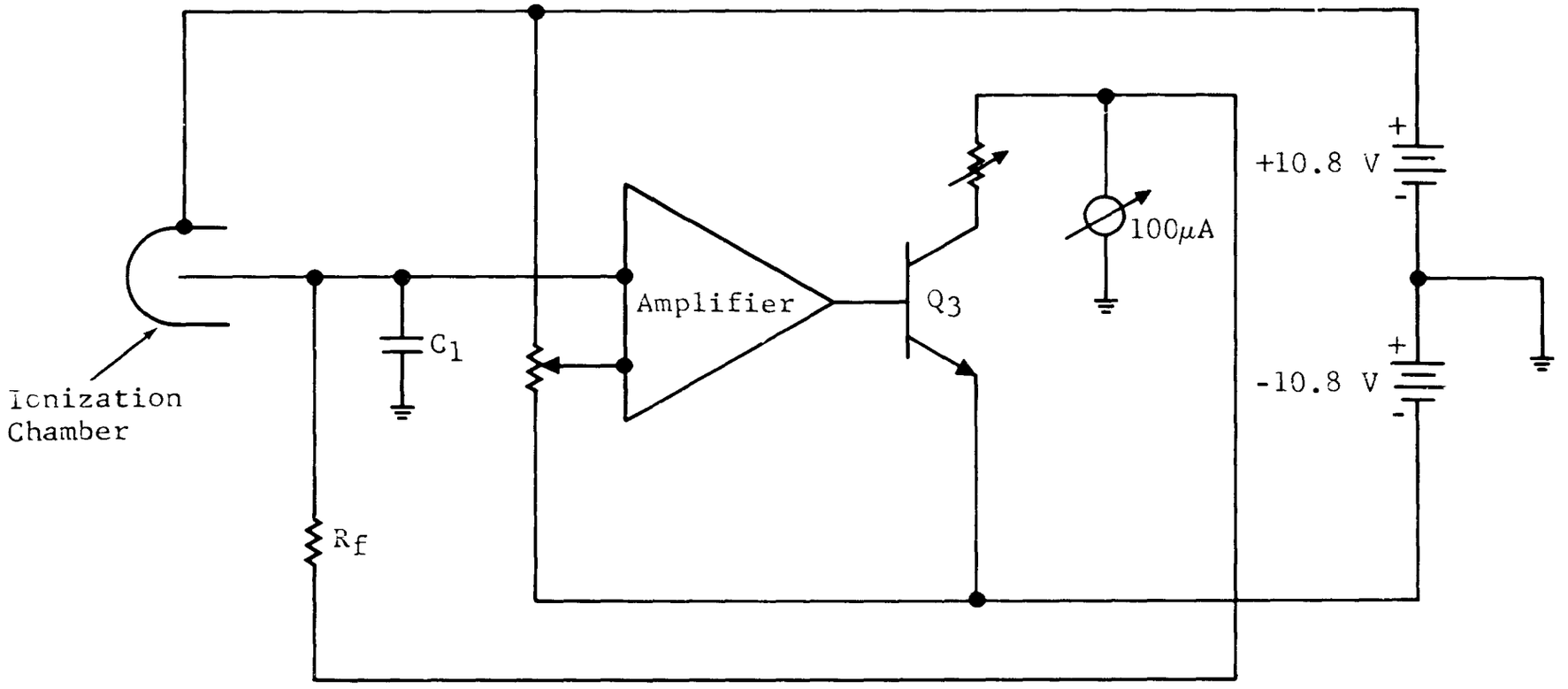

Figure 3-5 Simplified Circuit Schematic of Radiation Survey Meter

in the ion chamber are collected on the center electrode and flow as a signal current through R_f. The dc differential amplifier functions as an operational amplifier with R_f as the feedback element. The amplifier drives transistor Q_3, which has the indicating current meter in its collector circuit. The survey meter has a full-scale adjustment potentiometer and a zero adjustment potentiometer for calibration purposes.

3.2.1 Ionization Chamber

The RSM ionization chamber (Fig. 3-4) has an active volume of 12.4 cm^3 with a gamma sensitivity of 10^{-12} A/rad/h. The chambers are filled with ethylene gas to 760 mm-Hg at 86 ^oF and are 95% saturated at 6 V in a field of 90 rad/h (Fig. 3-6).

3.2.2 High-Impedance Module and Electronics Module

The basic survey meter schematic is shown in Figure 3-7 (for detailed schematic, see NLE 298-B). The high-impedance module contains transistor Q_1 and the feedback resistors and range switches. The leads on these components that connect to the signal output terminal of the ionization chamber must have approximately 10^{15} ohms insulation resistance. A resistance less than this would cause inaccuracies on the lowest range. This high insulation resistance, or input impedance, is maintained by careful selection of components and by placing these

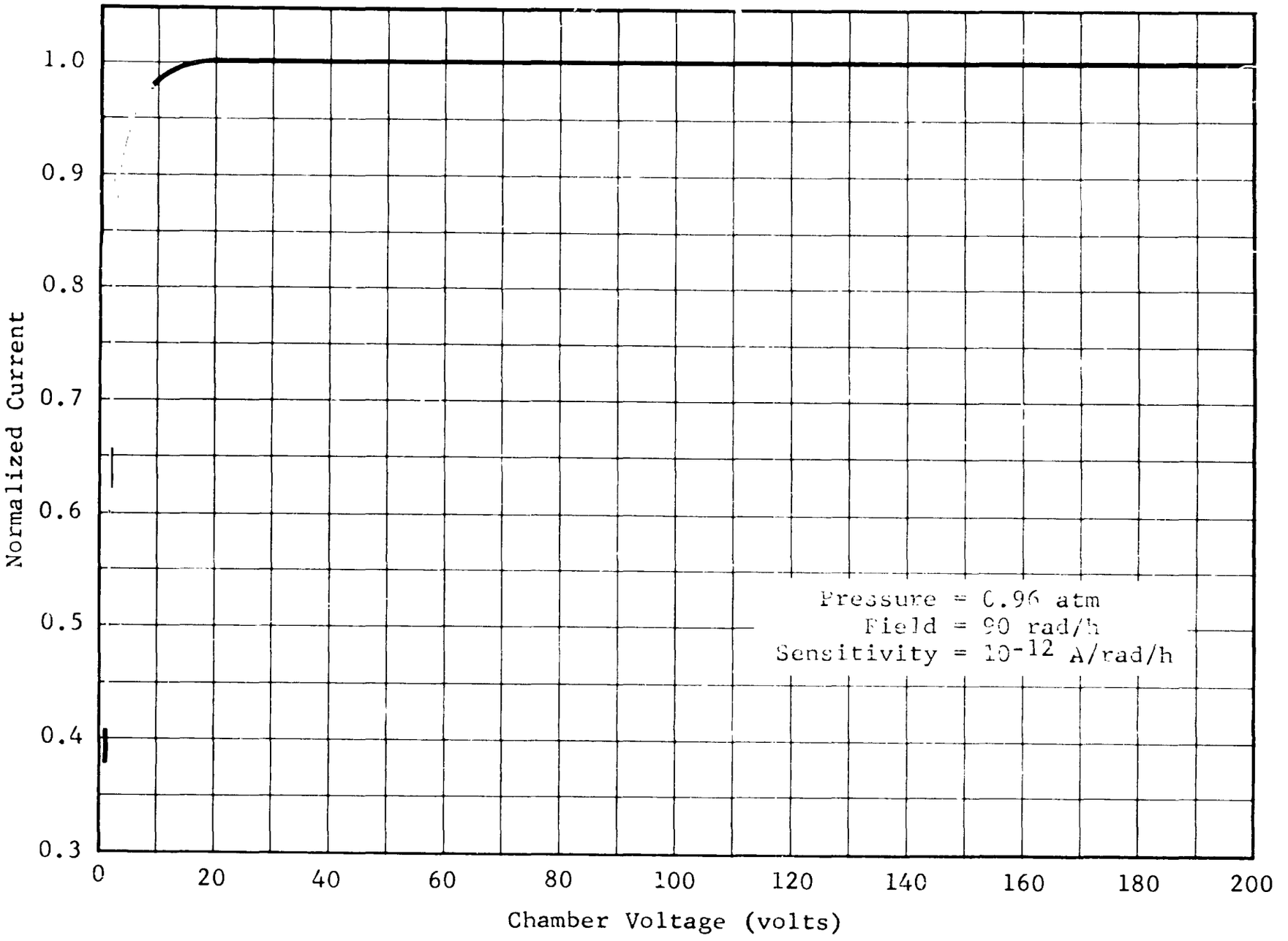

Figure 3-6 RSM Saturation Curve

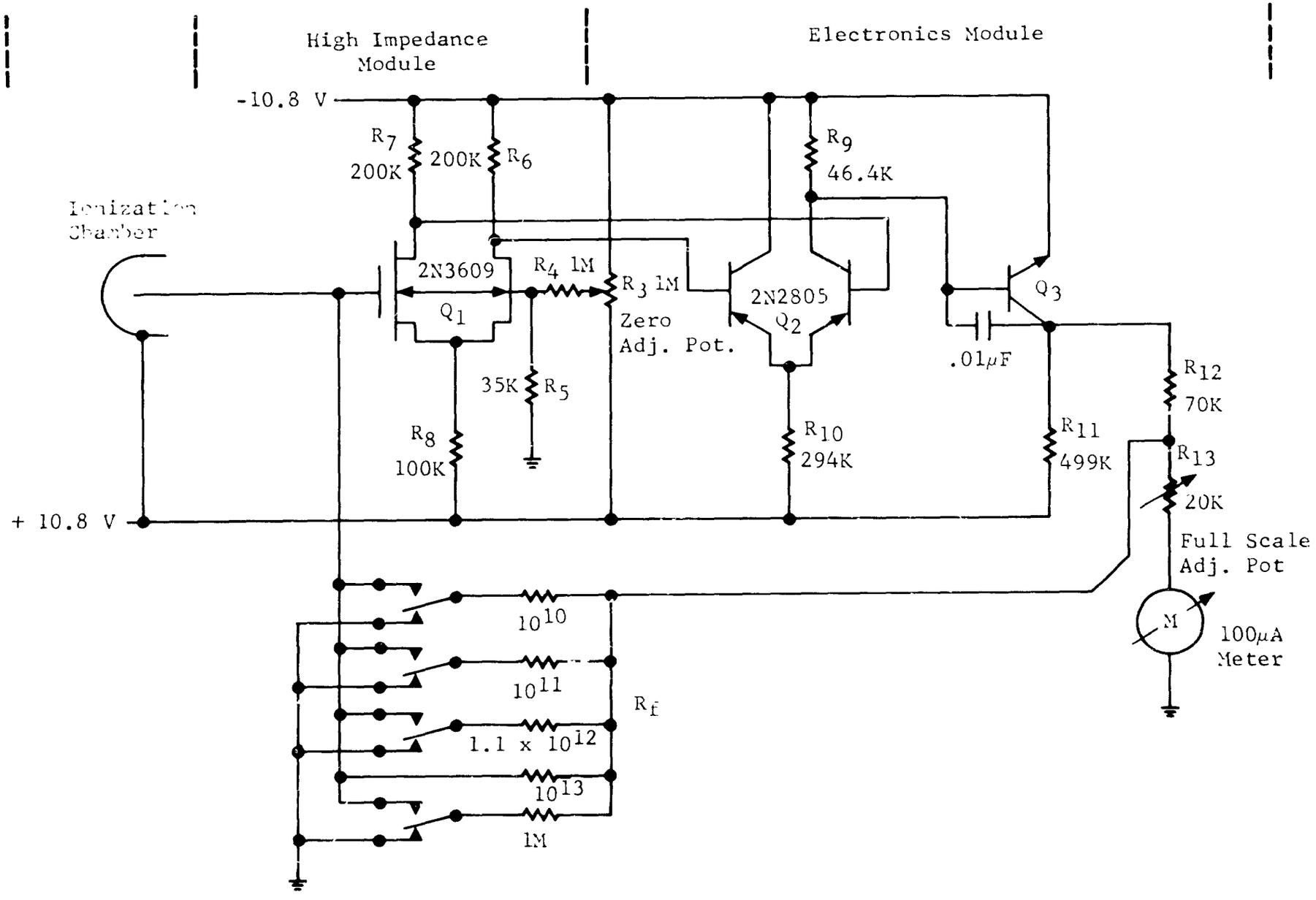

Figure 3-7 Electronic Circuit Schematic of Radiation Survey Meter

components in a polyethylene holder. The high-impedance module is evacuated and sealed after installation so that it will not act as a second ionization chamber.

The electronics module contains transistors Q_2 and Q_3 and their associated components. These parts are encapsulated in epoxy and form a plug-in unit in the handle.

The current from the ionization chamber is fed to the input of the differential amplifier (Fig. 3-7). This differential amplifier functions as an operational amplifier with R_f as the feedback element. The input time constant is approximately

$$t_c = \frac{C_1 \times R_f}{\text{Open Loop Gain}} + C_s \times R_f$$

where C_1 = input capacitance

R_f = range resistor (10^{10} to 10^{13} ohms)

C_s = shunt capacitance of R_f

The time constant that integrates the current from the detector is less than 10 sec on the most sensitive range and is faster on the higher ranges. Because of the high open-loop gain (on the order of 1×10^6) the effective input resistance is relatively low and the leakage problems are reduced.

For the 2N3609 input transistor, with V_{GS} matched to approximately 50 mV, the differential drift with temperature in

the first stage is not greater than 60 $\mu V/^{o}F$ (Changes in Q_3 with temperature, referred to the input, will produce a similar drift in the worst case.) These changes, referred to the 1-V effective full-scale signal at the input, give a zero shift of $\pm$ 2% for the unit over the temperature range. The effects of temperature on the survey meter are discussed in Subsection 3.3. The data indicate that the survey meter is stable within $\pm$ 2% over the required temperature range of -58^{o} to $+167^{o}F$.

The survey meter may be zeroed with no signal input by adjusting potentiometer R_3 until the zero offsets of the two input transistors are equal. The full-scale meter output is adjusted by the use of potentiometer R_{13}.

3.2.3 Readout Meter

The readout on the survey meter is a 100-μA current meter with an accuracy of $\pm$ 2%. The meter face plate is a linear scale from 0 to 1.0 rad/h and is 1.5 in. in diameter. The time constant of the meter movement, as used in the electronic circuit, is less than 10 sec on the most sensitive range. A meter zero potentiometer and a full-scale meter potentiometer are located in the electronics module. The meter movement, when in the snub position, has been environmentally qualified to the desired NASA specifications.

3.2.4 Range Switch

The range switch contains a permanent magnet that is physically moved around the outer perimeter of the high-impedance module to energize internally located reed switches. These reed switches, when energized, place feedback resistors in the amplifier circuit and change the gain, thus changing ranges. The range switch may be operated in one direction only. From the OFF position, the switch can only be turned to the 100-rad/h range, the highest and most stable range. This design concept of going from the highest range to the lowest (100 mrad/h) gives the unit more stability.

3.2.5 Battery Module

Each of the four Eveready E-114 batteries has a rating of 250 mA-h. Since the current required by the survey meter is less than 200 μA at a full-scale reading, the operating life of the meter is greater than 1000 hours.

The mercury cell has excellent high-temperature characteristics and will operate at 130°F for extended periods of time and at 200°F for a few hours. The only disadvantage to mercury batteries is a severe loss of capacity at about -40°F; however, the battery is usable at this temperature under the light load required in this application. Figure 3-8 gives the battery voltage versus temperature for a 100-μA current drain.

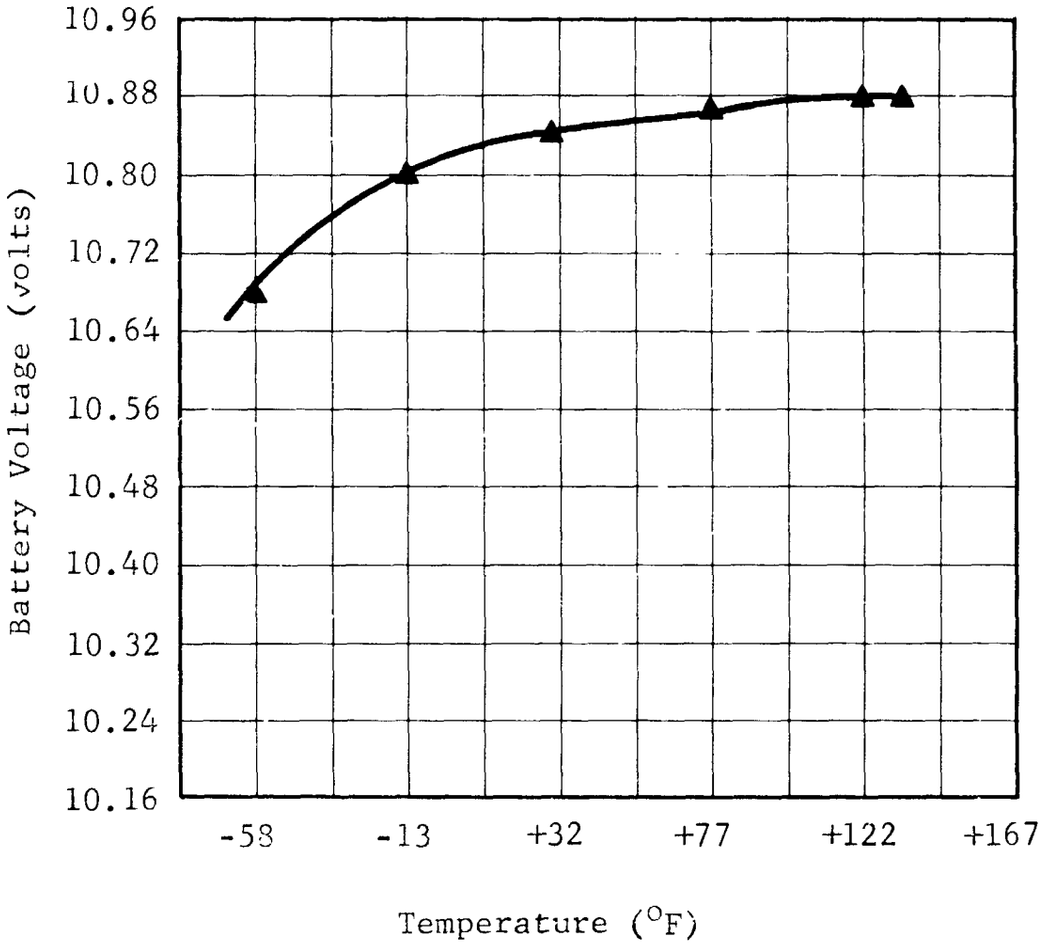

Figure 3-8 Mercury Cell Terminal Voltage vs Temperature at 100-μA Drain

Mercury cells were chosen for the RSM for the following reasons:

- High capacity current-to-volume ratio
- Flat discharge characteristics
- Excellent high-temperature characteristics
- High resistance to shock and vibration

3.3 Temperature Stability Data

A survey meter ionization chamber was temperature-cycled from -40° to $+180^{\circ}$F and the output current recorded. A source was placed near the ionization chamber for a signal and a picoammeter was used to monitor the current. The pressure inside the temperature chamber was reduced to 600 microns. The temperature of the ionization chamber was monitored by a thermocouple attached to its outer surface. The ionization chamber was allowed to stabilize at each temperature level by conducting the test over a two-day period. The data from this test are shown in Figure 3-9. As expected there was no significant change in the output current of the ionization chamber. The chamber output should be constant if the materials from which the chamber is assembled can withstand the change in temperature.

Two production RSMs with an anodized aluminum finish were temperature-cycled from -50°F to $+150^{\circ}$F at a pressure of 600

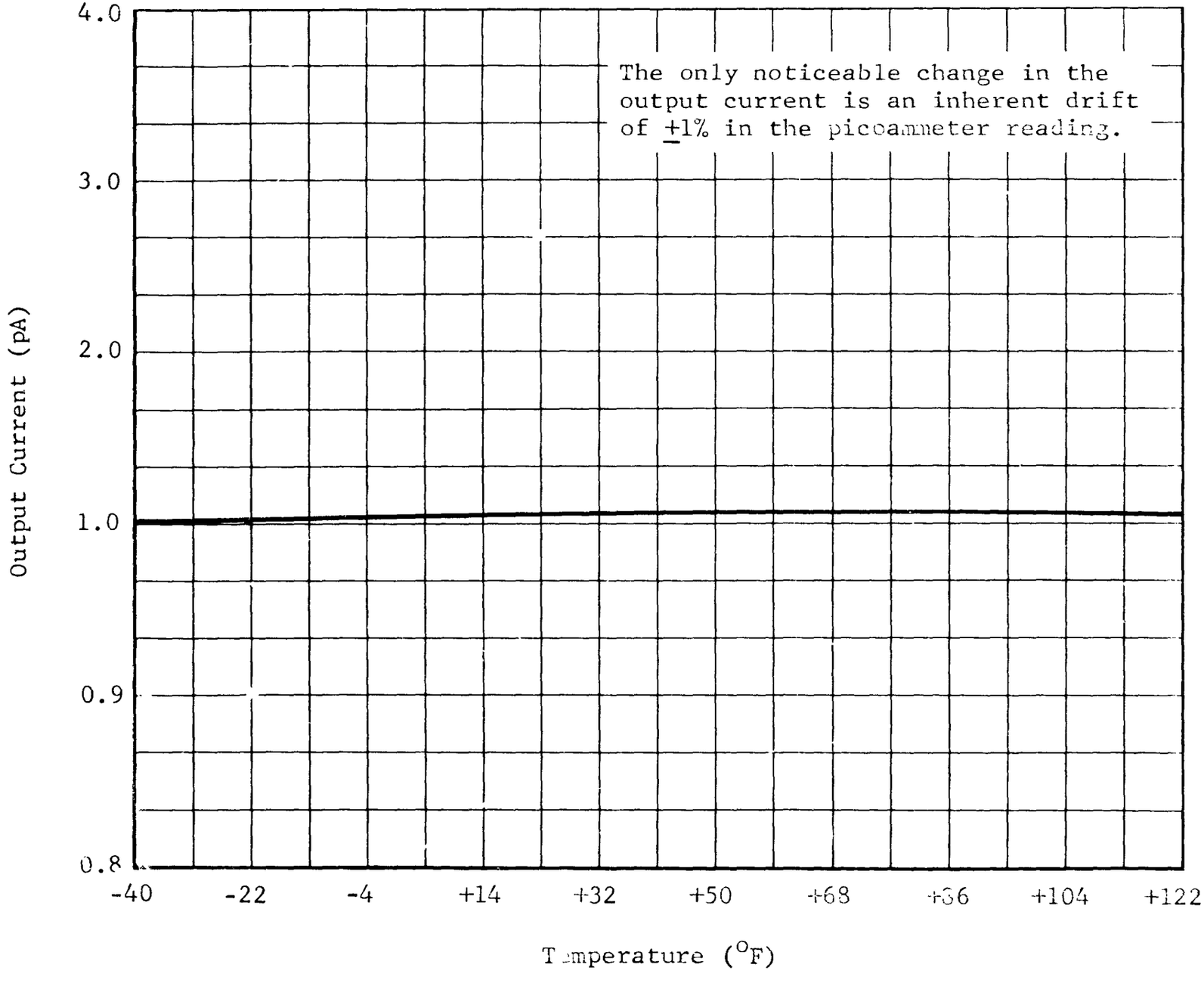

Figure 3-9 Ionization Chamber Current vs Temperature for Apollo Radiation Survey Meter

microns. A source was placed near these units to give a meter reading of midscale at 75°F; the reading was monitored over the complete temperature range. Figures 3-10 and 3-11 give the meter outputs on the 100-mrad/h and the 1-rad/h range, respectively. Both survey meters were checked on both ranges. Each test took approximately two days to allow the units to stabilize at the oven temperature. The output drift with temperature is a direct function of the value and temperature coefficient of the feedback resistor.

Two production survey meters and a polished aluminum dummy survey meter were operated in a hard vacuum at an elevated temperature of 200°F. The survey meters and the dummy were suspended in the center of a cylindrical temperature chamber. The chamber pressure was reduced to 10^{-6} torr and the wall temperature of the chamber was elevated to 200°F for 6 hours. A source was placed near the survey meters so they would read upscale. The meter output for the 6-h temperature and vacuum test is recorded in Figure 3-12. The temperatures of the chamber and the three survey meters are also shown in this figure. The survey meter outputs did not change and the maximum temperature reached by these units was 194°F.

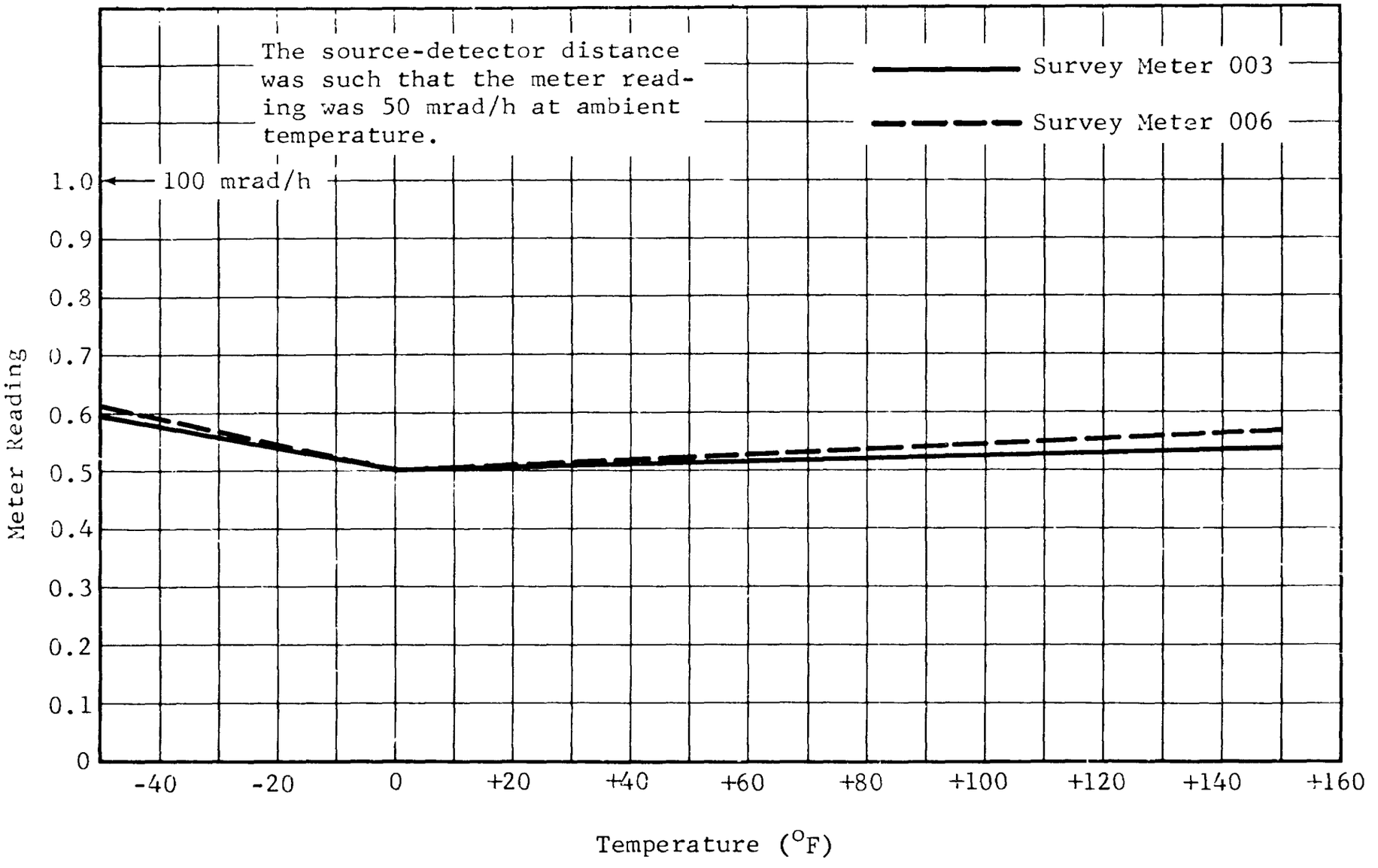

Figure 3-10 Meter Reading vs Temperature on the 0-100 mrad/h Range

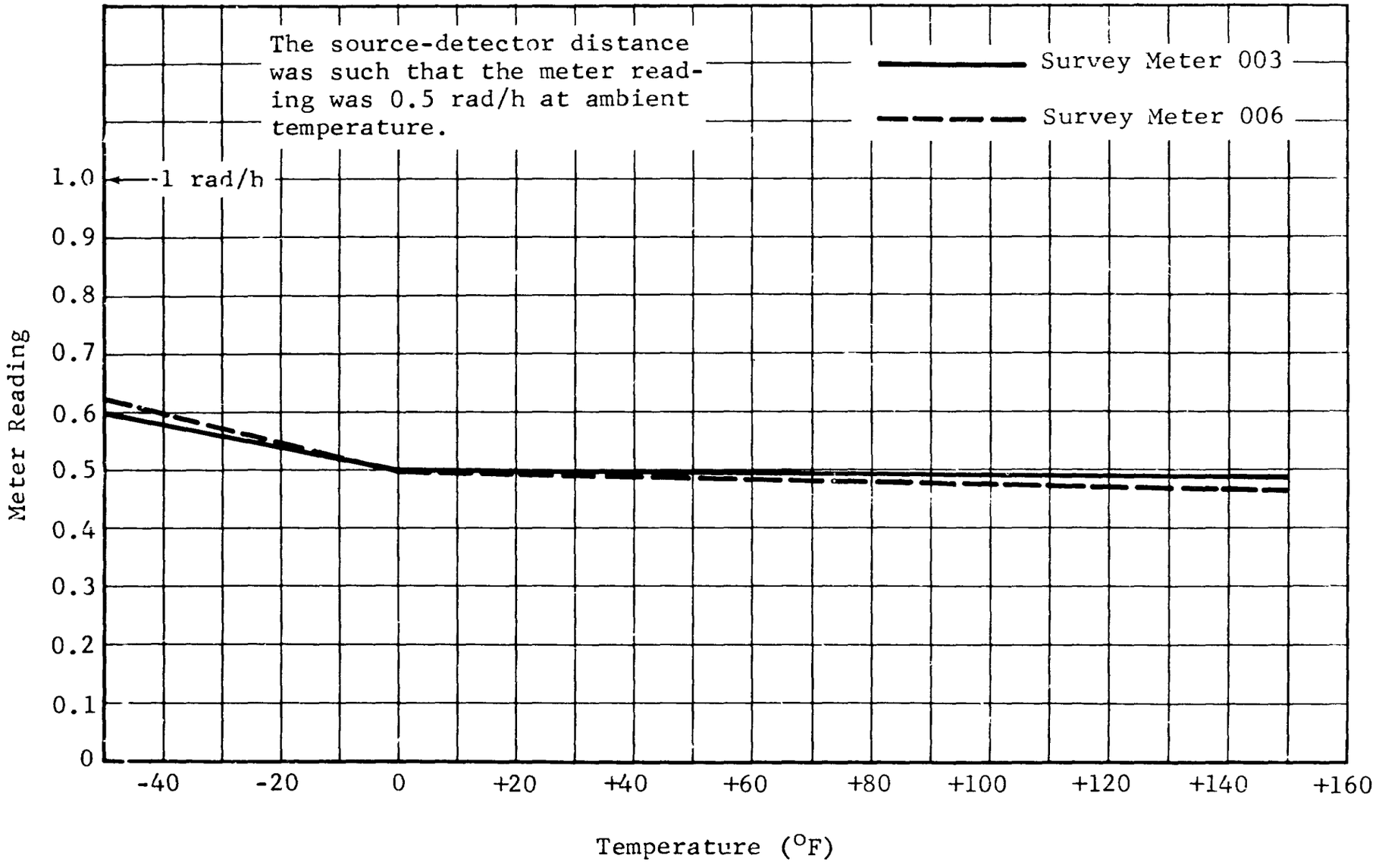

Figure 3-11 Meter Reading vs Temperature on the 0-1 rad/h Range

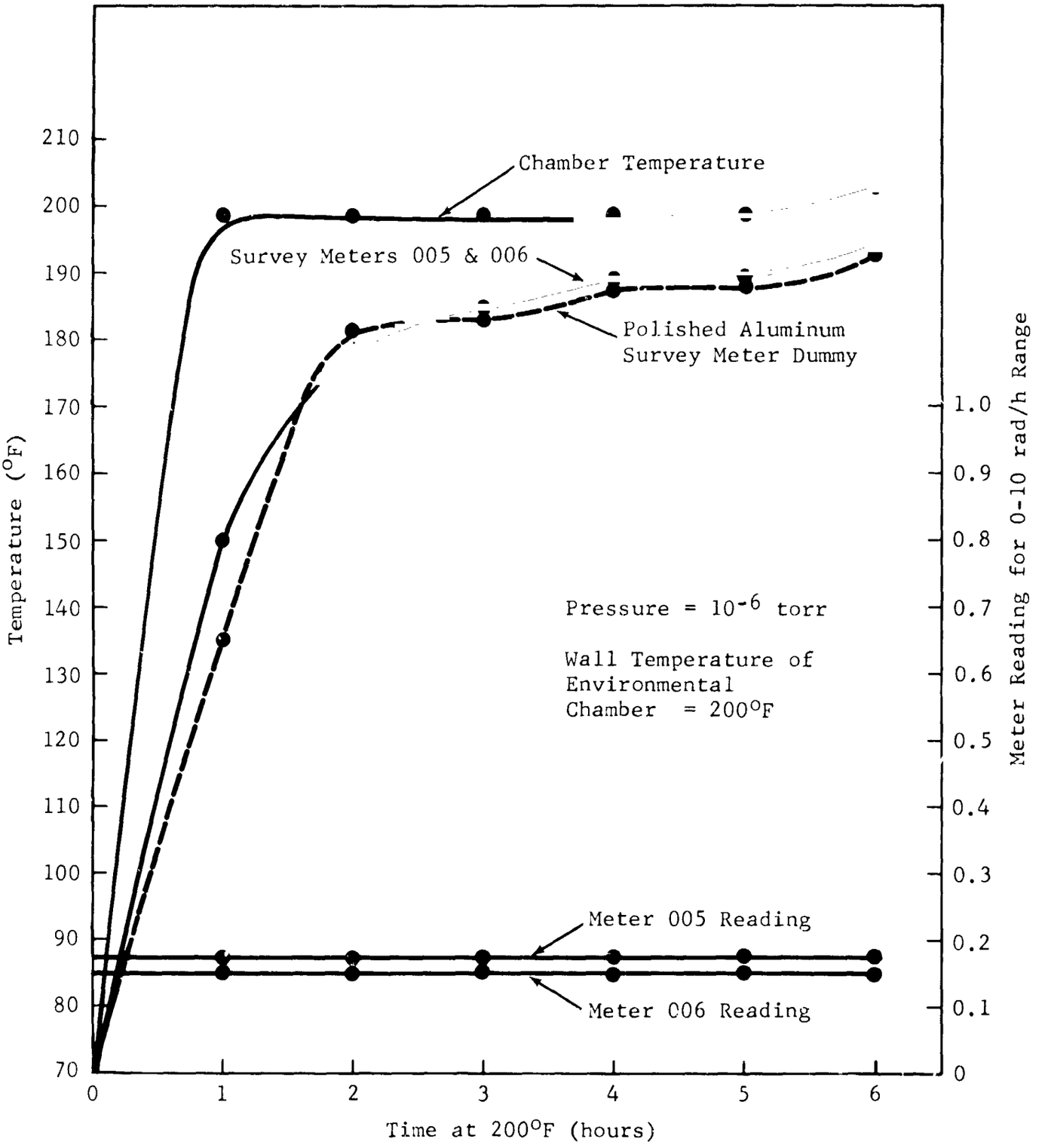

Figure 3-12 Effect of Hard Vacuum and High Temperature on Radiation Survey Meter

3.4 Radiation Survey Meter Bracket

The bracket designed to hold the RSM is shown in Figures 3-1 and 3-2. The vibration- and shock-absorbing cup and sleeve visible in these photographs were molded from silicon rubber (Dow Corning 93-055) and cemented to the bracket. The survey meter, when installed in the bracket, is firmly clamped by these silicon rubber molds so that it does not come into contact with the hard metal. The efficacy of the design and fabrication was verified in the vibration tests, during which it was used to hold the survey meter.

The survey meter is readily removed from the bracket by grasping the meter in the left hand and releasing the clasp assembly with the right hand.

The complete bracket, with the exception of the silicon rubber molds, is machined from 5052 aluminum and has a clear anodize finish. The nameplate and identification are engraved on the base of the bracket in accordance with NLM 227-B. The assembly of the bracket is discussed in detail in NIP-21.

IV TESTS AND CALIBRATION

All the delivered RSMs and PRDs were calibrated using Co-60 as a calibration source Several of these units underwent charged-particle calibration A description of these tests and the results are given in the following paragraphs.

4.1 Cobalt-60

The PRDs and RSMs were calibrated according to the procedures given in NIP-7 and NIP-20, respectively. The gamma field strength of the Co-60 sources was established with a Victoreen R meter.

4.1.1 RSM Linearity

The linearity of the RSM over the intended gamma dose-rate range is excellent The curve, shown in Figure 4-1a, is typical for the RSMs and shows the response to be within a few percent of the true dose rate over the entire dose-rate range. The contract specifications call for the response to be within 10% of full scale on each of the four ranges, which means the RSM Co-60 response is much better than contractually required

4 1.2 PRD Linearity

The linearity of the PRD is not as good as that of the RSM (Fig 4-1b) because of the high register pulse rate The high pulse rate loads the batteries down to a value that causes the potential throughout the circuitry to drop, which in turn does

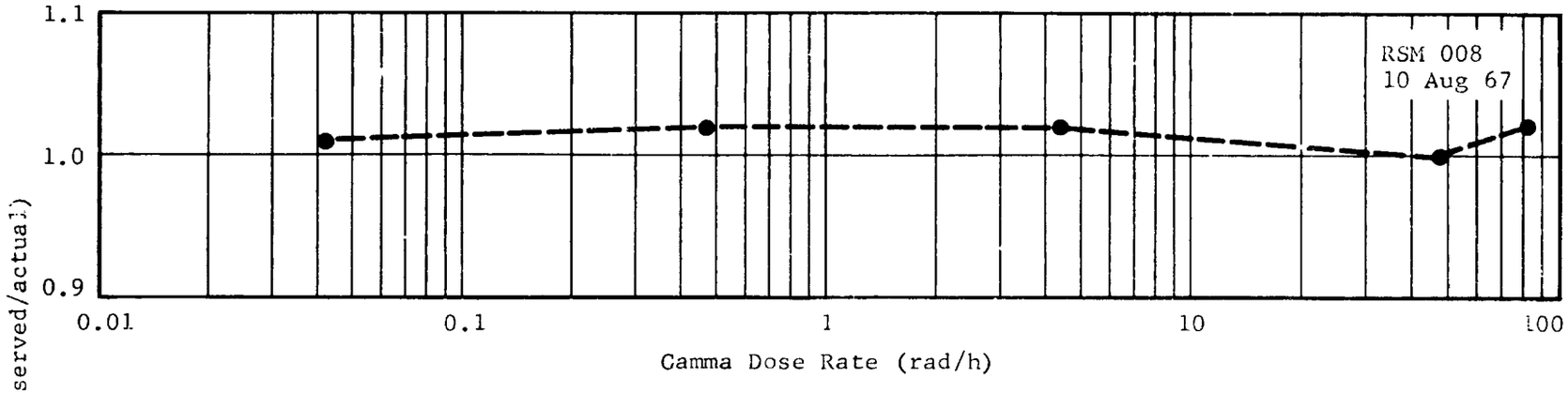

a. Radiation Survey Meter

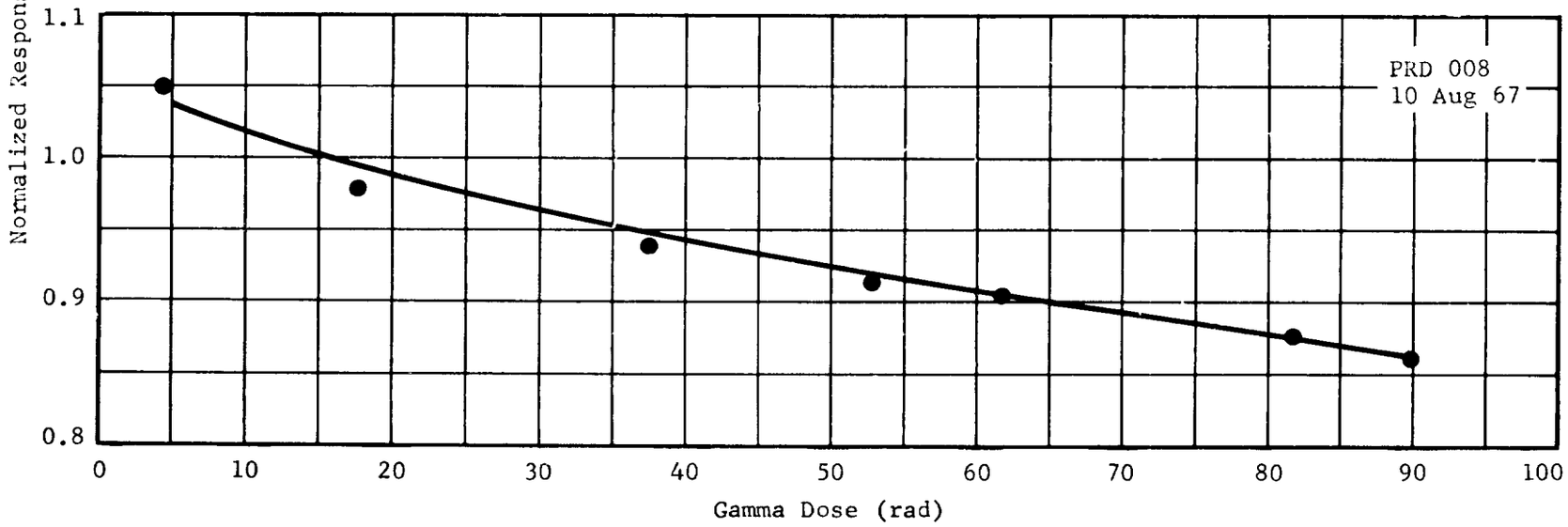

b. Personal Radiation Dosimeter

Figure 4-1 Typical Calibration Curves Showing Linearity of RMS and PRD Response to Cobalt-60 Source

not allow the PRD to count properly. The linearity of the PRD ionization chamber was checked in order to show that its response was not causing the PRD to roll off. The ionization chamber checked to within a few percent for rates up to 100 rad/h. The contractual specification for the PRD was ± 10% for rates less than 60 rad/h and ± 20% for rates greater than 60 rad/h up to 100 rad/h.

4.2 Proton Response

The responses of three RSMs and three PRDs to high-energy protons were measured at the Harvard 95-in. Cyclotron Facility on 15-16 February 1967. Both angular response and linearity of response with dose rate were measured at proton energies of 137, 100, and 50 MeV.

4.2.1 Experiment Description

The Harvard 95-in. Cyclotron is a frequency-modulated, pulsed accelerator with a primary proton energy of 160 MeV. The pulse width for this experiment was approximately 200 μsec at a repetition rate of 200 pulses/sec. The instantaneous dose rates are therefore approximately seventeen times higher than the average dose rates reported in this document.

Since a large area of uniform flux was necessary for this experiment, a 0.25-in.-thick lead scatterer was placed near the

medical quadrupole magnets in the beam tube. The primary proton beam was focused on the scatterer by means of the quadrupole magnets. The beam was diverged by the scatterer, and its energy was degraded to 137 MeV. The scattered beam then exited from the beam tube and passed through a thin-window ionization chamber which was used as a beam monitor.

The beam profile was measured with a diode in a test plane perpendicular to the primary beam at a distance of approximately 11 ft from the beam-tube exit. The beam intensity was found to vary less than 2% over a circular area 15 cm in diameter centered about the centerline of the beam.

The absolute beam calibration was accomplished by placing a Faraday cup in the test plane at the beam center. The flux measured by the Faraday cup was then related to the charge collected in the ionization chamber. This relative calibration of the ionization chamber permitted irradiations to be performed without locating a Faraday cup at the test plane.

The energy calibration of the scattered proton beam was performed by placing a series of polystyrene absorbers of known thicknesses in front of the Faraday cup aperture. With the resulting range curve, shown in Figure 4-2, and the data of Janni (Ref. 1) the energy of the beam was found to be 137 MeV with a standard deviation of 2.3 MeV.

Figure 4-2 Range Curve for Protons from Harvard 95-Inch Cyclotron

Attenuation of the beam energy to 100 and 50 MeV was accomplished by placing a series of polyethylene absorbers of known thicknesses in the beam near the ionization chamber. Total thicknesses of 5.338 and 10.436 g/cm^2 were used to attenuate the energy to 100 and 50 MeV, respectively. An absolute beam calibration was performed at each energy utilizing the Faraday cup and ionization chamber as described previously.

The range curve at 137 MeV and the straggling standard deviations of Janni were used to estimate the energy spread of the beam at 50 and 100 MeV. Standard deviations of 5.4 and 3.0 MeV, respectively, were obtained. Standard deviations of 4.3 MeV at 50 MeV and 2.1 MeV at 100 MeV were obtained by means of crystal spectroscopy in an identical experimental setup in April 1967 (Ref. 2).

The instruments were mounted on a remotely controlled turntable with the centers of detection lying directly above the center of rotation of the turntable. A selsyn provided remote readout of the angular position of the turntable with an accuracy of approximately one degree. The 0°-180° line lay along the centerline of the beam with 0° lying nearest the beam exit and the angles increasing in a clockwise fashion when viewed from above the turntable.

The detectors were exposed in pairs, one PRD and one RSM. The RSM was mounted directly above the PRD with 9.5 cm between the

centers of detection and with the centerline of the beam falling midway between the two detectors.

The average dose rate, as measured by the PRD during a data run, was obtained by counting with a scaler the number of pulses put out by the PRD during a measured time interval and equating each pulse to 10 mrad.

The average dose rate, as measured by the RSM, was obtained by measuring the output voltage across the test points and calculating the instantaneous dose rate from a knowledge of the full-scale voltage. Since the instantaneous beam intensity varied during each data run, it was necessary to take from 10 to 20 voltage readings and average them in order to obtain the average dose rate.

These average dose rates were then compared to the average dose rate measured by the Harvard ionization chamber. This dose rate was obtained by integrating the current from the ionization chamber over a measured time interval and applying the appropriate factor, as previously described.

The responses of RSM 003 and PRD 005 to 137-, 100-, and 50-MeV protons were measured in 15° increments from 0° to 90° and in 30° increments from 180° to $\pm 90^{\circ}$ in two planes: one plane was that in which the readout faces of the instruments were horizontal; the other plane was that in which the readout faces were vertical and facing toward the right as viewed from behind the instruments.

These complete data sets were not performed on the remaining instruments because of time limitations. The responses of RSM 001 and 002 and PRD 003 and 004 were measured in 30^{o} increments from 0^{o} to 90^{o} in the horizontal plane, only, at each of the three energies.

All of these measurements were performed at a dose rate of approximately 5 rad/h.

The linearity of response with dose rate of the RSMs was investigated at each energy by performing data runs at approximately 50, 5, 0.5 and 0.05 rad/h. The two lower dose rates were not investigated with the PRDs because of the excessive time required to accumulate a statistically significant number of pulses. The detectors were at 0^{o} for all of these measurements.

4.2.2 Results and Conclusions

The angular responses of the instruments to 137-, 100-, and 50-MeV protons are presented in Figures 4-3 through 4-10. The data are presented as the ratio of the PRD or RSM dose rate to the Harvard Cyclotron dose rate as a function of angular position of the detectors.

Analysis of the data shows that the PRDs for head-on (0^{o}) incidence agreed with the Harvard dose rate within $\pm$ 2% at both 137- and 100 MeV proton energies. At 50 MeV the measured dose rate was 6% higher than the Harvard dose rate. Agreement between the

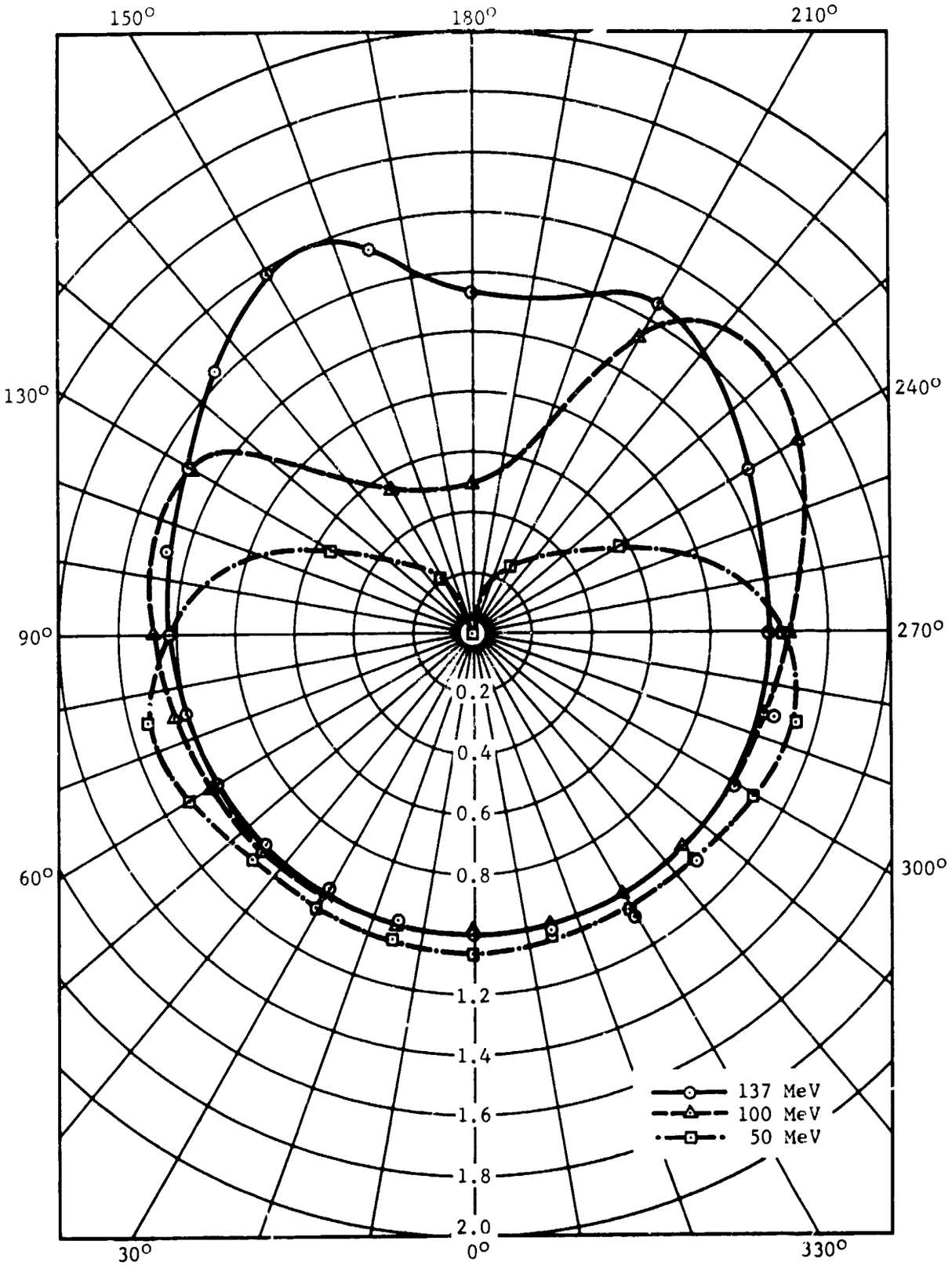

Figure 4-3 Proton Response of PRD 005 in the Horizontal-Dial Configuration

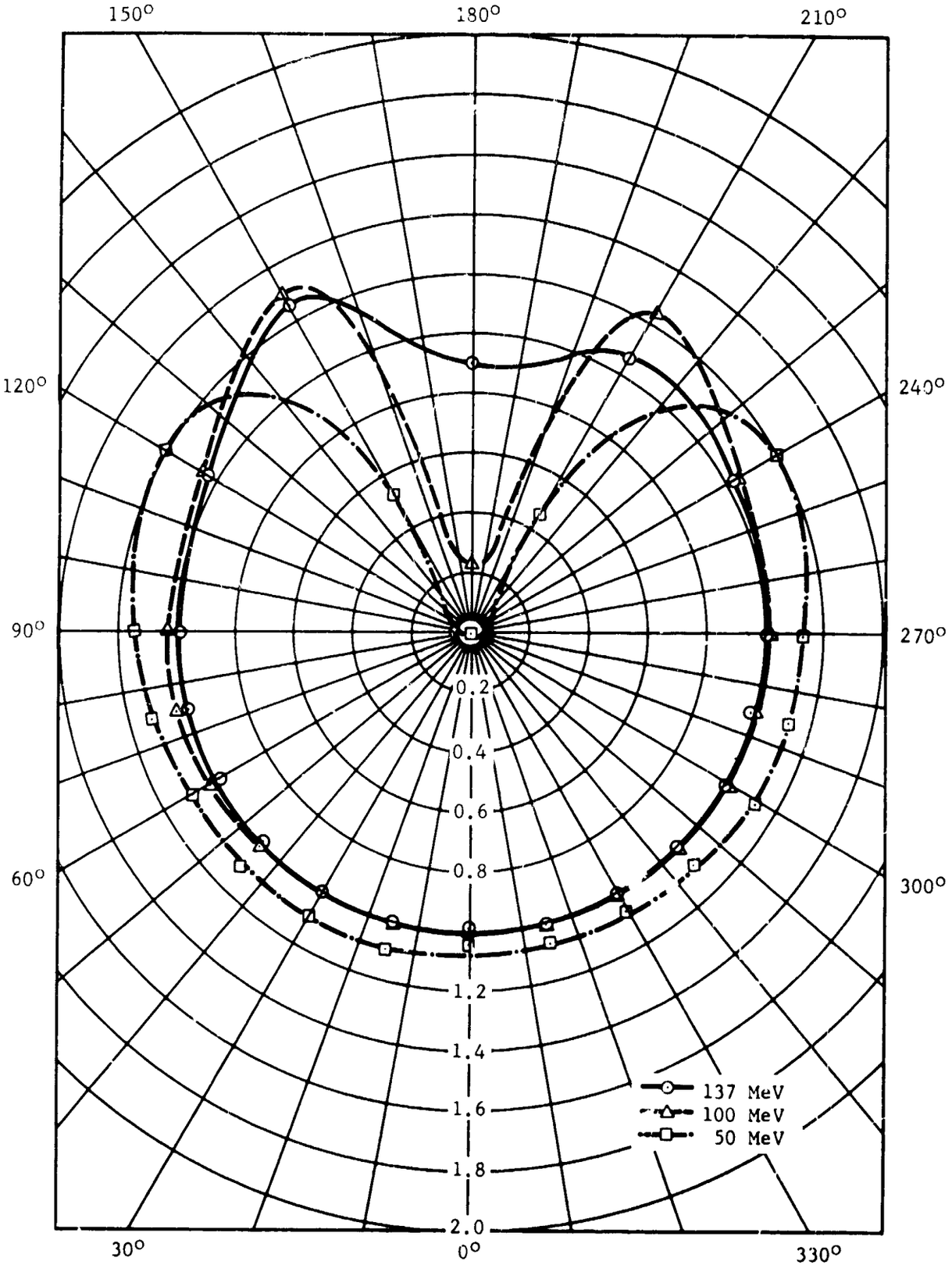

Figure 4-4 Proton Response of PRD 005 in the Vertical-Dial Configuration

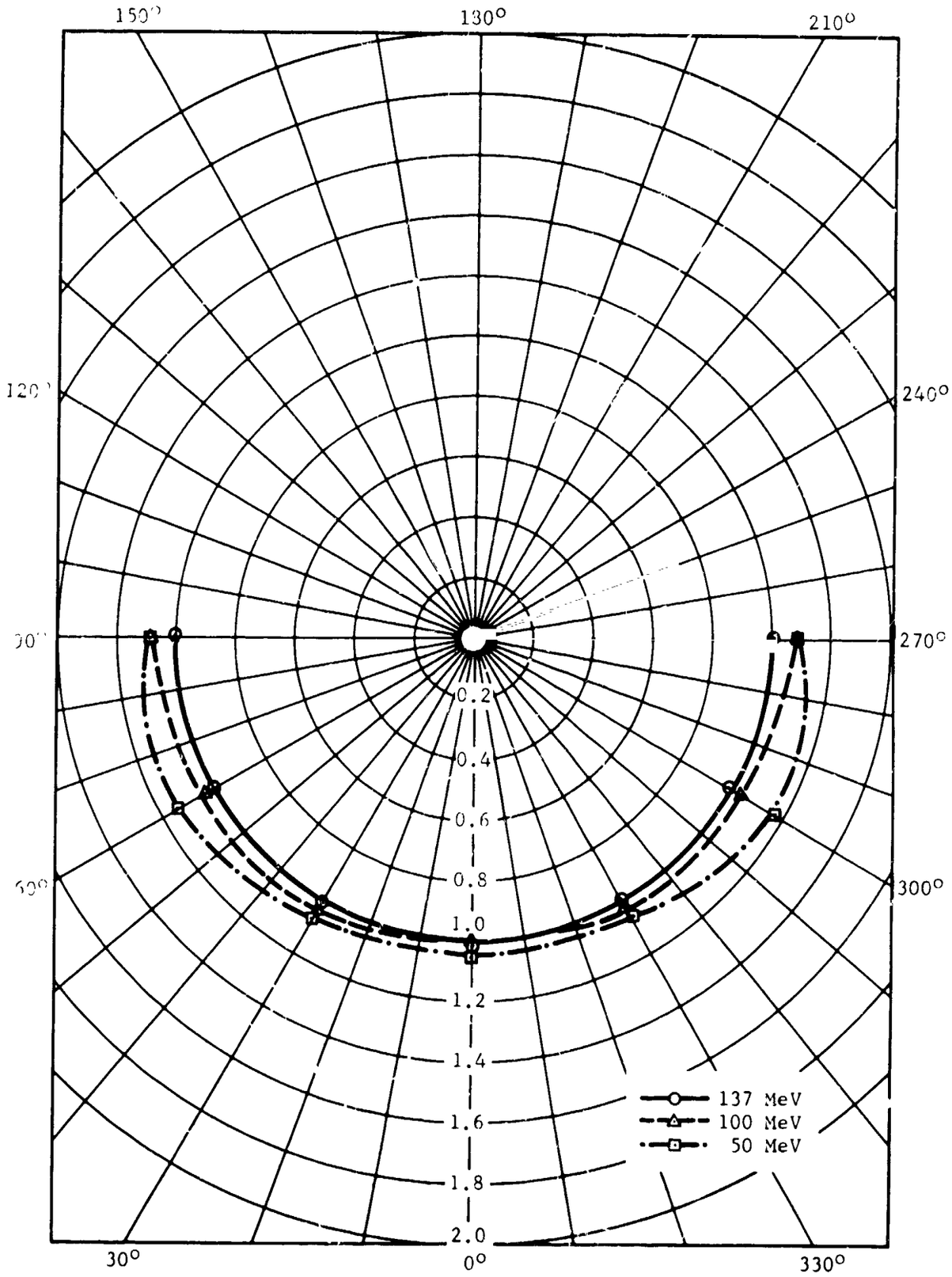

Figure 4-5 Proton Response of PRD 004 in the Horizontal-Dial Configuration

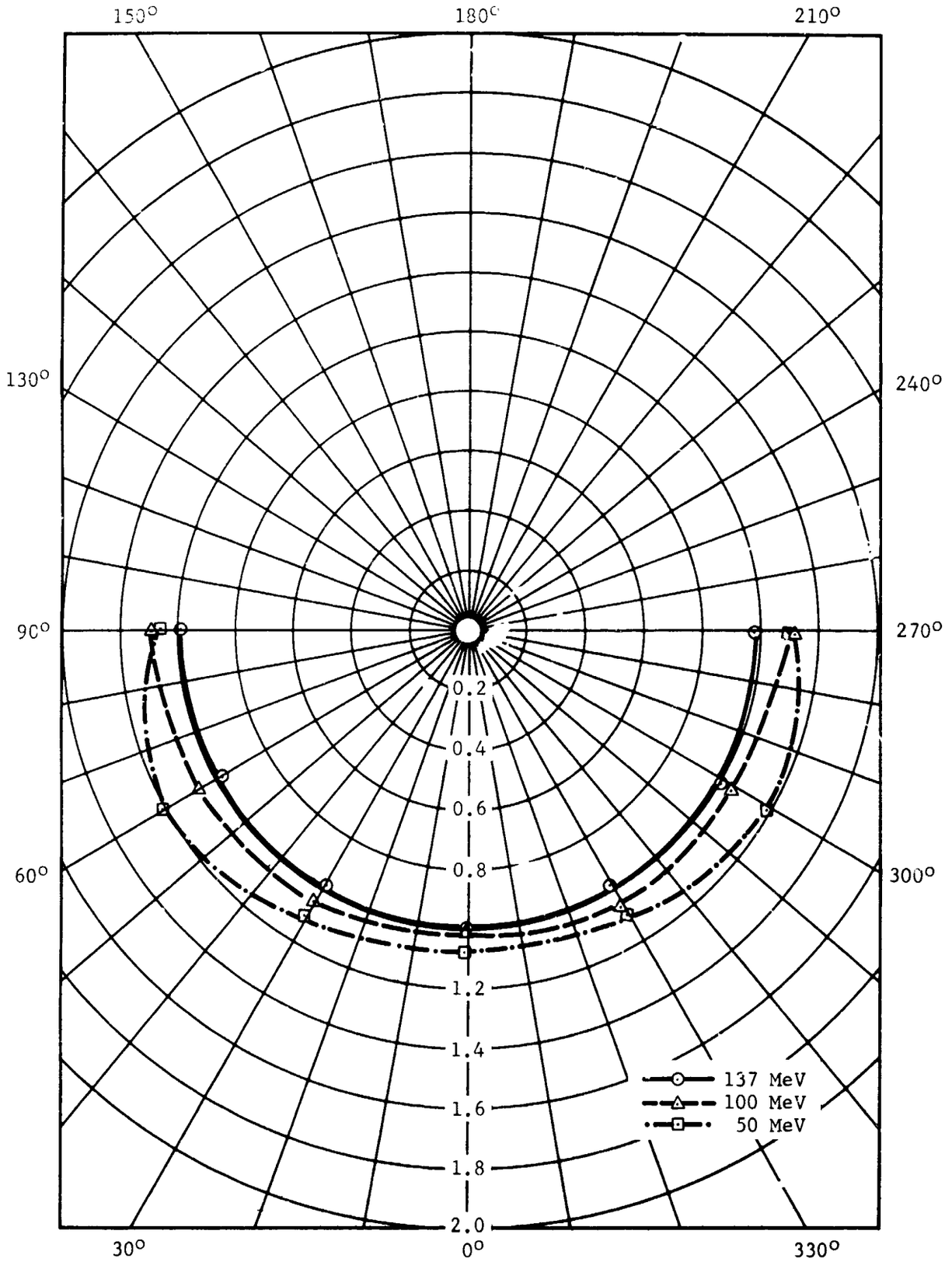

Figure 4-6 Proton Response of PRD 003 in the Horizontal-Dial Configuration

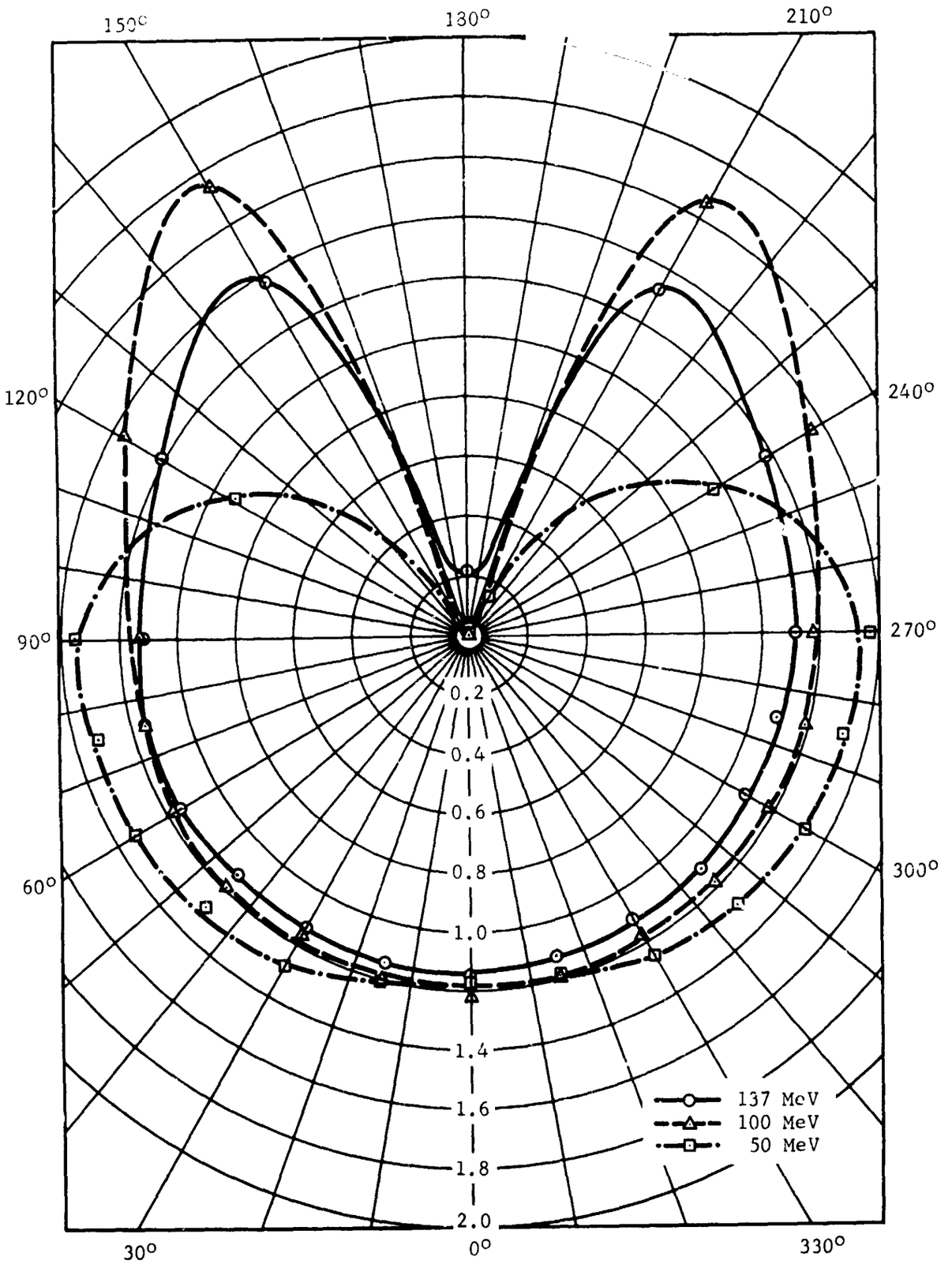

Figure 4-7 Proton Response of RSM 003 in the Horizontal-Dial Configuration

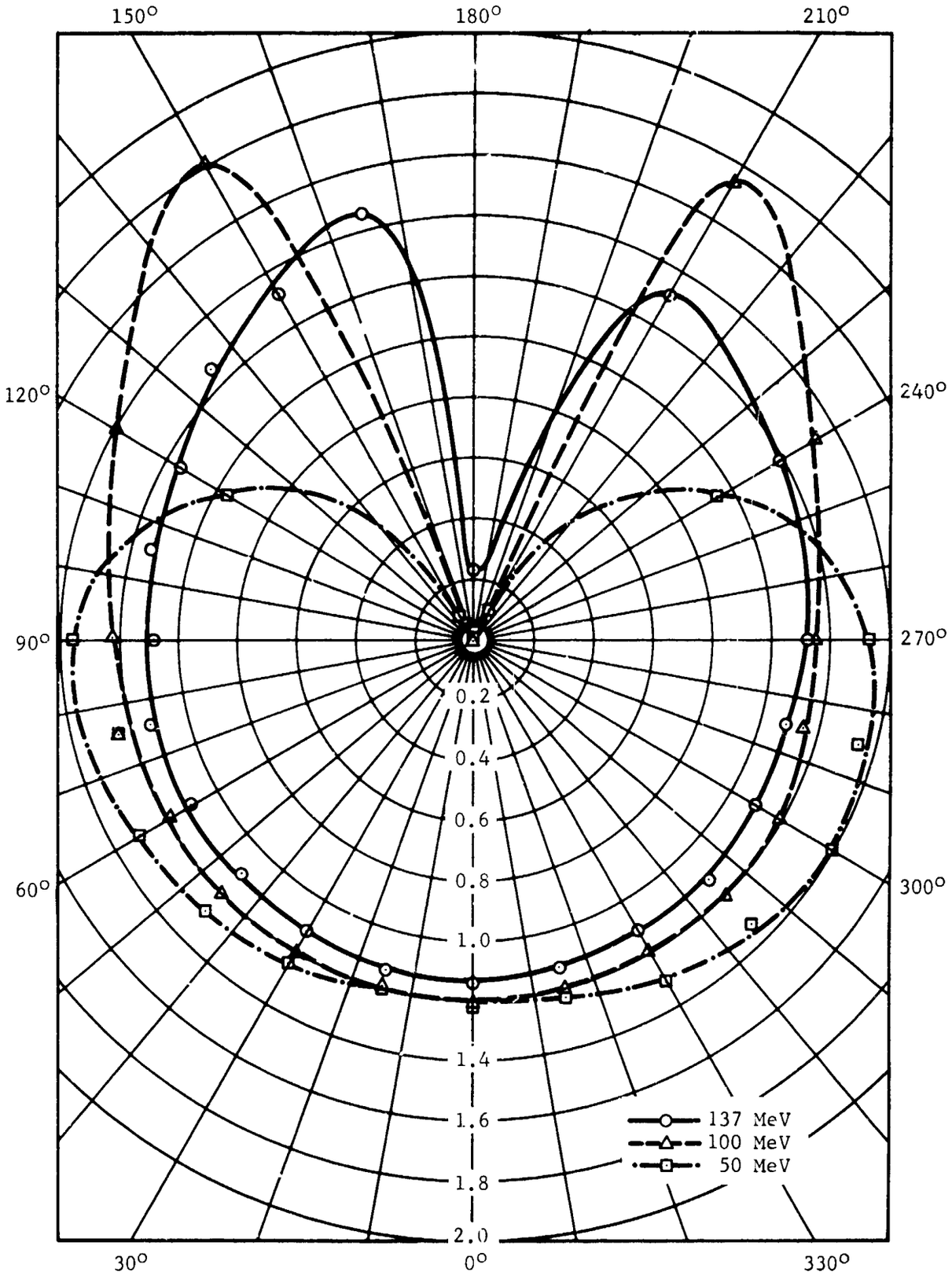

Figure 4-8 Proton Response of RSM 003 in the Vertical-Dial Configuration

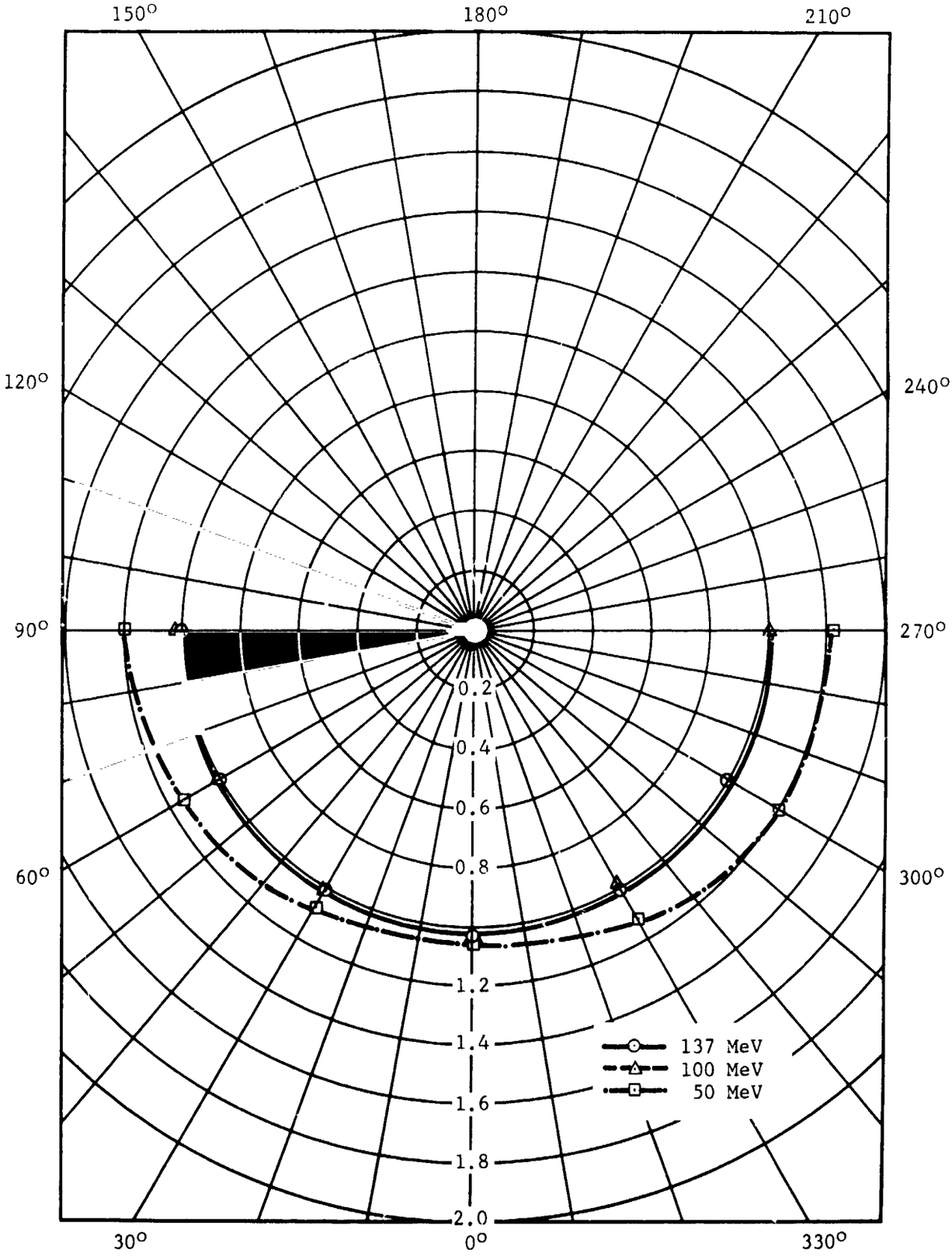

Figure 4-9 Proton Response of RSM 002 in the Horizontal-Dial Configuration

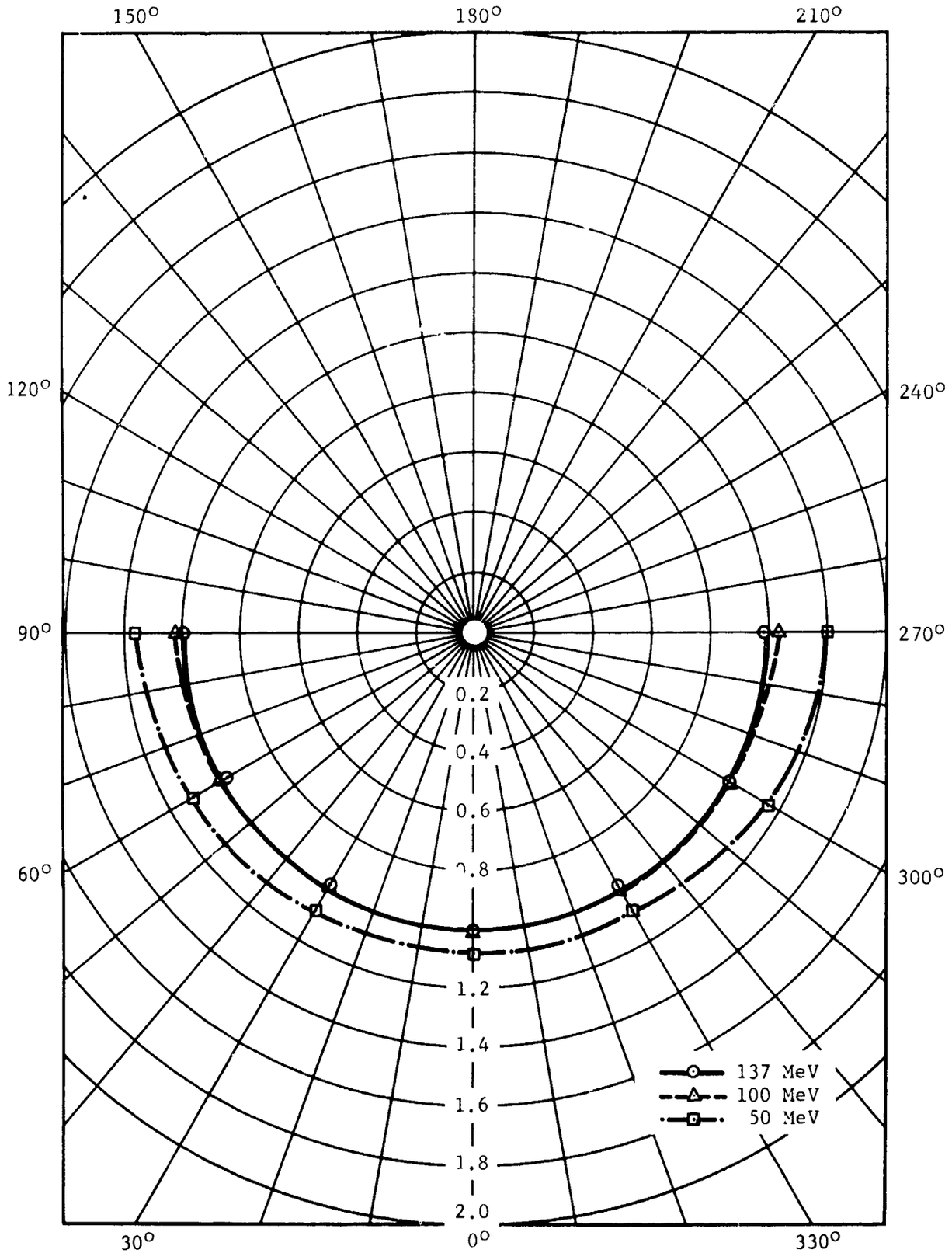

Figure 4-10 Proton Response of RSM 001 in the Horizontal-Dial Configuration

three PRDs was excellent - within $\pm$ 1.5% at all three energies. The angular response of the instruments was also excellent. At angles between 0^{o} and $\pm$ 90^{o} the response of the PRDs was essentially independent of angular position for 137-MeV protons and indicated maximum errors of approximately 10% and 20% for 100- and 50-MeV protons, respectively.

RSM 001 and 002 agreed within $\pm$ 1% with the Harvard dose rates at 137 and 100 MeV for head-on incidence. At 50 MeV the measured dose rate was 5% higher than the Harvard dose rate. RSM 003 indicated dose rates 13% higher than the Harvard dose rate at 137 MeV and 18% higher at 100 and 50 MeV for head-on incidence.

The angular response of the RSMs was superior to the PRDs, being essentially independent of angular position for 137- and 100-MeV protons at angles between 0^{o} and $\pm$ 90^{o}. At angles between 0^{o} and $\pm$ 90^{o} for 50-MeV protons, the maximum difference between an off-axis reading and head-on reading was approximately +20%.

The data taken to investigate the linearity of response with dose rate are given in Table 4-1. The dose rates listed in the table headings are only approximate and are given to indicate range rather than actual value.

The only conclusion that may be drawn from the RSM data is that there is no strong nonlinearity with dose rate. The scatter

Table 4-1

LINEARITY OF RESPONSE WITH DOSE RATE

Detector	Energy	Ratio of Measured Rate to True Rate			
	MeV	50 rad/h	5 rad/h	0.5 rad/h	0.05 rad/h
RSM 001	137	0.95	0.99	1.07	1.08
	100	0.94	1.00	1.06	1.02
	50	1.03	1.07	1.19	1.08
RSM 002	137	1.06	1.02	0.98	0.97
	100	1.06	1.03	1.05	0.99
	50	1.09	1.05	1.08	1.00
RSM 003	137	1.10	1.13	1.08	1.01
	100	1.10	1.20	-	-
	50	1.10	1.18	1.20	1.09
PRD 003	137	0.90	1.02		
	100	0.93	1.00	—	—
	50	0.95	1.07		
PRD 004	137	0.89	0.99		
	100	0.92	1.01	—	—
	50	0.96	1.06		
PRD 005	137	0.89	0.97		
	100	0.91	0.98	—	—
	50	0.96	1.04		

of the data reflects the lack of precision that is inherent in the data-taking method.

The PRD data indicate the nonlinearity with dose rate that has been observed previously with gamma radiation. The measured dose rates at 50 rad/h are an average of 10% lower than expected when compared to the 5-rad/h data.

4.3 Alpha Response

The responses of RSM 006 and PRD 008 to 118-MeV alpha particles were measured utilizing the 88-in. cyclotron at Lawrence Radiation Laboratory on 30 August 1967. The angular responses of the instruments were measured for angles within $\pm$ 90° of head-on incidence.

4.3.1 Experimental Description

The 88-in. cyclotron is a fixed-frequency, variable-energy accelerator with a maximum alpha particle energy of 120 MeV. The biomedical facility of the accelerator was used for this test, since it is well equipped for large-volume irradiations at low dose rates.

After extraction of the particle beam from the cyclotron into the biomedical facility, the beam is swept electromagnetically in order to obtain a large uniform area at the test plane. After exiting from the sweeper, the diverging beam drifts approximately

20 ft in an evacuated beam tube and exits into the test area through a thin aluminum foil. The beam then passes through two thin-walled, parallel-plate ionization chambers. The first of these is divided into quadrants, and its individual outputs are used to center the beam. The collection electrode of the second chamber is 1 cm in diameter and is located at the center of the beam pattern. This chamber is cross-calibrated against a Faraday cup and is used to measure the alpha dose rate incident on the test plane.

The test plane was parallel to and 2 in. from the monitor ion chamber. The beam profile is approximately a 3-in. square in this plane when the sweeper coils are operated at a current of 30A. The beam profile in the test plane was measured with a diode (Ref. 3) and is presented in Figure 4-11.

The beam energy at the test plane was measured by obtaining a Bragg ionization curve in water (Ref. 3). Analysis of these data yielded an alpha energy of 118 MeV (Fig. 4-12).

The experimental setup of the detectors and the method of data accumulation were identical to those previously described for the Harvard proton irradiations with three exceptions: (1) the two detectors were exposed individually because of the small irradiation volume available; (2) angular responses were measured only within head-on incidence $\pm$ 90^{o} because of the proximity (2 in.) of

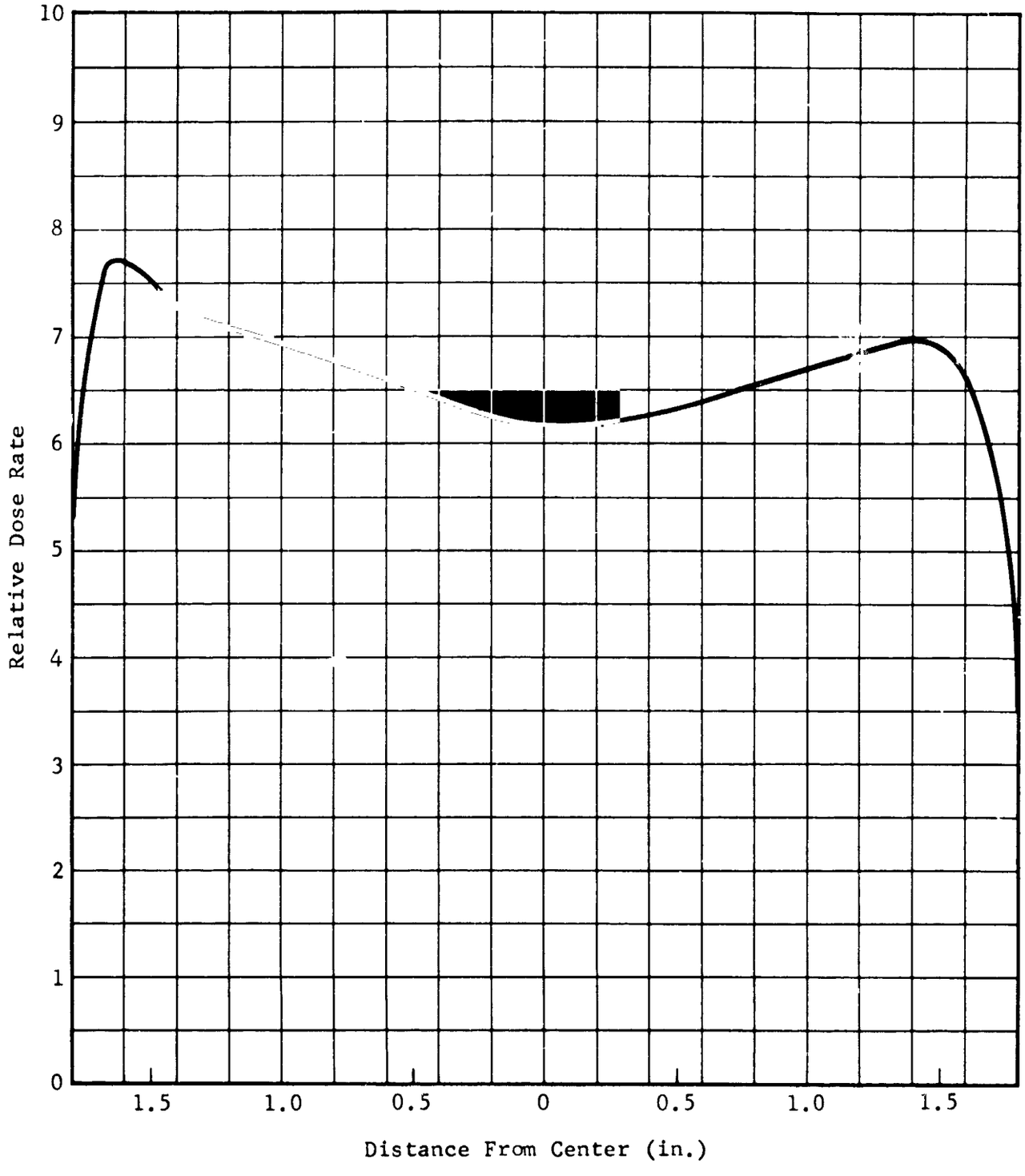

Figure 4-11 Alpha Beam Profile in Test Plane

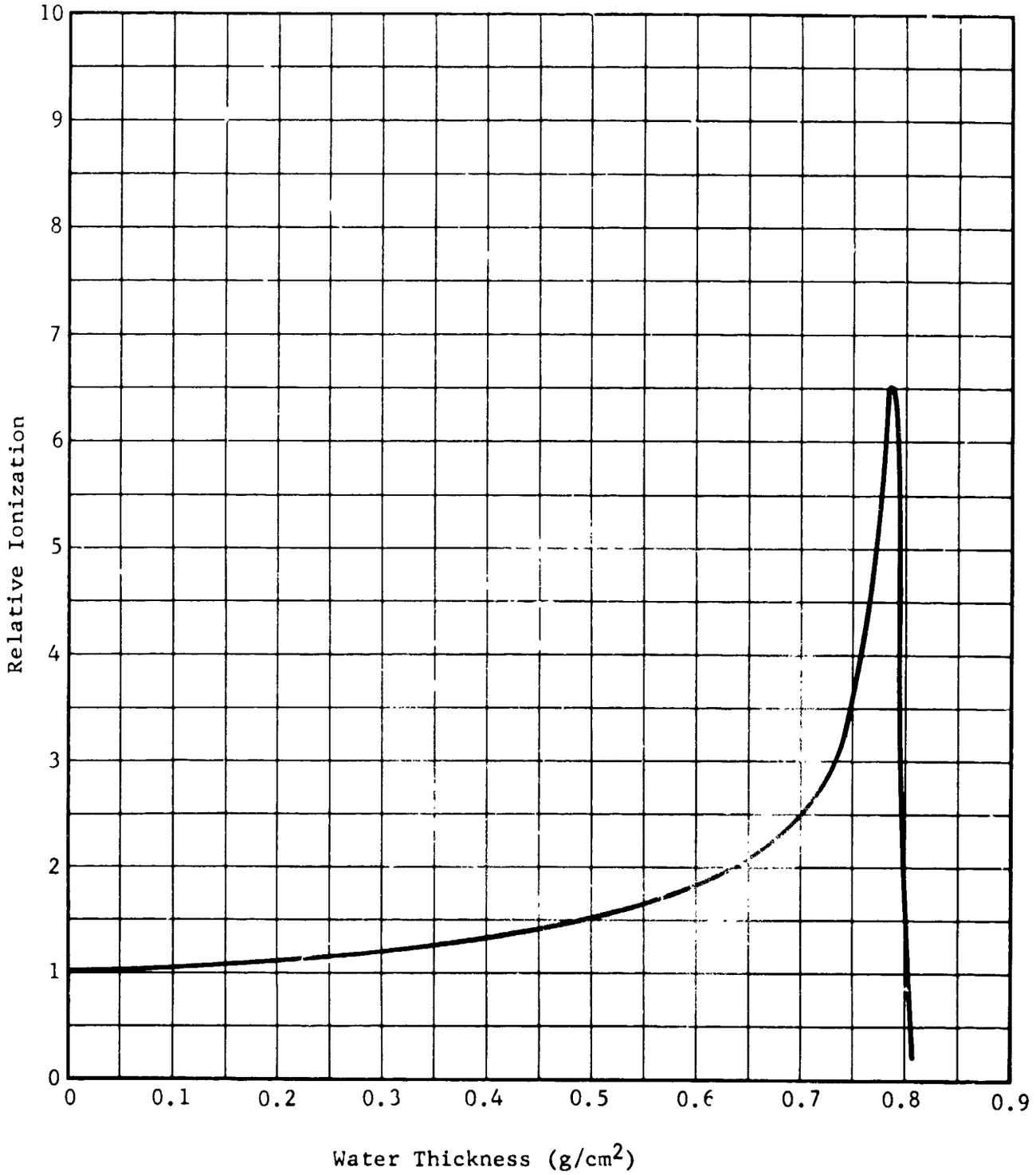

Figure 4-12 Bragg Ionization Curve of 118-MeV Alphas in Water

the detectors to the monitor ion chamber; and (3) the survey meter angular response was measured only in the horizontal-dial configuration because of time limitations.

The measurements were performed at alpha dose rates varying from 33 to 60 rad/h. The PRD data presented in this report were corrected for the nonlinearity of response with dose rate, which had been previously measured for this detector. A correction factor of -4.3% has also been applied to these data to correct for the nonuniformity of the beam profile.

4.3.2 Results and Conclusions

The angular responses of the two instruments to 118-MeV alphas are presented in Figures 4-13 through 4-15. The data are presented as the ratio of the PRD or RSM dose rate to the Lawrence Radiation Laboratory (LRL) dose rate as a function of angular position of the detectors.

Analysis of the data shows that PRD 008 agreed with the LRL dose rate within 6% for head-on incidence. This agreement was maintained within the limits of $\pm 45^{\circ}$ when the dosimeter was in the horizontal-dial configuration. When the dosimeter was in the vertical-dial configuration, the agreement was within 8% within the limits of $\pm 45^{\circ}$. At larger angles the measured-to-true dose-rate ratio dropped below unity to a minimum of 0.91.

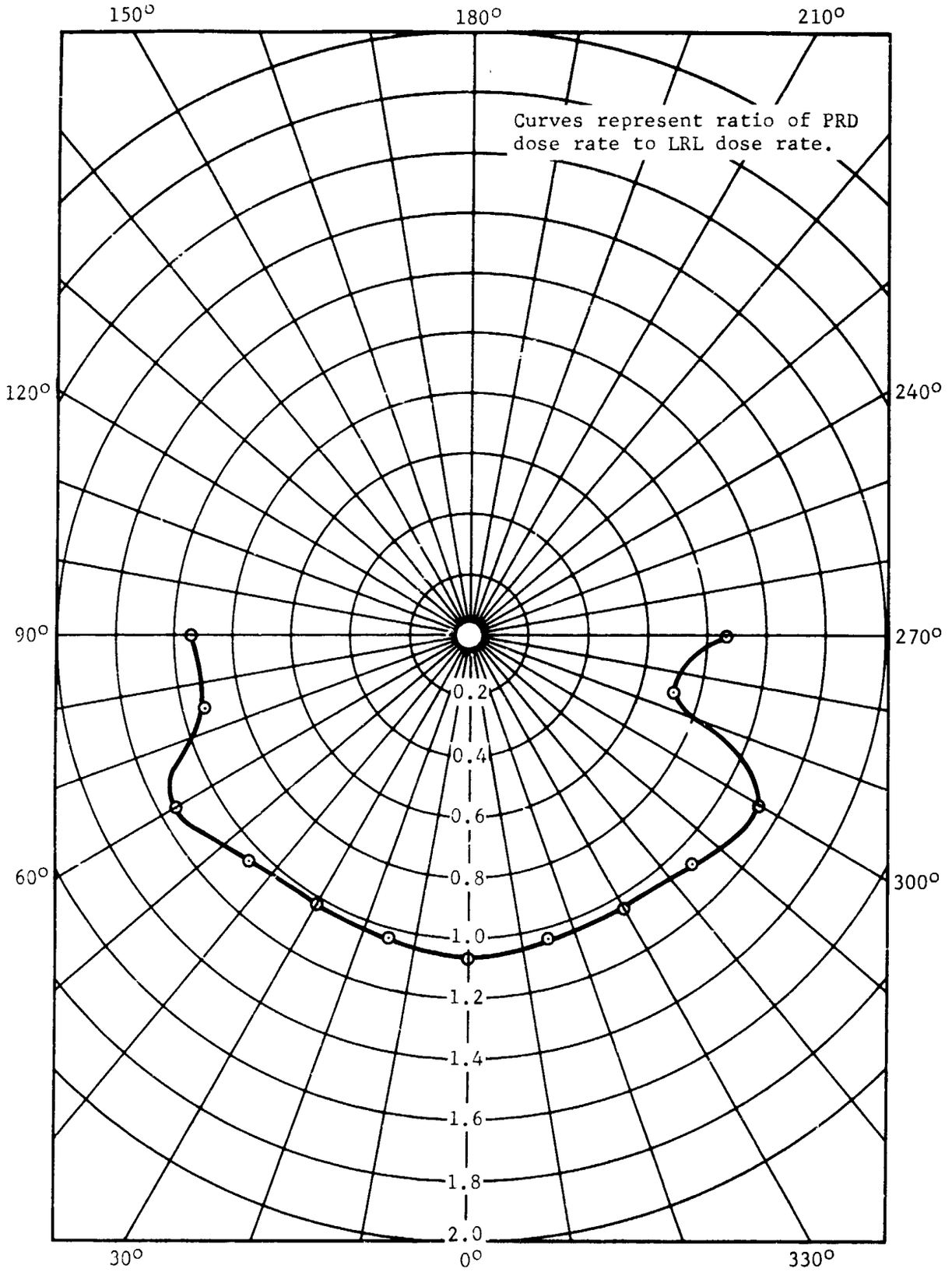

Figure 4-13 Response of PRD 008 to 118-MeV Alphas in the Horizontal-Dial Configuration

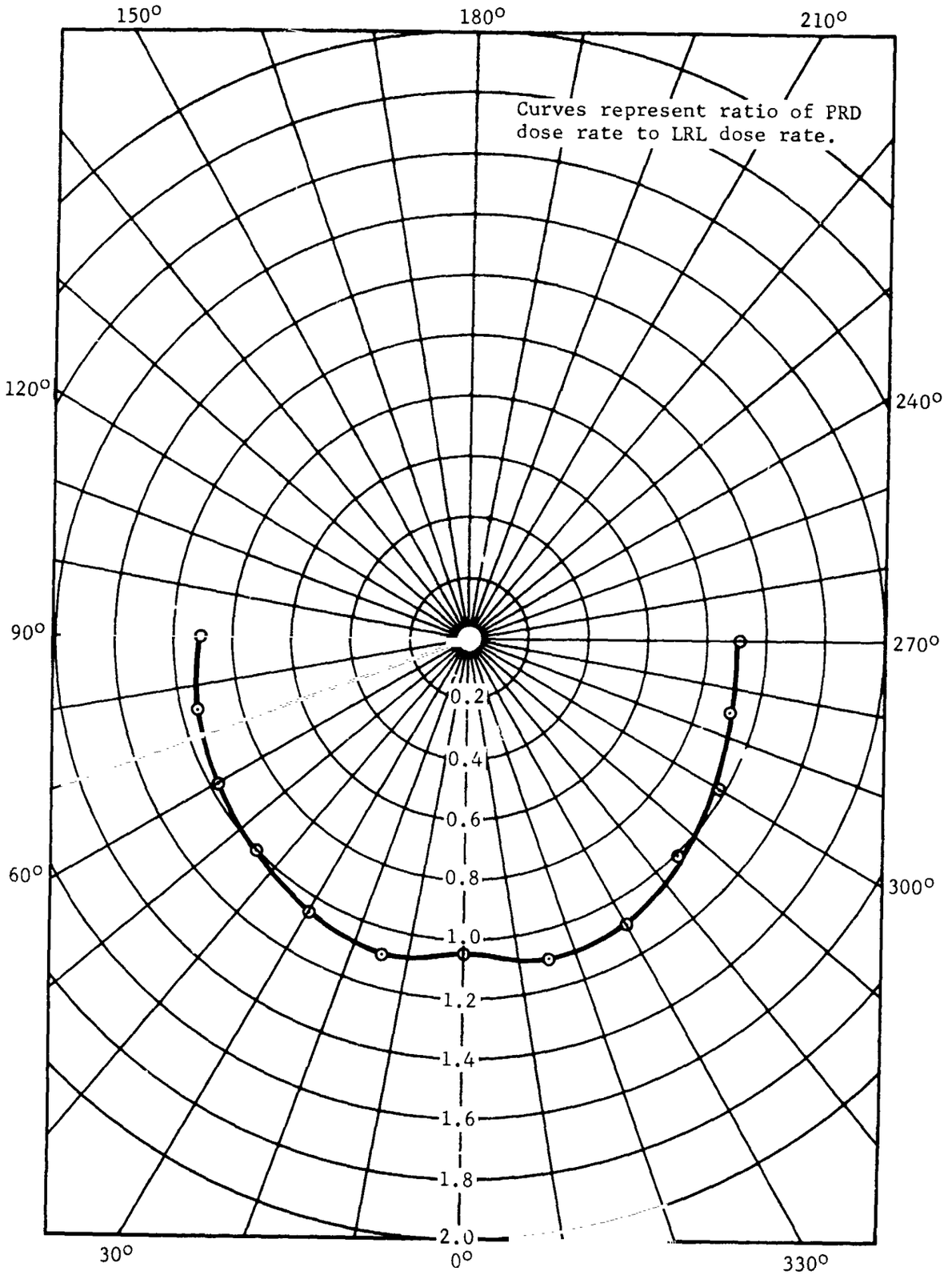

Figure 4-14 Response of PRD 008 to 118-MeV Alphas in the Vertical-Dial Configuration

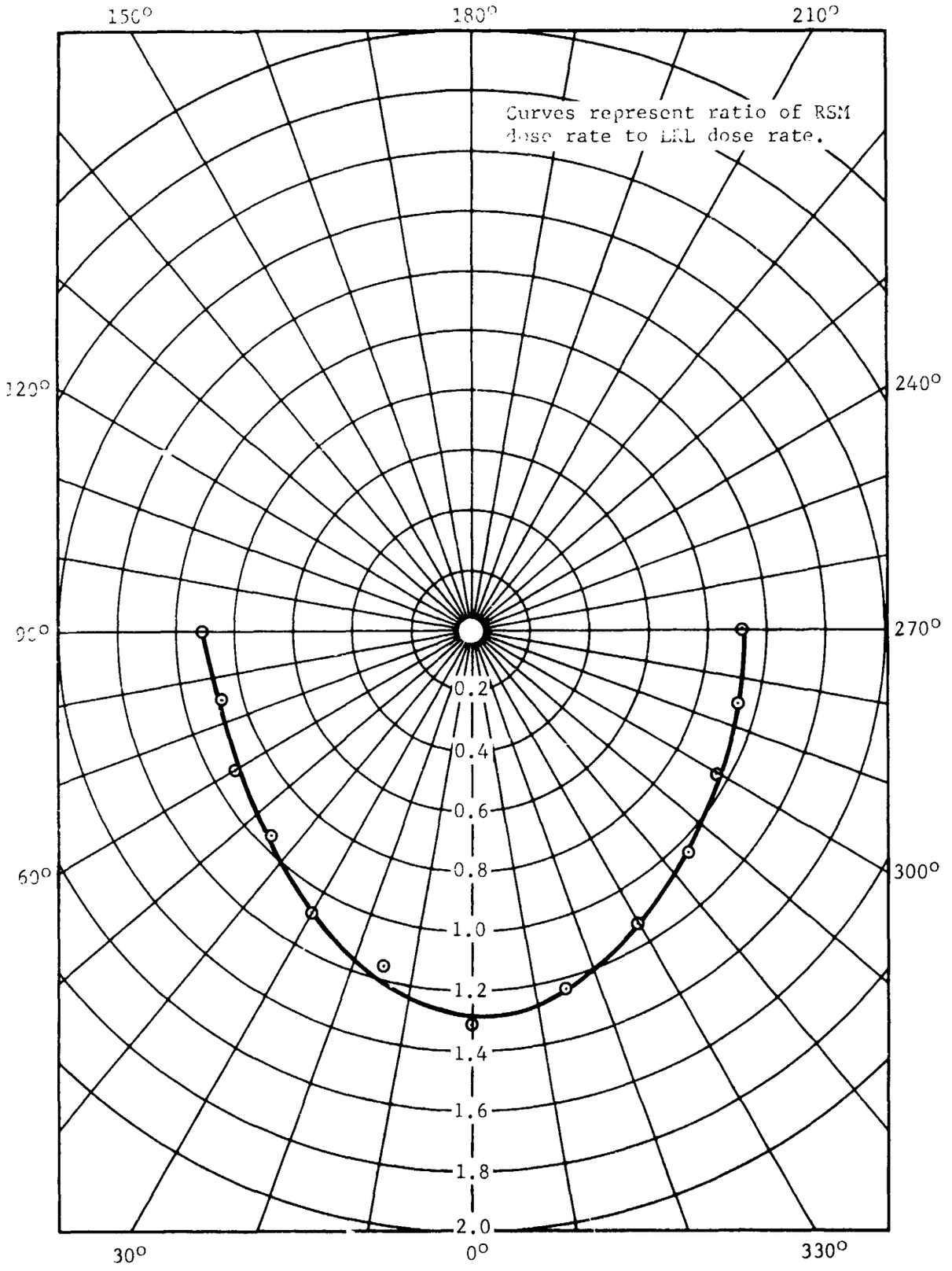

Figure 4-15 Response of RSM 006 to 118-MeV Alphas in the Horizontal-Dial Position

The dose rate measured by RSM 006 was approximately 28% higher than the LRL dose rate for head-on incidence. The response decreased monotonically from 0^{o} to $\pm 90^{o}$ to a minimum of approximately 0.9. This behavior is similar to that expected, since the effective thickness of the detector walls is approximately 20% larger at 0^{o} than at 90^{o}. Alphas passing through the detector walls into the active volume are subjected to energy degradation with a resultant increase in the flux-to-dose conversion factor. The detector would thus be expected to exhibit a larger response at 0^{o} than at 90^{o}. However, the magnitude of the difference is much larger than that expected from a theoretical analysis. The detector would also be expected to indicate a dose rate higher than the true dose rate at all angles.

4.4 Monoenergetic Electrons

The responses of RSM 006 and PRD 008 to monoenergetic (1-2 MeV) electrons were measured at NASA-MSC Van de Graaff Accelerator on 14, 18, 19 September 1967 (Ref. 4). Since these data were obtained at NASA-MSC, no experimental description will be given.

The angular responses of the two instruments to 1-MeV electrons are presented in Figures 4-16 and 4-17, and the angular response of the PRD to 2-MeV electrons is presented in 4-18. The data are presented as the ratio of the PRD or RSM dose rate to the

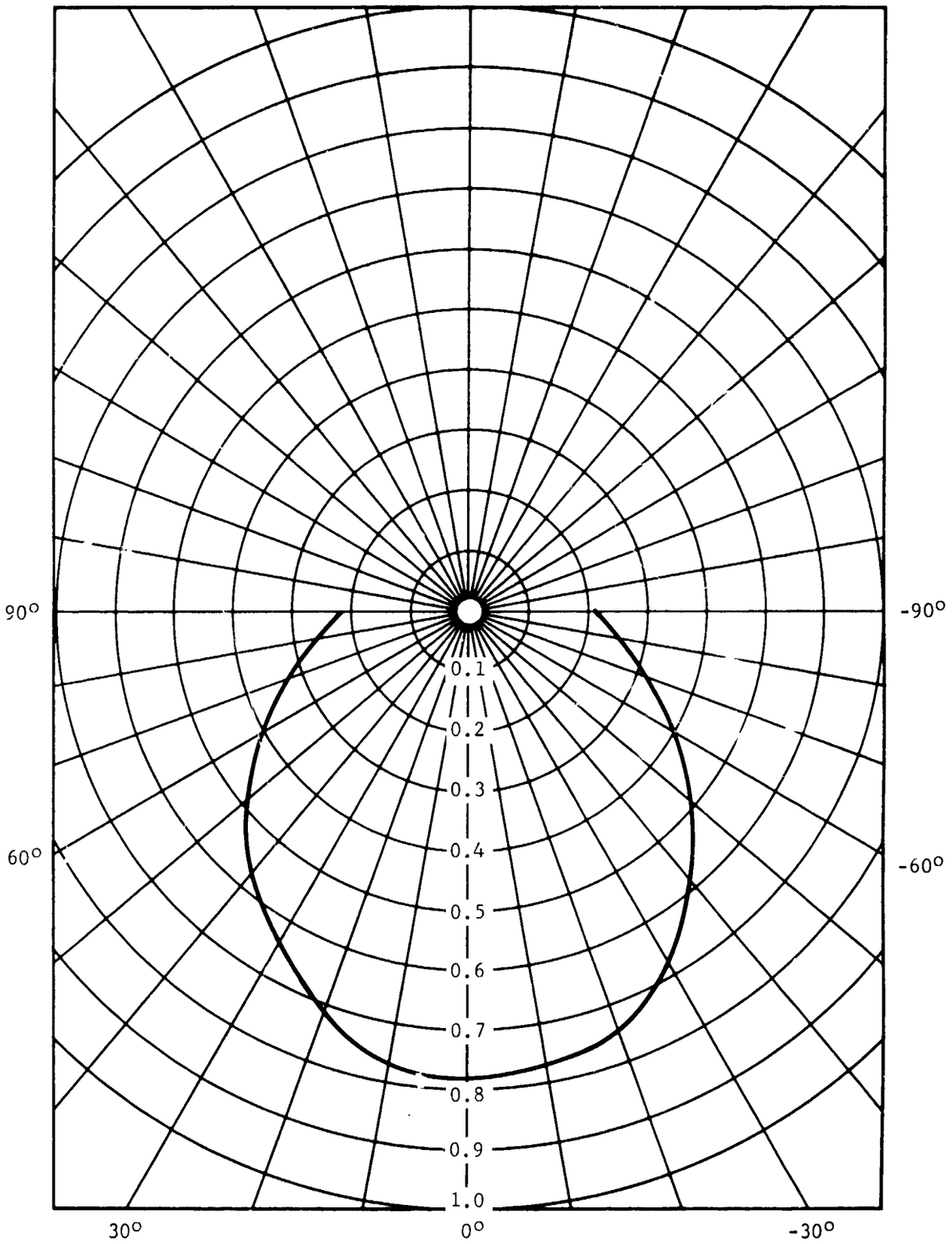

Figure 4-16 Response of PRD 008 to 1-MeV Electrons in the Horizontal-Dial Position

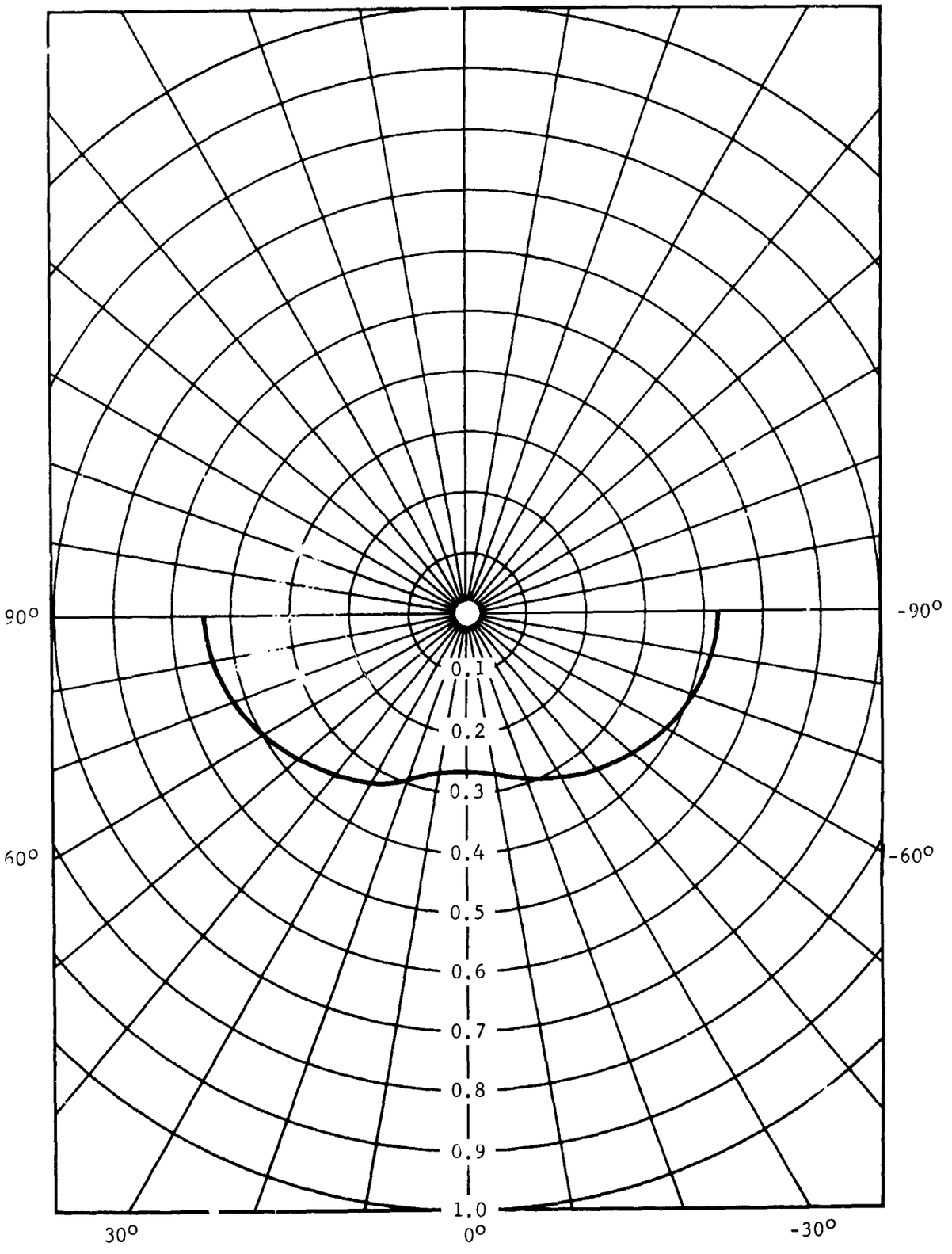

Figure 4-17 Response of RSM 006 to 1-MeV Electrons in the Horizontal-Dial Position

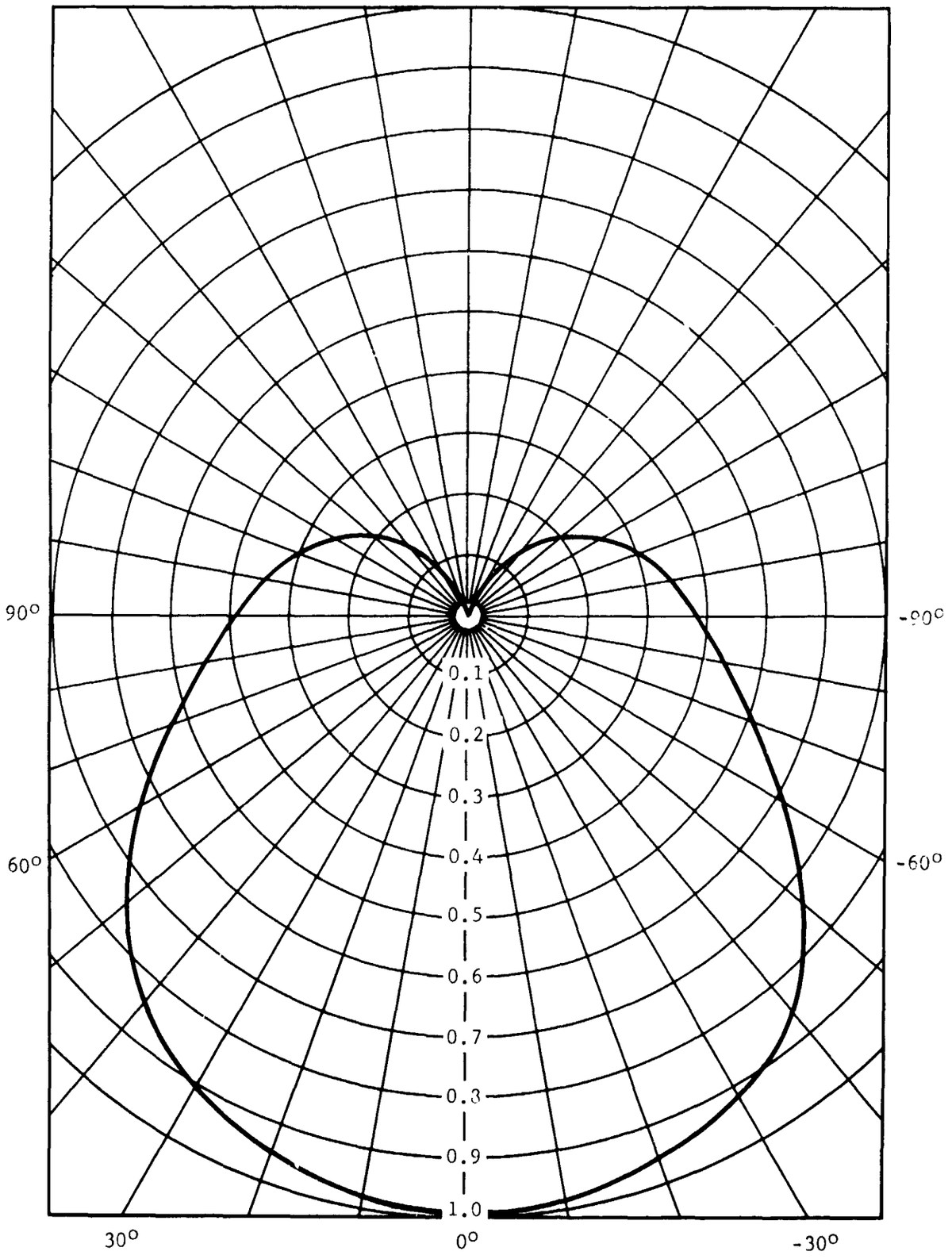

Figure 4-18 Response of PRD 008 to 2-MeV Electrons in the Horizontal-Dial Position

accelerator dose rate. The data for both instruments were obtained in fields of 20-25 rad/h.

For 1-MeV electrons, the PRD response decreased from 0.77 at 0^{o} to 0.21 at $\pm$ 90^{o}, while the RSM read 0.26 at 0^{o} and increased monotonically to approximately 0.43 at $\pm$ 90^{o}.

The PRD response at 0^{o} for 2-MeV electrons was 0.99 and monotonically decreased to zero at $\pm$ 180^{o}.

4.5 P-32 Betas

The responses of two PRDs and two RSMs to the P-32 betas were measured on 11 April 1967.

4.5.1 Source Preparation and Calibration

The P-32 source was prepared from one of the standard sulfur foils used by GDFWD for neutron-flux measurements. Three of these foils were irradiated for 60 hours at 3 MW utilizing the Ground Test Reactor. P-32 is produced by the S^{32} $(n,p)P^{32}$ reaction.

After irradiation, the specific disintegration rates (dis/sec-g) of two of the foils were determined by standard GDFWD counting techniques (Ref. 5). The remaining foil was crushed, and two pieces of the foil were weighed and burned separately on 2-mil aluminum sample mounts. It has been demonstrated (Ref. 6) that when an activated sulfur pellet is burned, 93.5% of the P-32 present remains in the ash. The sample was then sprayed with a

fast-setting plastic film to prevent sample loss during handling. A thin source with very little self-absorption is obtained by this technique.

The absolute disintegration rates of the two specimens were then calculated by knowledge of the measured specific disintegration rate, the weights of sulfur burned, and the correction for P-32 loss in burning.

The disintegration rates were then converted to beta dose rates by means of a flux-to-dose-rate conversion factor. This factor was calculated from the P-32 beta spectrum (Ref. 7) and the stopping power of electrons in muscle (Ref. 8). A conversion factor of 4.26×10^{-8} rad-cm^2/electron was obtained.

4.5.2 Response Measurements

The responses of PRD 003 and 009 and RSM 003 and 006 to the stronger of the two prepared sources were measured. In addition, the response of RSM 003 to the second prepared source was measured in order to check on the reproducibility of source preparation.

The instruments were placed at distances of from 1 to 12 in. from the sources, and the indicated dose rates at each distance recorded. The dose rate, as measured by the PRDs, was obtained by dividing the dose by the measured time interval.

4.5.3 Results

The variation of the measured dose rate with distance for each of the instruments is given in Figures 4-19 through 4-22. A $1/r^2$ curve is also given for purposes of comparison.

An examination of these curves shows that the instruments measure the dose rate from the sources as a $1/r^2$ dependence at distances greater than approximately 3 in. For closer approaches the instruments indicate a less than $1/r^2$ dependence, the deviation being greater for the PRD than for the RSM. This is in the direction expected, since the RSM is a closer approximation of a point detector than the PRD.

Examination of the data in Figure 4-21 reveals that the RSM accurately measured the difference between the two prepared sources. It was therefore concluded that the method of source preparation was reproducible.

The dose rate measured at 5 in. by each instrument was compared to the true dose rate at that position with the following results:

Instrument	Fraction of True Dose Rate
RSM 003	0.065
RSM 006	0.076
PRD 003	0.23
PRD 009	0.26

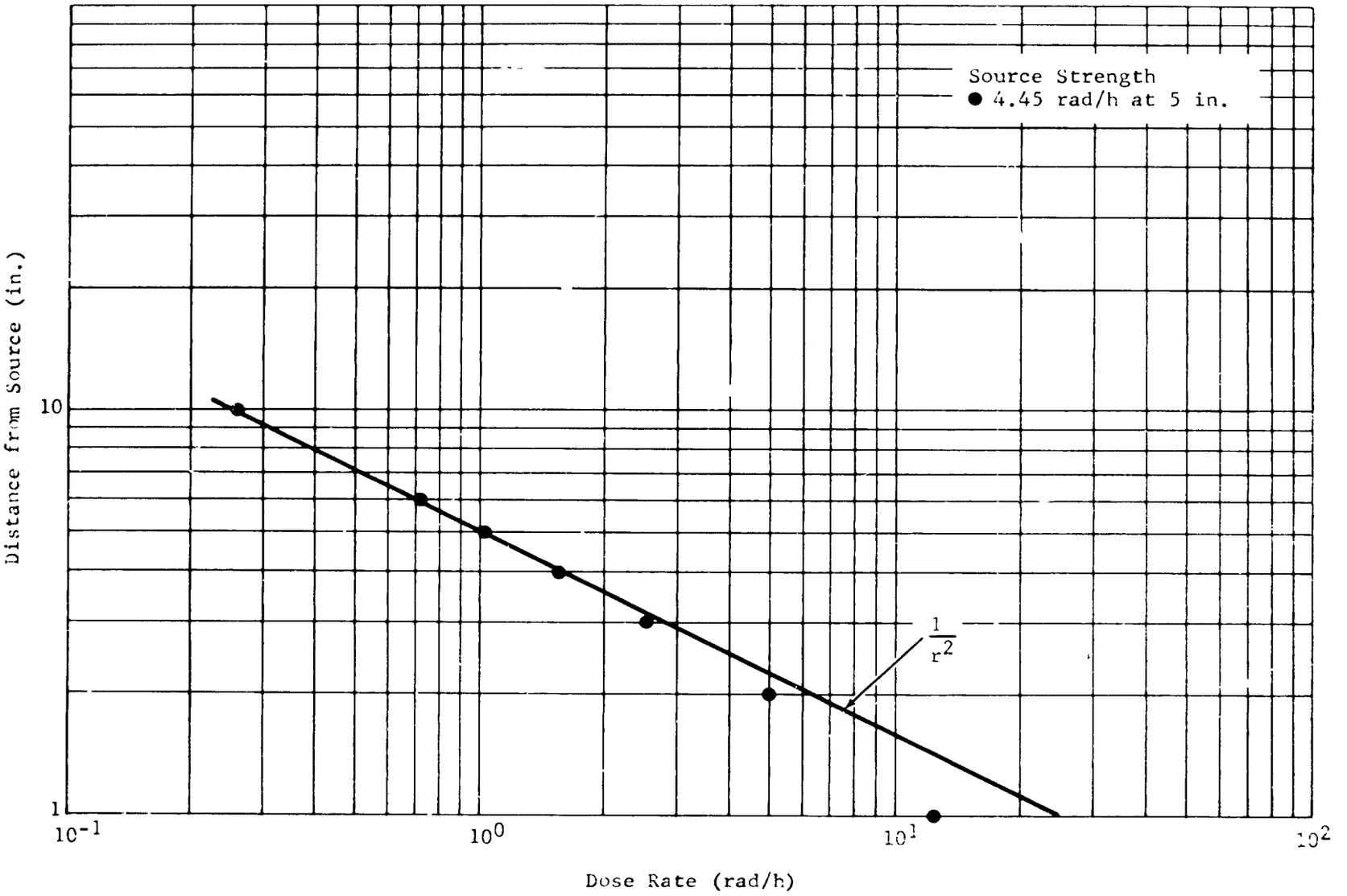

Figure 4-19 Response of PRD 003 to P-32 Beta Field with Distance

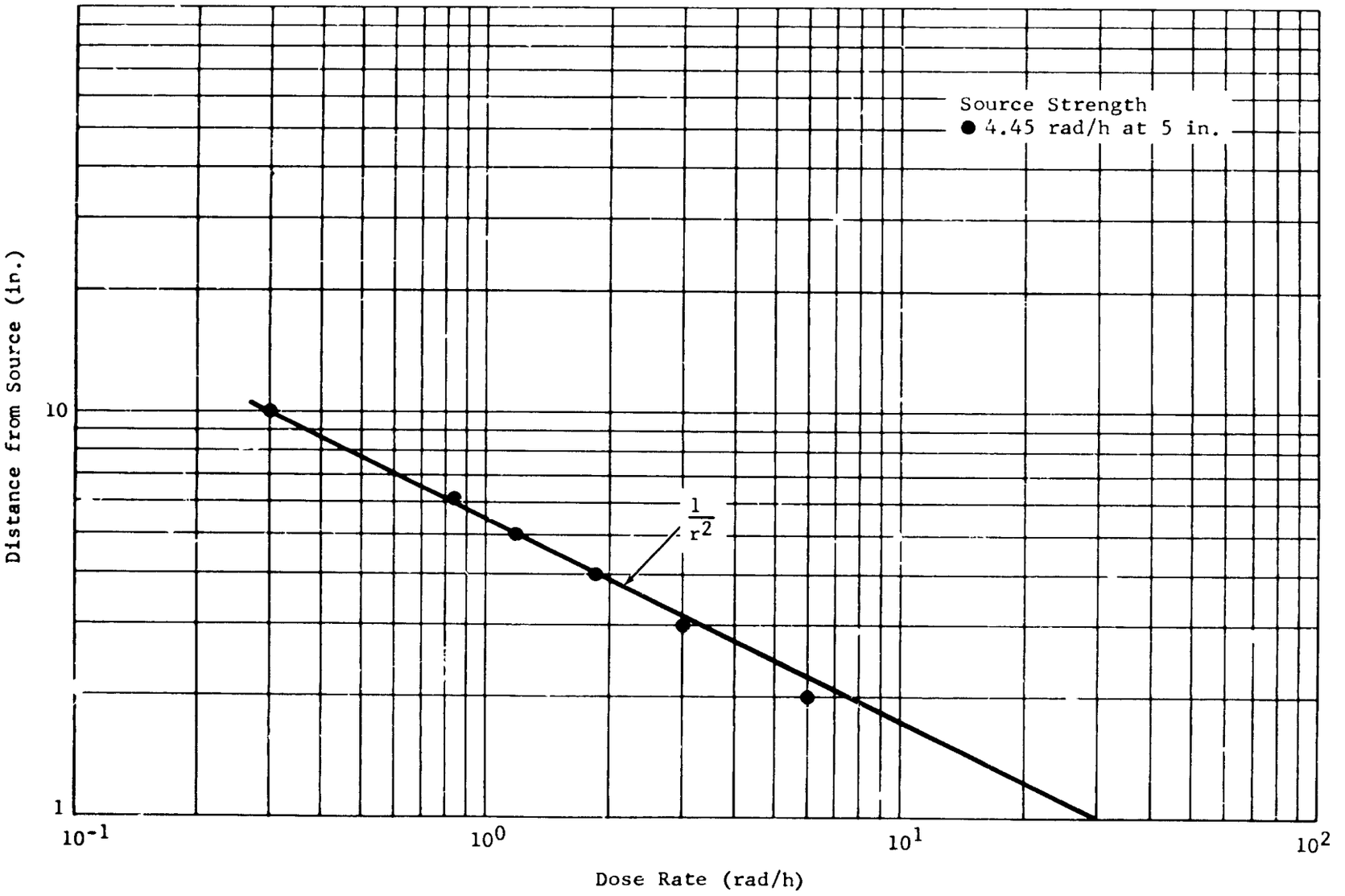

Figure 4-20 Response of PRD 009 to P-32 Beta Field with Distance

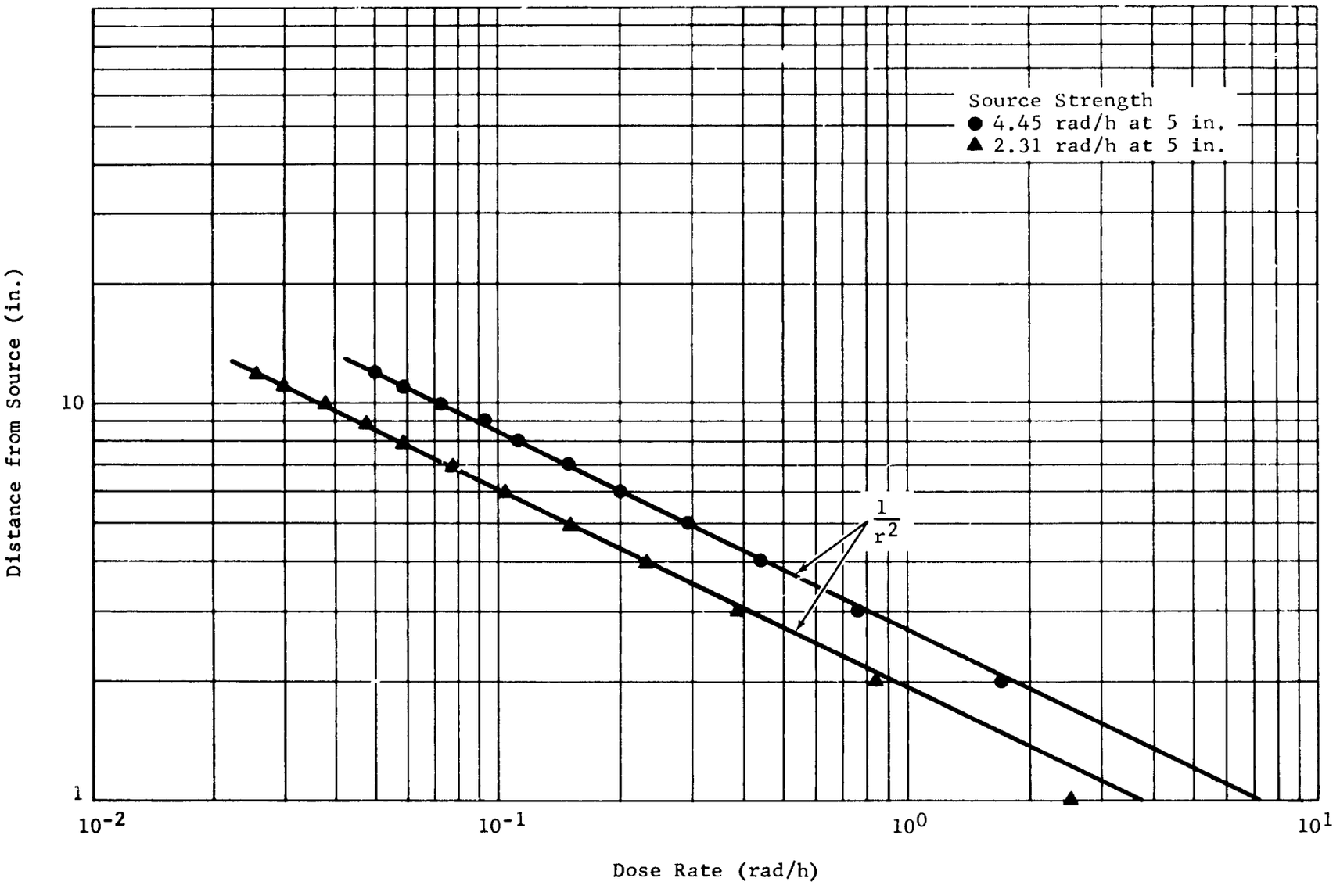

Figure 4-21 Response of RSM 003 to P-32 Beta Field with Distance

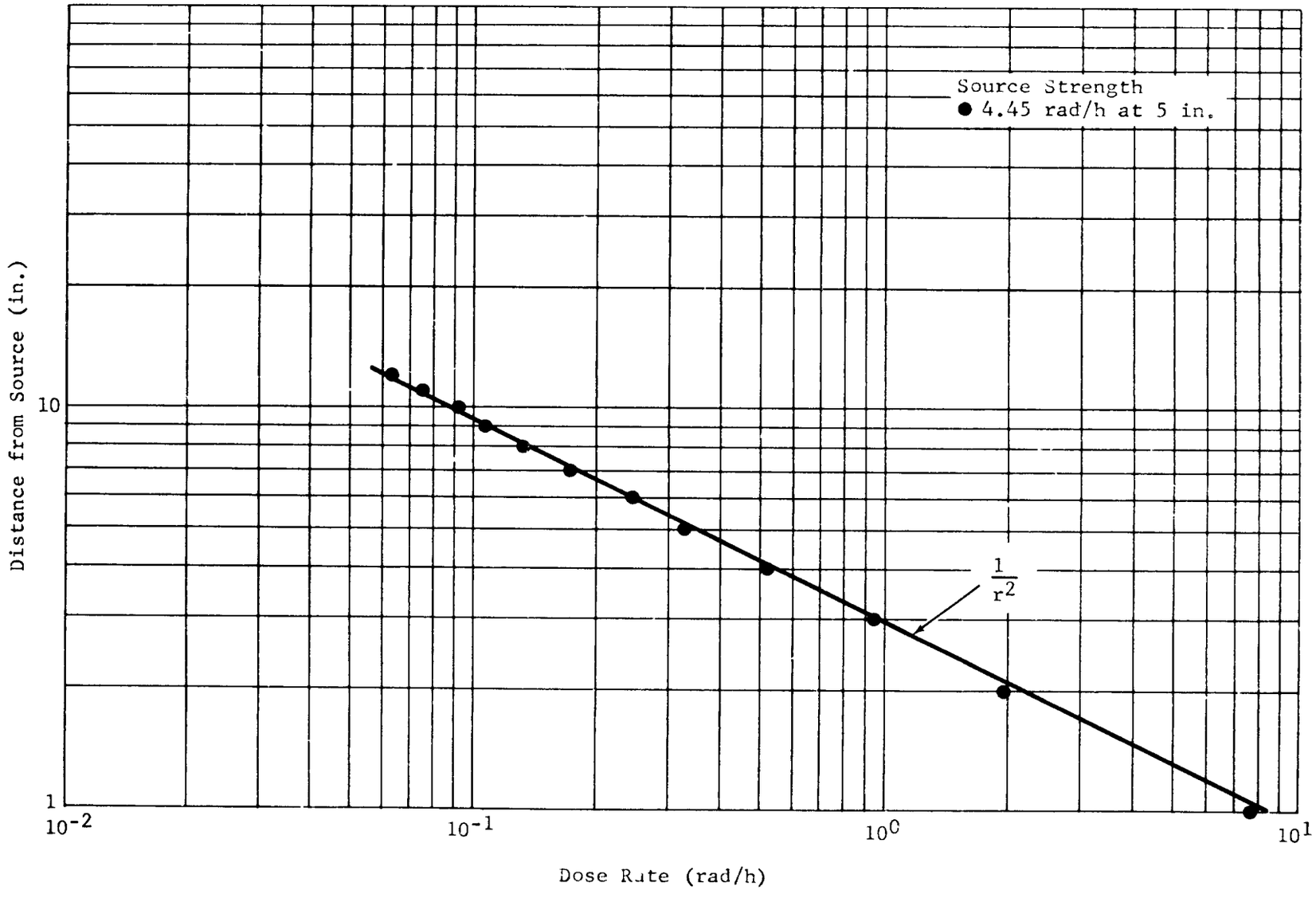

Figure 4-22 Response of RSM 006 to P-32 Beta Field with Distance

Explanation of the difference demonstrated between the two types of instruments is difficult, since it involves an integration of the P-32 beta spectrum passing through all the effective path lengths into the detector, i.e., at angles other than 0^{o}. However, as a relative measure, range-energy tables indicate that the shield and outer electrodes of the detectors will absorb all electrons with energies less than approximately 0.55 MeV for normal incidence. This constitutes 45% of the P-32 beta spectrum on a particle basis.

V. RECOMMENDATIONS

The program was successfully completed with no major difficulties or failures. The ease of performing the program can be attributed to the management and control plans plus the thorough design work performed on the prototype units.

The items or tasks that may possibly be improved are discussed below.

5.1 Personal Radiation Dosimeter Register

The PRD register is the smallest known five-digit register on the market. It suffers from several drawbacks which, if eliminated, would help the system's linearity and increase the readability of the unit.

The register is operated by a 7- to 11-V pulse having a minimum width of 4 msecs. At count rates less than 1.67 pulses/sec (~60 rad/h) the system operates satisfactorily; at pulse rates greater than this, however, the battery voltage decreases, resulting in a lower sensitivity. In addition, the readability would be improved if the numbers on the digit wheels were larger and were perfectly aligned after each count. A research and development effort to perfect a better register may prove fruitful.

5.2 Ionization Chamber Fabrication Techniques

The most difficult assembly is that required for the ionization chambers. A considerable effort was required to establish the procedures for aluminum deposition, cleaning, and sealing. Also, these procedures are expensive and time-consuming. A program to improve the method of construction should be performed.

APPENDIX A

DOCUMENTATION

All aspects of this Apollo program were documented so that MSC and GDFWD personnel could correctly assess progress and make decisions relative to the program.

The major categories of documentation include:

Program Planning	Information required to manage and plan the program.
Engineering Reports and Data	Information not specifically requested in the program. Includes design calculations and developmental test data.
Reliability & Quality Assurance	Information related to reliability and quality assurance other than the original program plans.
Support Procedures	Descriptions of special procedures, such as preservation, handling, and periodic maintenance.
Program Reports	Monthly and final reports.

In addition to the above reports, documentary photographs were furnished to MSC for evaluation of instrument assembly and external configuration. Most of the photographs appear in the body of this report.

There are three types of documents as follows:

Type I	Documents first submitted as review drafts and distributed only after approval by MSC.

Type II — Documents submitted to MSC for surveillance, information, review, and program monitoring.

Type III — Documents retained by GDFWD but submitted to MSC upon request.

Each document of this program is listed in Table A-1. The table also gives the document type and a brief summary of the contents.

Lists of the GDFWD drawing numbers and the Nuclear Instrumentation Procedures (NIP) are given in Tables A-2 and A-3, respectively.

Table A-1

DOCUMENTATION LIST

Title	Documentation Type	Brief Summary of Contents
Program Planning		
1. Program Plan	I	The master control plan that was used throughout the program. It contains a description of the personnel organization, cost-control procedures, milestone schedule, configuration control, and documentation schedule.
2. Test Plan	I	The plan describing all tests that were to be performed, including environmental qualification, energy dependence, and calibration.
3. Reliability Program Plan	I	Description of all reliability tasks; prepared in accordance with NPC 250-1.
4. Inspection Plan	I	Description of the procedures for inspecting various items such as purchase requests, resistance welds, and calibrations.
5. Drawing Specification and Documentation Lists	I	List of all drawings, specifications, and documents; revised as changes were made. (See Tables A-2 and A-3)
6. Technical Data, Reports, and Analyses	II	Results from various tests and analyses considered necessary to program planning.

Table A-1 (Cont'd)

Title	Documentation Type	Brief Summary of Contents
7. Specification:		
CEI Part I	I	Specifications documented for use at the various design meetings and for establishing assembly procedures. Specifications include drawings, performance criteria, manufacturing standards, and assembly procedures.
CEI Part II	I	
Company Specs.	III	
8. Drawings:		
Top Assembly	I	Drawings showing the external configuration and internal modules of each instrument.
Final Detail	II	Drawings used to manufacture detail parts.
9. Interface Control Documents	I	The only interface was the mounting of the RSM bracket and the bracket was fabricated to match the mounting already available.
10. Mass Properties Report	II	Monthly reports on the weight status of each item.
Engineering Reports and Data	II	Documentation of tests or analyses not anticipated in planning.
Reliability and Quality Assurance		
1. Qualification Test Plan and Test Procedures	I	Detailed plan for all environmental qualification tests, such as vibration and temperature.

Table A-2

LIST OF PRD AND RSM NUCLEAR INSTRUMENTATION PROCEDURES

Personal Radiation Dosimeter

NIP-1	Cleaning and Plating High-Density Polyethylene
NIP-2	PRD Ionization Chamber Assembly Procedure
NIP-3	PRD High-Impedance Electronic Module Assembly Procedure
NIP-4	PRD Electronic Module Assembly Procedure
NIP-5	PRD Final Assembly
NIP-6	PRD Finish and Identification
NIP-7	PRD Calibration Procedure
NIP-8	PRD Packing and Shipping Procedure

Radiation Survey Meter

NIP-10	RSM Ionization Chamber Assembly Procedure
NIP-11	RSM Ionization Chamber Plating Procedure
NIP-12	RSM High-Impedance Electronic Module Assembly Procedure
NIP-13	RSM Electronic Module Assembly Procedure
NIP-14	RSM Battery Module Assembly Procedure
NIP-15	RSM Meter Assembly Procedure
NIP-16	RSM Range Switch Assembly Procedure
NIP-17	RSM Meter Housing and Snub Mechanism Assembly Procedure
NIP-18	RSM Final Assembly Procedure
NIP-19	RSM Finish and Identification Procedure

Table A-1 (Cont'd)

	Title	Documentation Type	Brief Summary of Contents
2.	Qualification Test Reports	II	Exact test and inspection procedures in accordance with NPC 200-2. Details the qualification test results.
3.	Qualification Status List	II	A list submitted periodically on the status of qualifying each instrument.
4.	End Item Test Plan and Procedure	I	Description of procedure for "Government Pre-Delivery Acceptance."
5.	Failure Reports	II	Description of any failure; documented in accordance with NPC 250-1.
6.	Failure Analysis and Corrective Action	II	Detailed report on the correction of any failure.
7.	Failure Modes and Effects Analysis	II	Description of failure modes and the effects of possible failures.
8.	Equipment Log Book	II	Detailed history log of each individual piece of flight hardware.
9.	Reliability Prediction Model	II	Description of the reliability prediction and analysis of the PRD and RSM; prepared in accordance with NPC 250-1.
10.	Acceptance Data Package	II	Each shipment of hardware contains a data package in accordance with ASPO document entitled "Acceptance and Data Package, Requirements and Definition, Revision A, August 1964."

Table A-1 (Cont'd)

Title	Documentation Type	Brief Summary of Contents
Support Procedures		
1. Preservation and Handling Procedures	I	Description of the procedures for packaging, handling, transporting, and storing of flight hardware.
Program Reports		
1. Monthly Progress Report	II	Standard type of monthly progress report.
2. Final Report	II	Summary of the results of the entire contract.

Table A-2 (Cont'd)

NIP-20	RSM Calibration Procedure
NIP-21	RSMB Assembly, Finish, and Identification Procedure
NIP-22	RSM and RSMB Cleaning, Packing, and Shipping Procedure
NIP-23	Shipping and Packaging Instructions

Table A-3

LIST OF GENERAL DYNAMICS PRD AND RSM DRAWINGS

Personal Radiation Dosimeter

NLE 297-B	Printed Circuit of Battery Contact
NLE 299-B	Schematic, Personal Radiation Dosimeter and Parts List
NLE 300-B	Assembly of Welded Module
NLM 224-B	Ionization Chamber
NLM 228-B	Module, High-Impedance Electronics
NLM 236-B	Dosimeter Housing
NLM 237-B	Electronic Module Mold
NLM 249-B	Isometric Projection
NLM 250-B	Ionization Chamber Assembly
NLM 251-B	Assembly II, High Impedance Module & -9 Plate
NLM 252-B	Assembly III, Lower Housing

Radiation Survey Meter

NLE 298-B	Schematic, Radiation Survey Meter and Parts Lists
NLE 301-B	Assembly of Welded Module
NLM 223-B	Ionization Chamber
NLM 227-B	Bracket
NLM 227-13	Bracket Mold
NLM 229-B	Meter Housing
NLM 230-B	Range Switch

Table A-3 (Cont'd)

NLM 231-B Sheet 1	Module, High Impedance
NLM 231-B Sheet 2	Module, High Impedance
NLM 232-B Sheet 1	Battery Module
NLM 232-B Sheet 2	Battery Module
NLM 232-B Sheet 3	Battery Module
NLM 233-B	Meter Housing & Details
NLM 234-B	Meter Handle & Details
NLM 235-B	Snub Device
NLM 238-B	Mold Plate, Bracket
NLM 240-B	Electronic Module Mold
NLM 246-B	Assembly III Snub Mechanism
NLM 248-B	Isometric Projection
NLM 253-B	Assembly I Ionization Chamber
NLM 254-B	Assembly II Meter Housing & Handle

REFERENCES

1. Janni, J. F., Calculations of Energy Loss, Range, Pathlength, Straggling, Multiple Scattering, and the Probability of Inelastic Nuclear Collisions for 0.1- to 1000-MeV Protons, Technical Report No. AFWL-TR-65-150, September 1966.

2. Private communication from S. N. Hardee, National Aeronautics and Space Administration, Houston, Texas.

3. Private communication from Dr. G. P. Welch, Lawrence Radiation Laboratory, University of California, 5 October 1967.

4. Private communication from R. G. Richmond, National Aeronautics and Space Administration, Houston, Texas.

5. Bell, J. R., and Miles, J. K., Calibration of Foils for Neutron Flux Measurements, GD/FW Report MR-N-279, 6 June 1961.

6. Reinhard, P. W., and Davis, F. J., "Improvements in the Threshold Detector Method of Fast Neutron Dosimetry," Health Physics, Vol. 1, 1958, pp. 169-175.

7. Warshaw, S. D., et al., "The Beta-Spectrum of P^{32}," Physical Review, Vol. 80, 1950, p. 288.

8. "Studies in Penetration of Charged Particles in Matter," National Academy of Sciences - National Research Council Publication 1133, 1964.